Université d'Ottawa • University of Ottawa

Université d'Ottawa · University of Ottawa

FACULTÉ DES ÉTUDES SUPÉRIEURES ET POSTDOCTORALES

FACULTY OF GRADUATE AND POSTDOCTORAL STUDIES

Viorel CRACIUN

AUTEUR DE LA THÈSE - AUTHOR OF THESIS

M. A. Sc. (Electrical Engineering)

GRADE - DEGREE

School of Information Technology and Engineering

FACULTÉ, ÉCOLE, DÉPARTEMENT - FACULTY, SCHOOL, DEPARTMENT

TITRE DE LA THÈSE - TITLE OF THE THESIS

A Tunable Optical Add-Drop Multiplexer

O. Yang

DIRECTEUR DE LA THÈSE - THESIS SUPERVISOR

CO-DIRECTEUR DE LA THÈSE - THESIS CO-SUPERVISOR

EXAMINATEURS DE LA THÈSE - THESIS EXAMINERS

B. Syrett

J. Yao

J.-M. De Koninck, Ph.D.

LE DOYEN DE LA FACULTÉ DES ÉTUDES SUPÉRIEURES ET POSTDOCTORALES

SIGNATURE

DEAN OF THE FACULTY OF GRADUATE AND POSTDOCTORAL STUDIES

A Tunable Optical Add-Drop Multiplexer

by

Viorel Craciun

M.A.Sc. Thesis

submitted to the Faculty of Graduated Studies and Postdoctoral Studies
in partial fulfillment of the requirements
for the degree of Master of Applied Science in Electrical Engineering

April 2003

Ottawa-Carleton Institute for Electrical and Computer Engineering
Department of Electrical Engineering
School of Information Technology and Engineering
University of Ottawa

Your file Votre référence
ISBN: 0-612-90050-9
Our file Notre référence
ISBN: 0-612-90050-9

Abstract

Tuneable add-drop multiplexer systems that are feasible and exhibit good performance characteristics are highly desirable for building all-optical transmission systems. A novel sparse tuneable optical add/drop multiplexer subsystem consisting of eight tuneable single-ring resonator based optical filters, and two eight-channel phase array devices, is proposed to allow sparse optical channels add and/or drop. The design takes advantage of the main limitation of single ring resonator-based optical filters, namely the rather limited free spectral range and in effect the limited number of communication channels that can be processed. The tuneable filters provide add and drop functions of the selected channels whereas the phase array devices provide demultiplexing and multiplexing functions for the inbound and the outbound channels respectively. The coupled mode theory, its transfer matrix formalism, and the theory of spectral analysis of signals are used to carry out preliminary performance analysis of the single-ring resonator based tuneable add-drop filter, to optimize, and finally to characterize its performance. This approach allows an accurate evaluation of filter characteristics, namely the transfer functions between any ports of the device. A wavelength-domain simulation method, coupled with a time/frequency-domain simulation method, is used to analyse the performance of the tuneable OADM in linear, ring, and mesh all-optical wavelength-division multiplexing networks/transmission systems. Our performance evaluation demonstrates that the tuneable OADM could be successfully employed in linear, ring, and mesh all-optical dense-division multiplexing networks/transmission systems with bit rates up to 10 Gbit/s.

Acknowledgements

I would like to thank Prof. Oliver W.W. Yang, my thesis director, for his constructive criticism and encouragements. I am in debt and also like to thank Dr. Cristian Lambiri for teaching me the basics of typesetting in LaTeX.

This work is dedicated to my wonderful daughter Alexandra Erica and to my lovely wife Alina whose endless patience and constant encouragements kept me going throughout this endeavour.

Contents

List of Figures

List of Tables

Notations

Various symbols, superscripts, subscripts, and abbreviations frequently used in this work are summarized below.

Notation	Description	Section of First Appearance
α_i	loss coefficient	2.1.1
β_i	propagation coefficient	2.1.1
γ	scattering loss coefficient	2.1.1
λ_0	central wavelength	2.1.1
θ_i	phase delay	2.1.1
τ	group delay	1.2.8
$\Phi(f)$	phase response	2.1.4
a	coupler loss coefficient	2.1.1
a_i	incident wave at port i	2.1.1
b_i	reflected wave at port i	2.1.1
k	power coupling coefficient	2.1.1
k_t	thermal expansion coefficient	2.1.5
n_e	refractive index	2.1.5
r	radius of the resonator ring	2.1.5
AD_{factor}	add-drop factor	5.3
$AOTF$	acousto-optic tuneable filter	1.2.3
BW_{FWHM}	filter bandwidth at -3dB	3.3
C-band	conventional band	1.2.1
C_s	channel spacing	3.3
FBG	fiber Bragg grating	1.2.3
$FDTD$	finite difference time domain	1.2.8

FSR	free spectral range	1.2.8
IL	insertion loss	1.2.8
$IL_{add/drop}$	*add/drop* insertion loss	3.3
$IL_{through-adj}$	*through* insertion loss for adjacent channel	3.3
$IL_{through-non-adj}$	*through* insertion loss for non-adjacent channel	3.3
L-band	long band	1.2.1
$MEMS$	micro-electro-mechanical system	1.2.3
MMI	multi-mode interferometer	1.2.3
MZ	Mach-Zehnder	1.2.3
N_c	total number of channels	3.3
N_{cg}	number of channel per group	3.3
N_g	number of groups of channels	3.3
$OADM$	optical add-drop multiplexer	1.2.1
$OCDM$	optical code division multiplexing	1.2.1
$OSNR$	optical signal to noise ratio	1.2.1
$OTDM$	optical time domain multiplexing	1.2.1
RF	radio frequency	1.2.4
S-band	short band	1.2.1
SCM	sub-carrier mutiplexing	1.2.1
$SiON$	silicon-oxynitride	1.2.3
SOA	semiconductor optical amplifier	1.2.3
$VLSI$	very large scale integration	1.2.6
WDM	wavelength division multiplexing	1.2.1
$Xtalk_{adj}$	adjacent crosstalk	3.3
$Xtalk_{non-adj}$	non-adjacent crosstalk	3.3

Chapter 1

Introduction

1.1 Overview

The tremendous growth of Internet traffic led to an increase in demand for data transmission. It is a clear trend that while the voice traffic demand is steady increasing linearly, the data traffic demand has surpassed the voice growth in a quasi-exponential evolution.

A number of technologies such as optical time division multiplexing, optical code division multiplexing, wavelength division multiplexing, and subcarrier multiplexing have been considered [1] for realizing the next generation Optical Internet. It is generally accepted that wavelength division multiplexing represents the most attractive transport technology, offering extreme flexibility in terms of optical channel granularity and large transport capacities.

The main requirements for the next generation all-optical networks at the photonic layer are agility, scalability, intelligence, easy management and control, simplicity and robustness, and low cost. Configurable wavelength division multiplexing transmission systems [2] meet most of the requirements outlined above and offer significant performance improvement over non-configurable counterparts in terms of agility, easy management and control, lower blocking probabilities, and improved network utilization.

Extensive research and development effort is being dedicated to configurable optical add-drop multiplexers for wavelength division multiplexing networks as they represent key building blocks for realizing next generation, flexible optical networks.

1.2 Literature Review

1.2.1 All-Optical Networking

A number of multiplexing techniques have been studied for building the optical transmission layer of next generation all-optical networks. Examples of such techniques are optical time division multiplexing (OTDM) [3, 4], optical code division multiplexing (OCDM) [5] wavelength division multiplexing (WDM) [6, 7], subcarrier multiplexing (SCM) [8, 9, 10]. Hybrid solutions employing WDM in combination with SCM [11], OCDM [12, 13], OTDM [14], and OCDM/OTDM [15] have also been proposed in an attempt to decrease the complexity, to improve the flexibility, to increase the capacity, and to decrease the costs of next generation all-optical networks.

OTDM has been demonstrated as an effective technology for building optical networks. In spite of difficulties in generating very short spectrally pure pulses, recent experiments have demonstrated a record-length, 208 km standard singlemode fiber transmission of an 80 Gbps optical time division multiplexing signal using a return-to-zero modulation scheme [4]. Therefore, OTDM is viewed as the technology that would tremendously increase the capacity of the optical networks.

OCDM is regarded as a stand alone or complementary transmission technology that will allow for realization of next generation all-optical networks [5]. It was envisioned that by increasing the number of optical codes, and by expanding the wavelength transmission region to short (S), conventional (C), and long (L) band, the transmission capacity can be potentially increased to 40 Tb/s per optical fiber pair. A record of 1.6 b/s/Hz spectral efficiency has been achieved in OCDM/WDM link by quaternary phase shift keying and a transmission system of 6.4 Tb/s OCDM/WDM has been experimentally demonstrated [13].

SCM has been proposed as a cost effective approach for transmitting of a large numbers of optical channels over optical fibers [8], and has been acknowledged as an effective way of dividing WDM channels into low speed bit streams to mitigate the mismatch of the speed of the electronics at the edge and of the speed of the optical core [9]. SCM/WDM transmission systems have been successfully demonstrated for high speed optical transmissions [10, 16], wireless backbones [11], and for distribution

networks [17], and has been shown to benefit from low cost, readily available, low speed base-band electronics. However, the technology has fundamental limitations due the analog modulation of the transmitted signals [8, 18].

WDM has been identified as a serious candidate for high capacity transport networks [19] as a pure WDM optical network or as part of a hybrid solution. High capacity 10.92 Tb/s (273 x 40 Gb/s) triple-band, ultra-dense WDM optical repeated transmission fully utilizing S, C, and L band transmission window [6], and 10.2 Tb/s (256 x 42.7 Gb/s) PDM/WDM transmission over 100 km fiber with 1.28 bits/s/Hz spectral efficiency [7] have been reported. Most of today's commercial implementations are WDM optical networks/transmission systems.

1.2.2 Benefits of Configurability

Configurable optical transmission systems offer significant performance improvement over non-configurable counterparts. Lower blocking probabilities, improved network utilization, and added flexibility can be achieved through configurable network elements, wavelength translation, wavelength routing, and optimized wavelength assignment algorithms.

Models to quantify the blocking probability in all-optical networks under various assumptions have been proposed and described. Computationally intensive techniques such as Markov chains [20], and more efficient techniques based on inclusion-exclusion principle of combinatorics [21] or path decomposition approach [22] have been developed.

The above performance issues of all-optical network have been summarised in [2] and issues associated with implementing flexible all-optical networks have been analysed in [23]. Subramaniam et al. [24] introduced the concept of sparse wavelength conversion as a mean of improving the network utilization and blocking probability of all-optical networks and concluded that the performance improvement is highly dependent on the architecture of the network.

It has also been demonstrated that sparse configurable networks are far more cost effective than a fully configurable network [25, 26], and the blocking probability of a network with sparse conversion converges to that of the same network with full conversion if the network nodes have 25% to 50% reconfigurability capabilities [27, 28].

1.2.3 Configurable Optical Filters and Add-Drop Multiplexers

Significant research efforts have been dedicated to realizing configurable OADM for WDM networks, as they have been identified as key building blocks for realizing next-generation flexible optical networks [29]. Their main element is the tuneable wavelength-selective add-drop filter.

Various technologies have been actively studied to build such filters, including Bragg gratings [30, 31], acousto-optic effect [32, 33], Mach-Zehnder interferometer [34, 35], electro-optic effect [36], and a number of Fabry-Perot based on micromachined structures [37, 38], or Fabry-Perot based liquid crystals structures [39, 40]. A summary of technologies employed in realizing tuneable optical filters can be found in [41]. According to their speed of tuning, we can categorize tuneable optical filters as (i) slow-speed: generally thermo-optical or mechanical filters used in circuit switching optical networks, and (ii) high-speed: generally acousto-optic or electro-optic based filters used in packet switching optical networks. The first category is in advance stages of development while the latter is still in early stages.

A number of configurable OADMs for WDM networks, based on various underlying technologies and device architectures, have been proposed, demonstrated, and analyzed. They were based on Mach-Zehnder (MZ) interferometers in silicon-oxynitride (SiON) [42] or Bragg grating assisted MZ interferometers [43], coupled semiconductor waveguides [44], semiconductor optical amplifiers (SOA) [45], liquid crystals [46], fiber optical tapped delay lines [47], micro-electro-mechanical systems (MEMS) tilting mirrors [48, 49], and acousto-optic tuneable filters (AOTF)[50]. Also, a large number of solutions were based on Bragg gratings in conjunction with circulators [51, 52, 53, 54, 55, 56, 57], thermally-tuneable Bragg gratings [58], MEMS pitch-tunable Bragg gratings [59], Bragg-assisted multi-mode interferometer (MMI) coupler based OADM [60], Bragg grating loaded directional coupler [61], polymer Bragg gratings [62], and temperature-compensated fiber Bragg gratings (FBG) [63]. Most of the mentioned designs suffer from inherited limitation in the underlying technology. SOA-based OADMs suffer mainly from large fiber-chip insertion loss due to the large difference in the mode size, limited bandwidth due to the amplification profile, and additional noise inherent to the SOA. Liquid-crystal and MEMS add-drop filters suffer from long term stability

while Bragg gratings add-drop filters are relatively difficult to manufacture.

1.2.4 Tuning Mechanisms for Optical Filters

Each filter technology has a specific tuning technique [41]. Examples are temperature tuning for ring resonators [64], current injection for semiconductor-based Fabry-Perot filters [38], refractive index-shifting for long-period Bragg gratings [65], electro-optic effect for electro-optic filters [36], radio frequency (RF) signal control for AOTF filters [33, 50], micromachine for MEMS Fabry-Perot filters [48, 49], crystal orientation for liquid crystals Fabry-Perot filters [66], and piezoelectric transducer for fiber-based Fabry-Perot filters [67]. Although some methods are easier to design, implement and control choosing the tuning mechanism is limited to the underlying technology. As an example, the current injection tuning mechanism is simple to implement, it can prove very difficult to control and is applicable to semiconductor based OADMs only.

1.2.5 Integrated Optics and Materials

The concept of integrated optics was introduced by Miller [68] as a way of manufacturing solid state devices. The advantage, on one hand, is that a number of optical functions can be achieved by integrating a number of distinct optical components onto the same physical substrate. On the other hand, the fabrication processes can be automated leading to high volume manufacturing, high fabrication yields, and consistent product performance.

A number of optical materials have been characterized and employed for manufacturing integrated optical components. Semiconductor materials such as InGaAsP/InP and GaAlAs/GaAs can be successfully used for monolithic integration of passive and active components and exhibit good long-term stability, large thermo-optical coefficients, but large waveguide and fiber-to-chip loss. Other materials such as Lithium Niobate (LiNbO3), glass, and polymers exhibit better performance characteristics in terms of waveguide loss and fiber to chip loss but do not allow for monolithically integrating active and passive components, or do not exhibit a very good long term stability [69].

A fine balance between all the optical and mechanical properties must be achieved in order for a specific optical material to allow for successfully manufacturing a given

integrated optical circuit. Important parameters to consider are the thermo-optical coefficient, thermal expansion coefficient, waveguide loss, fiber-to-chip loss, long-term stability, wafer size.

1.2.6 Ring Resonator-Based Filters

Ring resonators were proposed for optical filters three decades ago by Marcatilli [70]. These filters are interferometric filters in which an incoming signal is split into multiple wavelength independent paths, delayed and recombined to obtain the output signal. The splitting and recombination ratios as well as the delays influence the frequency response of the filter.

Since their first proposal as optical filters, ring resonators have found applications in all-optical time recovering circuits, spectrum analysers, optical equalizers, soliton generators, and pulse generators [71]. Oda et al. [72] proposed the first ring resonator based filter for WDM applications and soon after a number of other applications have been proposed and analysed: all-fiber compound ring resonator [73], ultra-compact micro-ring silica on silicon resonator [74], vertically coupled resonators in Si-SiO2 [75], semiconductor [64, 76] or in polymer [77], race track microrings [78] or periodically coupled rings [79], multiple filters on an optical chip [80], and microring resonator arrays for very large scale integration (VLSI) photonics [81].

The dielectric waveguides of the ring resonator filter can be parallel or crossed. The first layout is advantageous due to the lack of cross talk between the two waveguides, while the latter allows for effectively integrating multiple add-drop filters onto the same substrate into add-drop filter arrays. The crossed waveguides design can feature a single ring, a maximum of two rings cascaded in parallel, or a number of ring resonators cascaded in series. Although cascading more rings improves the magnitude response, it also renders more difficult the task of successfully tuning the add-drop filter to the desired central wavelength.

1.2.7 Ring Resonator Building Blocks

A ring resonator based optical filter is comprised of optical waveguides and optical couplers.

Optical Waveguides

Optical waveguides were identified as basic building blocks for integrated optical components in general since the pioneering days of photonics by Wilmot [82], and for ring resonator based filters in particular shortly after by Marcatilli [83].

An optical waveguide consists of a dielectric core embedded into a medium with a lower dielectric constant and in general are rectangular in cross section. Rectangular waveguides confines the waves in both lateral directions. The optical waves are bounced back and forth between the four boundaries that may or may not have the same dielectric constant. The propagation of light within the waveguides is described by the wave equations that can be obtained from the Maxwell's equations and can be solved as described in [84].

In general, integrated optical components employ single mode dielectric waveguides. A number of single mode waveguide designs in polymer [85], silicon [86], silicon-on-insulator [87], or siloxane polymer on Cu-polyimide substrate [88] have been proposed and analysed.

Directional Couplers

A directional coupler is made of two waveguides placed in close proximity. Coupling occurs due to the overlap of the evanescent electromagnetic fields travelling through the cladding of two waveguides with the electromagnetic fields travelling through the core of the other waveguide.

A number of guided-wave directional couplers have been proposed and analyzed in search for integrated directional couplers with flat frequency response [89, 90, 91, 92, 93]. The featured interaction length between the two dielectric waveguides was in the range of hundreds of microns to 1 mm. Takagi et al. [94] categorized them into four types: uniform symmetric coupler, uniformly asymmetric coupler, point-symmetric tapered coupler, and non-symmetric directional coupler. To analyse optical couplers one can employ coupled mode theory to derive the solutions of the coupled mode equations, as presented in details in [95].

Multimode Interference Couplers

Multimode interference (MMI) couplers are based on the self-imaging property of multimode dielectric slabs, suggested in [96] and further described in [97]. Self-imaging is a property of multimode waveguides by which an input field profile is reproduced in single or multiple images at periodic intervals along the propagation direction of the waveguide. A detailed description of the operating principle of MMI couplers can be found in [98].

Soldano et al. gave a theoretical description of self-imaging in multimode waveguides [99] using the effective index method, a general matrix formalism of self-imaging in MMI couplers has been presented in [100], and the theory of variable-ratio power splitting multimode interference couplers has been presented in [101].

Recognizing the importance of small optical couplers for optical integrated circuits a number of ultracompact multimode interference couplers [102, 103, 104] have been proposed and analyzed. Along with the small size the MMI-based couplers can exhibit a reduced sensitivity to fabrication tolerances [105, 106].

1.2.8 Ring Resonator Analysis Methods

A number of methods have been proposed to analyze optical structures in general and optical ring resonator-based photonic circuits in particular. A signal processing method [64, 107, 108, 109] based on the Z-transform technique, couple mode theory [110, 111, 112] with its matrix formalism [113, 114, 115], and finite difference time domain (FDTD) method [116, 117], have been described and used to analyse ring resonator-based filters designs. All these methods take advantage of a very important property of optical filters, namely their full characterization by their magnitude and phase response.

The signal processing method uses the Z-transform digital filter analysis and design techniques. Given a desired magnitude and phase response of the filter, the method allows the synthesis of its physical dimensions. Performance characteristics such as free-spectral range (FSR), insertion loss (IL), adjacent and non-adjacent crosstalk, and group-velocity delay (τ), can be determined as extensively explained in [108].

The coupled mode theory has been developed in the 1950s to analyse and design microwave waveguides and passive devices [118]. The approach was rather heuristic, as

the couple mode equations were determined from power considerations only. A rigorous derivation of coupled mode theory was developed directly form the Maxwell's equations by expanding the unknown electromagnetic fields of the coupled systems in terms of the known modes of the uncoupled systems [119]. Yariv [120] adapted the coupled mode theory to optical waveguides in the 1970s. The coupled mode theory can be employed by coupling the modes in time or by coupling the modes in space. The coupling of modes in time approach can describe coupling of two resonators, parametric amplification and oscillation, while coupling of mode in space is applicable to periodic structures like gratings, periodic space-time phenomenon like an optical pump in a parametric amplifier, waveguide coupler, and traveling wave tube [121].

The coupled mode theory approach is tedious and lengthy when solving a large resonating circuit consisting of more than two directional couplers [122], and as a result a matrix formalism, previously used for electrical circuits, has been extended to analyse integrated optical circuits [114, 123].

The matrix formalism method transforms the simultaneously linear equations of the electromagnetic field intensities into matrices [113] and is straightforward in deriving the solutions of the coupling mode equations using computer algorithms [124]. Schwelb proposed a generalized matrix formalism method for linear interferometric networks, which simplifies the analysis and design of microwave and optoelectronic components by rearranging the interferometric network into a chain of cascaded four-ports, single-mode lumped-element 2 x 2 coupler with arbitrary coupling paths [115]. The method is computationally efficient for analysis of a wide variety of lattice networks.

FDTD method has been used for microcavity ring and disk resonators analysis [116], [117] and in modelling of photonic crystal structures [125]. Key optical design parameters such as transmission characteristics, coupling efficiencies and resonant frequencies can be obtained using FDTD solutions of the full-wave Maxwell's equations. The results include the effects of waveguide dispersion and bending and scattering losses [126]. A complete mathematical description of the FDTD method for electromagnetics has been provided by Kunz [127].

Although the FDTD method is the most accurate, its accuracy comes at the expense of computational complexity. Comparison between the coupled mode theory and finite

difference time domain methods indicated that the difference in accuracy of the two is within 1% making the coupled mode theory a very attractive method for analysing ring resonator based filters [110].

1.3 Motivation

It is generally accepted that WDM represents the most attractive transport technology as it offers extreme flexibility in terms of optical channel granularity and lends itself for large capacity reconfigurable network architectures as pure WDM or a combination of WDM with SCM, OCDM, and/or OTDM. Therefore, tuneable optical add-drop multiplexers that exhibit good performance characteristics are highly desirable for building all-optical networks/transmission systems.

A number of solutions for tuneable optical add-drop multiplexers and add-drop filters, employing novel techniques, materials, and device architectures, have been summarized in Section 1.2. Add-drop filters based on ring resonators are attractive due to their dimensions, integrability, optical performance, and flexibility [72, 128]. However, to the best of our knowledge, none of the proposals considered tuneable ring-resonator filters to realize sparse tuneable OADMs, nor thoroughly analysed the performance of such tuneable OADMs in all-optical WDM networks/transmission systems.

1.4 Objectives

The objectives of this thesis are to propose a novel ring-resonator-based sparse tuneable add-drop multiplexer, to demonstrate its feasibility, and to evaluate its performance in a number of all-optical WDM networks/transmission systems.

1.5 Methodology and Approach

To pursue our objectives, we shall propose a novel sparse tuneable OADM architecture based on tuneable ring-resonator-based add-drop filters.

Next, we shall devise a mathematical model of the tuneable add-drop filter, based on the coupled mode theory and its transfer matrix formalism, and implement the model

in Matlab. Using the developed computer model we shall design a filter prototype, determine its transfer characteristics, and optimize the design.

Next, we shall develop a computer program in Matlab, based on the theory of spectral analysis of signals, which shall allow us to determine the performance parameters of the tuneable OADM from the transfer characteristics of its constituent components. Performance parameters such as insertion loss, channel pass bandwidth, adjacent cross talk, non-adjacent cross talk, group-velocity delay, and operating temperature mapping shall be determined.

Finally, we shall evaluate the performance of our tuneable OADM in linear, ring and mesh all-optical networks/transmission systems in terms of optical power spectrum, bit error rate, optical signal to noise ratio, maximum number of possible cascaded OADM, and eye diagram. We shall accomplish this by employing an optical transmission system simulator, Optsim [129], to run two-step simulations that couples a wavelength-domain simulation step with a time-domain/frequency domain step. Since the simulator uses a Monte-Carlo technique as presented in [130], all the stochastic processes shall be randomly generated, the noise shall be propagated at the same time as the signals, and all the optical signals shall be represented by sets of samples in time and frequency domain as described in [131].

The simulation shall take into account all the linear and non-linear effects in the fiber, in addition to transmission impairments such as amplified spontaneous noise, cross-talk, polarization-dependant loss, polarization mode dispersion, chromatic dispersion, fiber non-linearities, transmitter chirp, and signal distortion due to filtering.

1.6 Contributions

The contributions of this thesis are:

- Devising a novel ring-resonator based tuneable OADM that can be used in linear, ring, and mesh all-optical networks/transmission systems
- Devising a mathematical algorithm that allows for designing and optimizing ring-resonator based filters

- Designing a tuneable add-drop optical filter, analysing and optimizing its performance characteristics
- Characterizing the proposed tuneable OADM, determining its optimum channel allocation plan, and proposing a possible physical layout
- Devising system level simulation scenarios and simulation models that accurately reflect the performance characteristics of the tuneable OADM and of the simulation scenarios
- Evaluating the performance of the proposed tuneable OADM in a number of all-optical WDM networks/transmission systems and demonstrating its applicability in linear, ring, and mesh all-optical network/transmission system.

1.7 Thesis Organization

The reminder of the thesis is organized as follows.

Chapter 2 presents the network architectures in which our sparse tuneable OADM would operate. Next, it presents the architecture, the suggested physical layout, the principle of operation, and the wavelength allocation plan of our sparse tuneable OADM. The assumptions made throughout this research along with important definitions are also presented for further usage and reference.

Chapter 3 presents a mathematical model, based on the coupled mode theory and its matrix formalism, which determines the magnitude and phase transfer functions of single-ring resonator based optical filters. It also gives the design, the performance characteristics and the optimization of the tuneable add-drop filter, the main component of our sparse tuneable OADM.

Chapter 4 presents the optimization of the design of the tuneable add-drop filter, using the mathematical model developed in the earlier chapter, and summarizes its design and performance parameters.

Chapter 5 presents the mathematical model based on the theory of spectral analysis of signals, which determines the performance parameters of our sparse tuneable OADM. Next, the performance parameters of our sparse tuneable OADM are determined and presented.

Chapter 6 evaluates the performance of our tuneable OADM in linear, ring, and mesh all-optical networks/transmission systems. Component models, network models, and simulation scenarios are devised and presented. Next, the performance is evaluated in terms of optical power spectra, bit error rates, optical signal to noise ratios, eye diagrams, and maximum number of cascadable sparse tuneable OADM by using Optsim, an optical transmission system simulator.

Chapter 7 provides guidelines and considerations for designing sparse tuneable optical add-drop multiplexers.

Chapter 8 concludes our research, and suggests further work.

1.8 Publications

The contents of Chapters 3 and 4 will be presented in [132] and that of Chapter 5 in [133].

[132] V. Craciun and O. W.W. Yang, "Ring resonatorbased sparse reconfigurable optical adddrop multiplexer. Part I: Filter analysis", Active and Passive Optical Components for WDM Communications, ITCOM, 2003 - to appear.

[133] V. Craciun and O. W. W. Yang. "Ring resonatorbased sparse reconfigurable optical adddrop multiplexer. Part II: Node level analysis", Optical Transmission Systems and Equipment for WDM Networking, ITCOM, 2003 - to appear.

Chapter 2

The Sparse Tuneable OADM

In this chapter, we shall presents the network architectures in which our sparse tuneable OADM would operate. Next, we shall present the architecture, the suggested physical layout, the principle of operation, and the wavelength allocation plan of our sparse tuneable OADM. We shall also present for further usage and reference all the assumptions made throughout this research along with important definitions.

2.1 The Applications

We envision a novel tuneable OADM that can be utilized in linear, ring, and mesh all-optical WDM networks/transmission systems. As illustrated in Figure 2.1(a) the linear network/transmission systems can have a number of optical add-drop nodes in between two terminal nodes. The ring network/transmission system, depicted in Figure 2.1(b), feature a terminal node along with a number of add-drop nodes and matched nodes. The matched nodes allow the ring to connect to subsequent rings yielding multiple ring architectures. The mesh network/transmission system features a number of optical add-drop nodes along with a number of optical cross connects as one can see in Figure 2.1(c).

A number of add-drop nodes may be present in the all-optical network. The tuneable OADM will allow any channel to be dropped providing the channel exists, will allow any channel to be added providing wavelength blocking will not occur, or will allow any channel to pass through towards its destination. The maximum number of channels that could be added and/or dropped at any add-drop node is a fraction of the total number of channels passing through the node.

The optical signals can be generated at any node and reach any other node within the

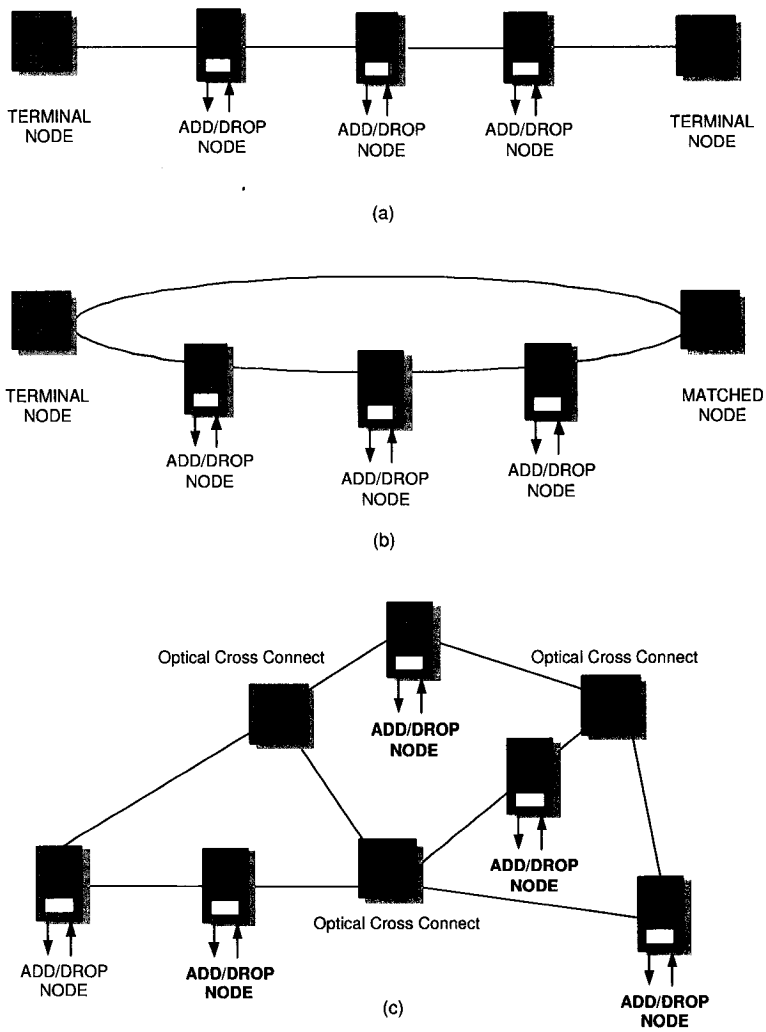

Figure 2.1: Tuneable OADM Applications: (a) linear, (b) ring, and (c) mesh transmission system

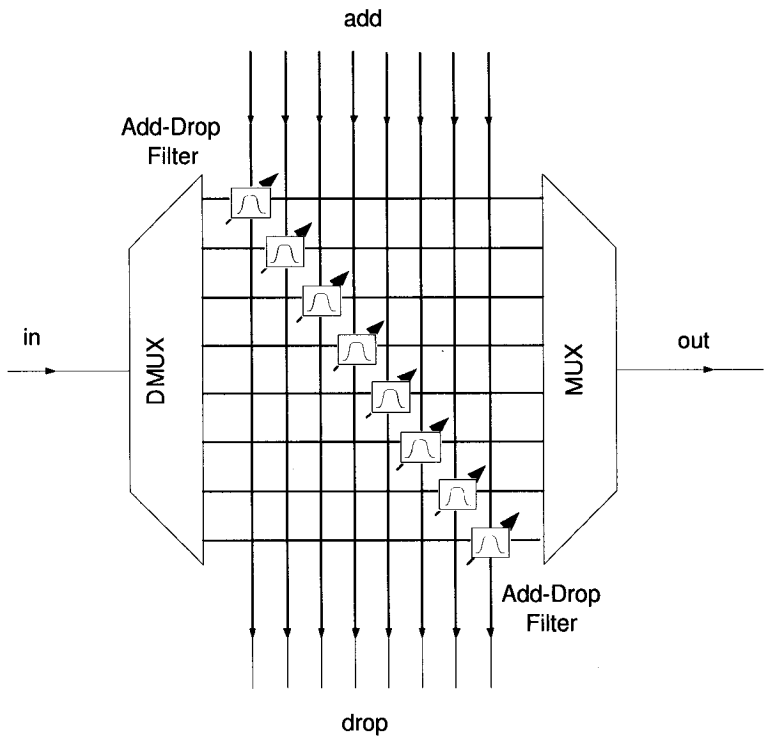

Figure 2.2: The architecture of our sparse tuneable OADM

transmission system without undergoing any conversion to electrical domain, provided that no wavelength blocking will occur. For example, in Figure 2.1 (a) an optical channel could be generated at one of the terminal nodes, travel through the add-drop nodes and arrive at the other terminal node, or could be dropped at any node along the path.

2.2 Architecture

2.2.1 Description

Our tuneable OADM is an integrated optical circuit with 32 optical channels at 0.8 nm spacing, which can selectively add and/or drop any channel. Its add-drop factor is 0.25[1] and therefore the maximum number of channels added and/or dropped at the same time is eight. Since the tuneable OADM does not add and/or drop all the 32 channels at the same time, we shall call it sparse tuneable OADM.

The design takes advantage of the main limitation of ring resonator-based optical

[1]The definition of the add-drop factor is provided in the Section 2.5.

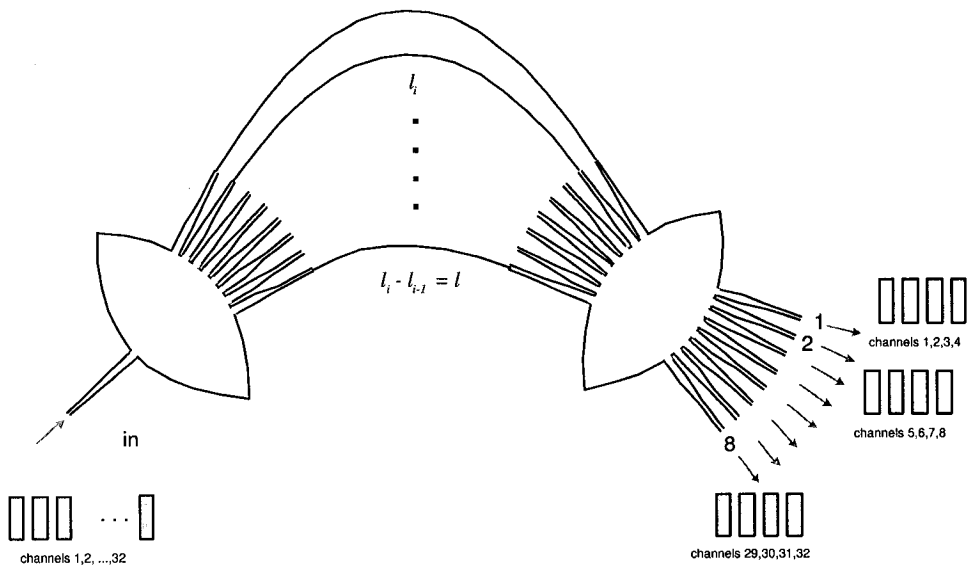

Figure 2.3: The phase-array demultiplexer

filters, namely the rather limited free spectral range and in effect the limited number of communication channels that can be processed by such filters. This is achieved by covering the desired pass bandwidth with an array of ring-resonator-based add-drop filters, each with a fraction of the desired pass bandwidth. The main element of our tuneable OADM is therefore the array of eight tuneable add-drop filters based on single-ring resonators, as illustrated in Figure 2.2. The tuning mechanism is temperature control, an inherent tuning mechanism for ring-resonator-based optical filters.

2.2.2 Constituent Components

The building blocks of our tuneable OADM are two eight-channel phased-array planar devices and eight tuneable ring resonator-based filters. The first phased-array device acts as optical demultiplexer, the tuneable ring resonator-based filters act as selective add-drop filters, and the second phased-array device acts as optical multiplexer.

The Phased-Array Demultiplexer

In Figure 2.3 we show a schematic representation of the phased-array device. It consists of two star couplers, connected by a dispersive grating in a planar grating arrangement. Each star coupler is a waveguide slab of constant refractive index while the dispersive

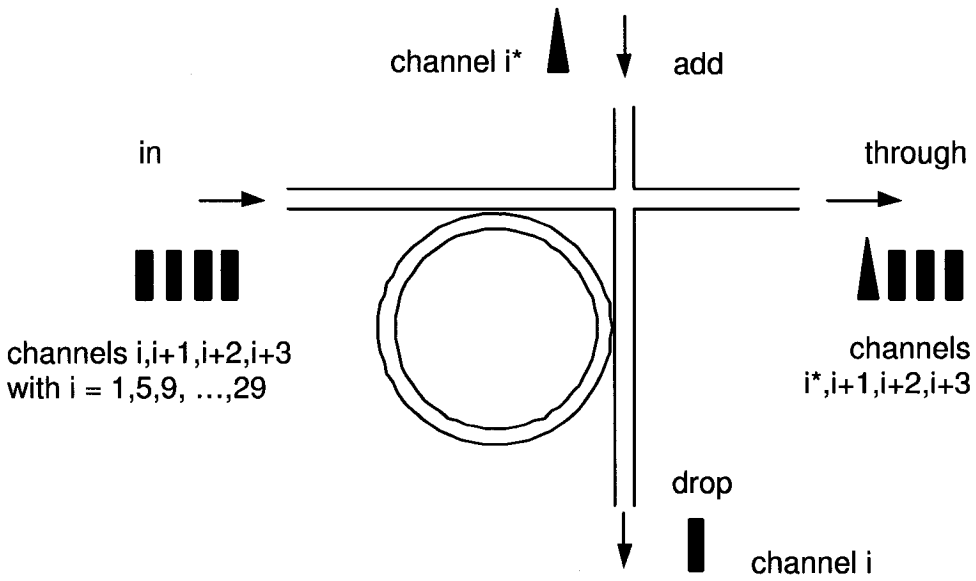

Figure 2.4: The tuneable ring-resonator-based add-drop filter

grating is an array of eight uncoupled waveguides with unequal lengths, such that the difference between the lengths of two subsequent waveguides is constant $l_i - l_{i-1} = l$. Each waveguide is a strip of constant refractive index bounded by strips of a different refractive index. The phase array demultiplexer splits the incoming signal into eight optical bands of equal bandwidths.

The Tuneable Add-Drop Filters

The tuneable add-drop filters consists of two dielectric waveguides, in a cross layout, coupled to one resonator ring as depicted in Figure 2.4[2]. The waveguides and the resonator rings are strips of optical material of constant refractive index delimited by material of a different refractive index. The dynamic ranges of the add-drop filters cover the bandwidth of the equal optical bands resulted from the phase-array demultiplexer. The tuneability of the add-drop filters is ultimately achieved by controlling the refractive index and/or the physical dimensions of the optical resonator through temperature variation, an inherent control mechanism for ring resonator filters.

[2]the control logic and the heating pad required for tuning the add-drop filter are not illustrated

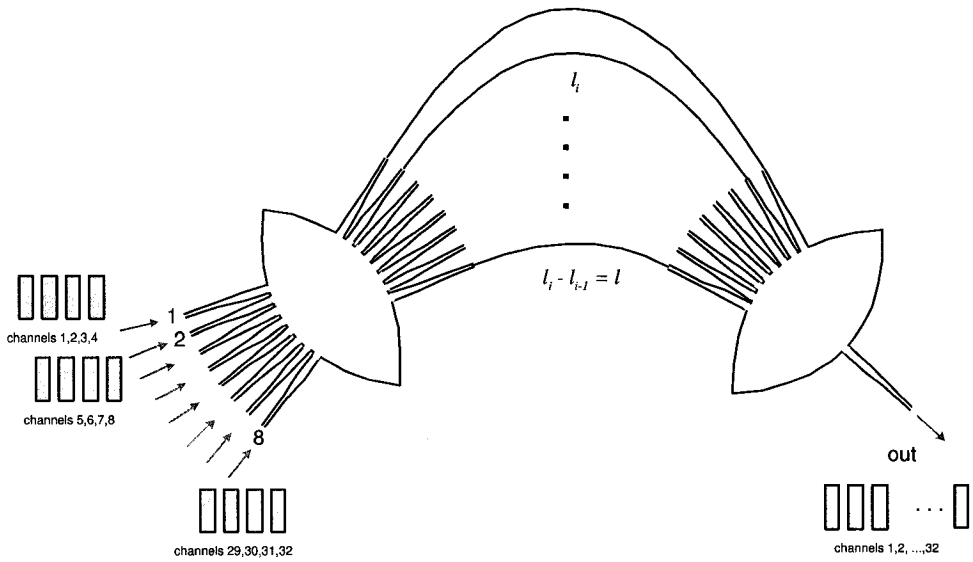

Figure 2.5: The phase-array multiplexer

The Phased-Array Multiplexer

The phase-array multiplexer uses the same type of design as the phase-array demultiplexer, two star couplers connected by a dispersive grating, as depicted in Figure 2.5. The only difference is that in this case the first star coupler has a number of eight input waveguides and the second one only one output waveguide, which is just the opposite of the phase-array demultiplexer. In fact the phase-array demultiplexer can function as multiplexer due to the reversal principle that governs this type of optical device as described by Marz [69].

A number of optical signals that occupy adjacent frequency bands of equal widths, entering the phase-array multiplexer will be combined into one optical signal with width equal to the sum of the widths of the constituent signals.

2.2.3 Physical Layout

The envisioned physical layout of the tuneable OADM is planar, as illustrated in Figure 2.6. The two phase-array devices and the single-ring resonator based tuneable add-drop filters shall reside on a single optical substrate yielding a so-called integrated optical circuit.

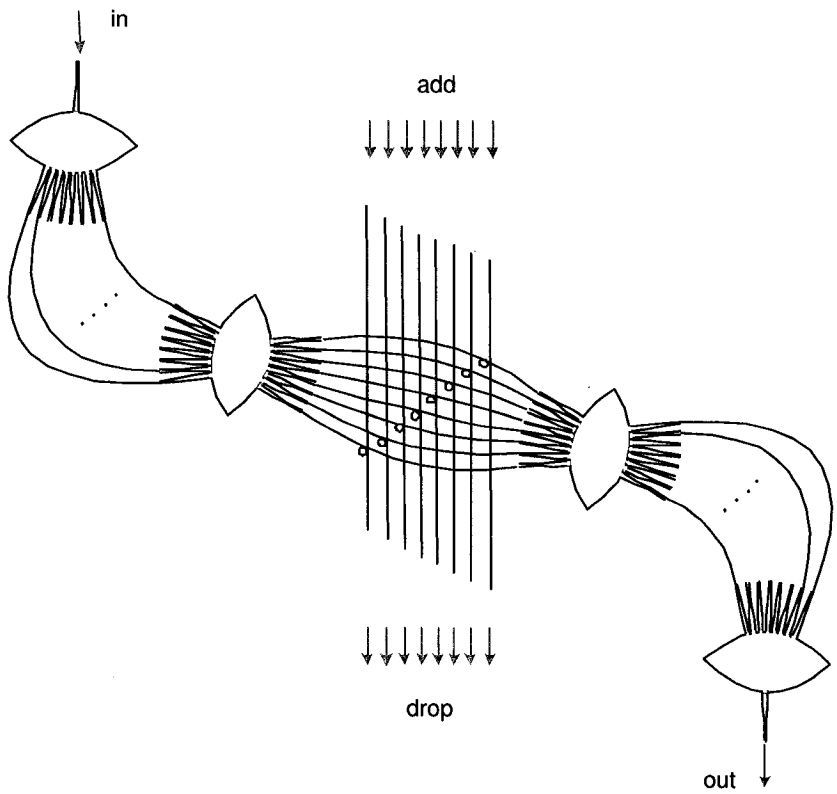

Figure 2.6: The envisioned physical layout of our sparse tuneable OADM

2.3 Principle of Operation

The principle of operation of the OADM can be summarized in three main steps:

- signal demultiplexing in eight groups of four adjacent optical channels,
- drop and/or add maximum one individual optical channels at a time from each group of adjacent channels.
- multiplexing the modified eight adjacent groups of four adjacent optical channels

Signal Demultiplexing

Light entering the *in* port will be coupled into the array grating via the first star coupler of the phase-array demultiplexer, shown in Figure 2.3. In the first star coupler, eight similar images with one eighth of the input signal intensity will be created in accordance

to the self-imaging principle of multimode dielectric slabs suggested by Brynggahl [96] and further described by Ulrich et al. [97].

Each image i travels through its optical waveguide of length l_i and enters the second star coupler with a phase shift $\Delta\phi$ relative to the image i-1. The phase-shifted images interfere constructively in the second coupler of the phase-array demultiplexer and emerge as eight adjacent partial images of the original signal. The bandwidth of each partial image spans over four adjacent optical channels, while their intensities will be less than the intensity of the original input signal or equal in ideal conditions.

Channel Add-Drop

Each one of the eight partial images propagating out of the phase-array demultiplexer is coupled into one of the tuneable add-drop filters, as shown in Figure 2.2, such that the electromagnetic wave emerging from port i of the phase-array demultiplexer enters the *in* port of the *i-th* tuneable add-drop filter.

The signal associated with a particular channel can be dropped from, or added to, the *in-through* waveguide through energy coupling between the two waveguides of the add-drop filter. Only the signal traveling through the first waveguide that have frequencies around the resonant frequency of the ring-resonator will be transferred to the second waveguide, while all the other signals will continue traveling through the first waveguide.

For example, assuming that signals associated with all four optical channel are present at the *in* port and the optical filter is tuned to channel i, $i \leq 4$, signal i will be dropped at the *drop* port while all the other signals will exit at the port *through*. A new signal i^* can be added instead through the *add* port and will exit port *through* along with the other signals, as illustrated in Figure 2.4. The resulting optical signal emerging from the port *through* will be a modified adjacent partial signal with respect to the original input signal.

Signal Multiplexing

The modified adjacent partial signals enter the phase-array multiplexer shown in Figure 2.5 through ports 1 to 8, respectively. The modified adjacent partial signal interfere constructively in the first star coupler and enters the waveguide grating as a signal with the bandwidth of the original input signal but an eighth of its original optical intensity.

Each image travels through its waveguide of length l_i and enters the second star coupler with a phase shift $\Delta\phi$ relative to image i-1. The geometry of the second star coupler enables the phase-shifted images interfere constructively and emerge as a composed signal at the *out* port of the phase-array multiplexer. The bandwidth of the resulting signal spans over 32 adjacent optical channels, and its intensity is less than the intensity of the modified adjacent partial signals or equal in ideal conditions.

2.4 Wavelength Allocation Plan

As per architecture presented in Section 2.2 our sparse tuneable OADM features a total of 32 channels organized in eight groups of channels, each with four channels spaced at 0.8 nm apart. The channel spacing is done in accordance to the recommendations of the International Telecommunication Union (ITU) [134].

In order to avoid significant performance degradation of the optical channels situated close to the edges of the pass bandwidth of the group of channels, our sparse tuneable OADM uses four consecutive channels and skips one before using the next block of four channels, in a so-called four-skip-one architecture. The wavelength allocation plan is presented in Table A.1 in Appendix A.

For the same reason the central wavelength of the add-drop filters in the *all-through* position[3] is selected at a distance of two channels from the channel with the highest wavelength of the related group. This can be seen by comparing Table A.2 with Table A.1.

2.5 Definitions

A number of parameters are characteristics to our tuneable OADM design in particular and optical networks/transmission systems in general. We shall define and/or present the performance characteristics applicable to our design as follows.

(i) Channel Spacing

We define channel spacing of a WDM transmission system as the difference between the central wavelengths of two adjacent optical channels.

[3]The definition of the *all-through* position is provided in Section 2.5.

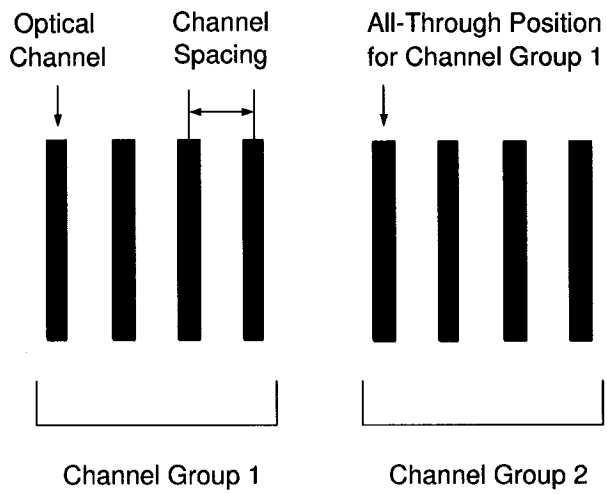

Figure 2.7: Tuneable OADM, the group of channels.

(ii)Group of Channels

We define a group channels of the tuneable OADM as the group of four adjacent optical channels, as illustrated in Figure 2.7. The concept is specific to the tuneable OADM and is inherent to its architecture.

(iii) All-Through Position

We define *all-through* position the position of the central frequency of the tuneable add-drop filter at room temperature (24.6^oC). This is also referred to as "parking" position by some authors. In the *all-through* position the add-drop filter allows all the channels within its bandwidth to pass through without affecting any them.

(iv)Insertion Loss

We define the insertion loss (IL) of our add-drop filter or tuneable OADM as the loss in optical intensity experienced by the input electromagnetic field $I_{IN}(f)$ while passing through the device and can be expressed as:

$$IL(f) = I_{IN}(f) - I_{OUT}(f) \tag{2.1}$$

where f is the frequency of interest and I_{OUT} is the intensity of the output optical signal.

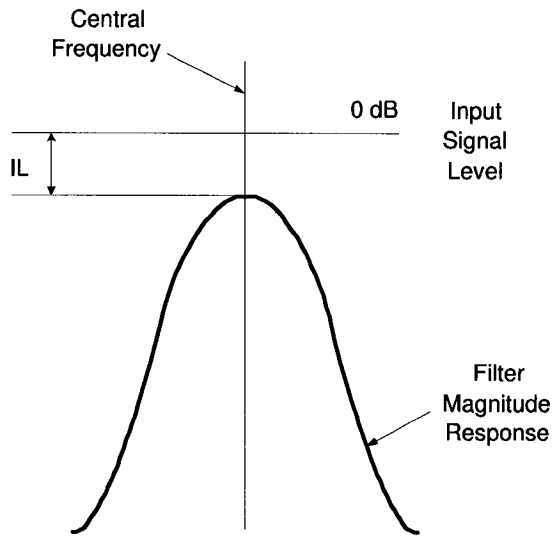

Figure 2.8: Optical filter, the insertion loss.

(v) Central Frequency/Wavelength

The central frequency of the add-drop filter is the resonant frequency of the ring resonator. Ring resonators show resonant transmission peaks at frequencies given by the following equation:

$$f_n = \frac{mc}{2\pi r n_e} \tag{2.2}$$

or wavelengths given by

$$\lambda_n = \frac{c}{f_n} \tag{2.3}$$

where m integer, n_e is the refractive index of the material, c is the speed of light in vacuum, ε_{eff} is the effective dielectric constant, and r is the radius of the resonator ring.

(vi) Add/Drop

We define *add/drop* the action of transferring one electromagnetic wave between the *in* port and the *drop* port or the *add* port and the *through* port of the tuneable add-drop

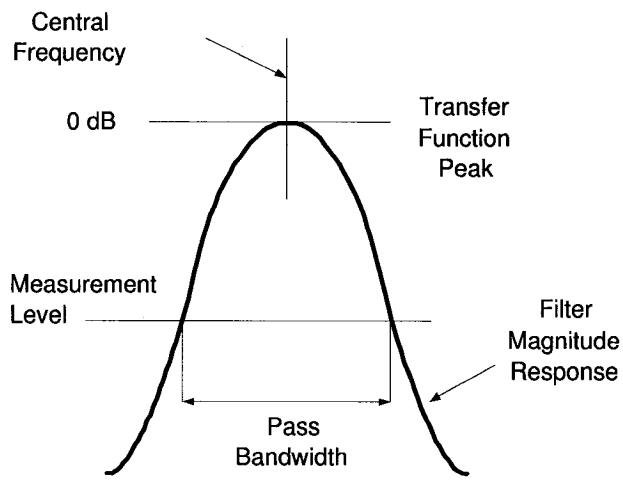

Figure 2.9: Optical filter, the pass bandwidth.

filter. Likewise, the transfer between the *in* port and any of the *drop* ports or any of the *add* ports and the *out* port of the tuneable OADM.

(vii) Through

We define *through* the action of transferring one or more electromagnetic waves between the *in* port and the *through* port of the tuneable add-drop filter. Likewise, it also refers to the transfer between the *in* port and the *out* port of the tuneable OADM.

(viii) Filter Bandwidth

The bandwidth of a filter is defined as the width of its transfer function measured at a given level from the peak-level of the transfer function.

(ix) Pass Bandwidth

We define the *pass bandwidth* as the bandwidth of a filter which allows the incoming electromagnetic waves to be transmitted through the filter. All the frequencies outside the *pass bandwidth* will not be transmitted through the filter. The measurement of the *pass bandwidth* is done at the $-3dB$ level as illustrated in Figure 2.9.

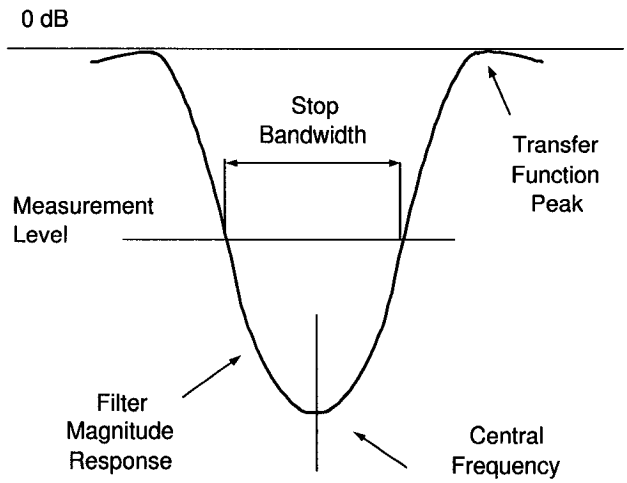

Figure 2.10: Optical filter, the stop bandwidth.

(x) Stop Bandwidth

We define the *stop bandwidth* as the bandwidth of a filter which prevents the incoming the electromagnetic waves from being transmitted through the filter. All the frequencies outside the *stop bandwidth* will be transmitted through the filter. The measurement of the *stop bandwidth* is done at the $-3dB$ level as illustrated in Figure 2.10.

(xi) Add-Drop Factor

We define the add-drop factor as the ratio between the number of channels that can be simultaneously added and/or dropped with respect the total number of channels.

(xii) Dynamic Range

We define the dynamic range of the add-drop filter as the difference between the highest achievable central wavelength and the lowest achievable central wavelength.

$$\Delta\lambda_0 = \lambda_{0MAX} - \lambda_{0MIN} \tag{2.4}$$

where λ_{0MIN} is the minimum central wavelength and λ_{0MAX} is the maximum central wavelength.

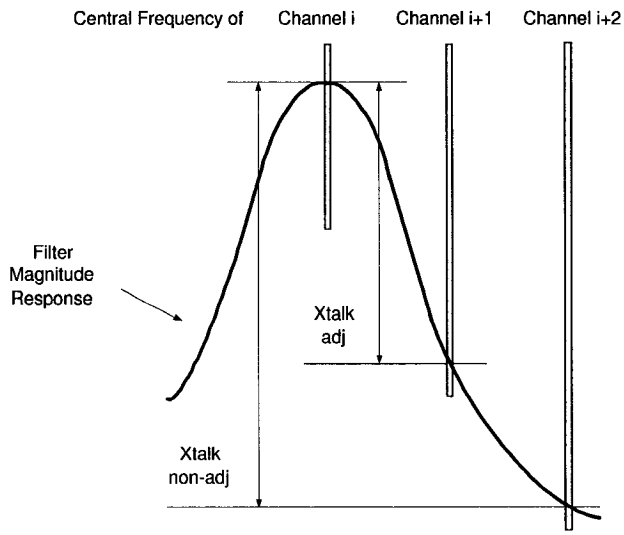

Figure 2.11: Optical filter, the adjacent and non-adjacent crosstalk

(xiii) Cross-Talk

The cross-talk of the filter is the amount of unwanted power in a given channel i from other channels, relative to the input power. There are two types of cross-talk characteristic to optical filters, the adjacent cross-talk $Xtalk_{adj}$ and the non-adjacent cross-talk $Xtalk_{non-adj}$, both illustrated in Figure 2.11. ITU-T [134] measures adjacent and non-adjacent cross-talk as the difference between the magnitude of the transfer function of the filter at the central wavelength and its magnitude at the edge of the adjacent and non-adjacent channel respectively. The method is channel-width dependent and leads to loss of generality.

As opposed to ITU-T, we define the adjacent cross talk as the difference between the magnitude of the transfer function at the central wavelength of channel i and its magnitude at the central wavelength of the adjacent channel i+1. We also define the non-adjacent as the difference between the magnitude of the transfer function at the central wavelength of channel i and its magnitude at the central wavelength of a non-adjacent channel, e.i. i+2.

We believe that our definitions will help in further analysis involving channels of different widths, since they are channel-width independent.

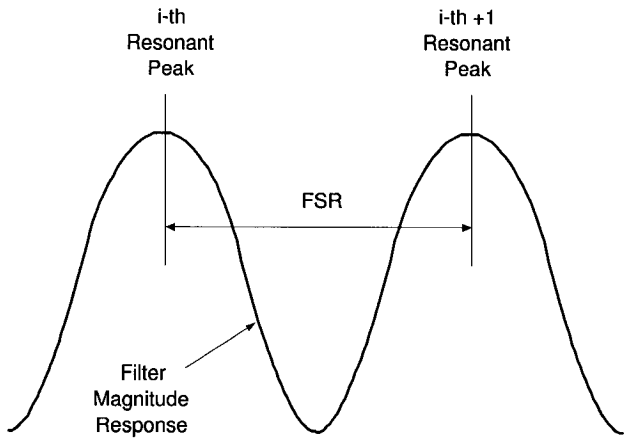

Figure 2.12: Optical filter, the free spectral range

(xiv) Group Delay

The group delay of an optical signal traveling through a transmission medium is defined as the rate of change of the total phase shift θ with respect to angular frequency ω. The phase shift is the change in phase experienced by the input electromagnetic field while traveling through the optical filter.

$$\tau = \frac{d\theta}{d\omega} = \frac{d\theta}{2\pi \cdot d(f)} \tag{2.5}$$

(xv) Free Spectral Range

The free spectral range (FSR) of an optical filter is the separation between two adjacent resonant peaks with the frequencies f_i and f_{i+1}:

$$FSR = f_i - f_{i+1} \tag{2.6}$$

For a ring resonator the free spectral range is

$$FSR = \frac{c}{L_{eff}} = \frac{c}{2\pi r n_e} \tag{2.7}$$

where L_{eff} is the effective length of the resonator ring, c is the speed of light, n_e is the refractive index of the resonator ring, and r is the radius of the resonator ring.

2.6 Assumptions and Considerations

The following is a list of assumptions used in our research:

(1) The optical material used for designing our tuneable add-drop filters is hybrimer, a polymer proposed by Kang at al. [135]. The thermo-optical coefficient is -2.0×10^{-4} K^{-1}, the thermal expansion coefficient is 10^{-6} K^{-1} and the refractive index at room temperature ($24.6°C$) is 1.47875, since these are reported values.

(2) In our filter analysis, we disregard manufacturing variation and therefore the coupling coefficients and the coupler loss coefficients between the ring-resonator and the two waveguides have the same values. This is because the manufacturing variations are highly dependent on specific manufacturing process and technique.

(3) Our tuneable optical filters are linear time-invariant, namely systems that behave linearly with respect to their input and have all their parameters stationary in time. This is because the tuneable add-drop filters behave like static filters while operating in optical transmission systems.

(4) The loss coefficient in the waveguides is ignored. This is because it has been established by Schwelb [115] that the loss coefficient does not have a significant influence on the performance of ring-resonator-based filters.

(5) Only the magnitude and phase functions for the *in-drop* and *in-out* is considered in the performance analysis of our add-drop filter. This is because the transfer functions for the *in-drop* and *add-out* shall prove to be identical.

(6) The magnitude transfer function of the phase array devices is quasi-rectangular, as per design proposed by Dragone [136] and the phase transfer function is ideal. This is because we do not design the phase array devices and are interested in the ring-resonator based tuneable add-drop filter.

(7) In our tuneable add-drop filters, only half of each resonator-ring is heated to vary the central wavelength of the filter in an attempt to avoid unnecessary performance degradation. This is because the optical couplers are sensitive to temperature changes.

(8) All optical cross connects employed in the mesh simulation scenario are ideal. This is because particular optical cross connects designs will not be considered in our performance analysis.

Chapter 3

Tuneable Add-Drop Filter Design

The tuning mechanism of our add-drop filters is temperature variation of the resonator rings. This will allow for selectively dropping and/or adding optical channels from/to the all optical network/transmission system, as described in Section 2.3.

Since the add-drop filters perform the very function of dropping and/or adding optical channels, it is reasonable to ascertain that they are the most important elements of our tuneable OADM.

In this chapter, we shall present a mathematical model of our single-ring resonator based add-drop filters. Next, we shall design a prototype of the tuneable add-drop filter, determine and analyse its transfer functions and performance characteristics.

3.1 Mathematical Model of the Tuneable Add-Drop Filters

As per our assumptions presented in Section 2.6 our tuneable add-drop filters can be considered linear time-invariant systems, namely a systems that behave linearly with respect to their input and have all their parameters stationary in time. Their performance characteristics are fully described by, and can be obtained from, their magnitude intensity, simply magnitude throughout this research work, and their phase transfer functions [108]. The most important characteristics of our tuneable add-drop filters, such as resonance frequency, free spectral range, bandwidth, adjacent and non-adjacent cross-talk, insertion loss, finesse, quality factor and group-velocity delay, are defined in Section 2.5.

The developed mathematical model is based on the coupled mode theory [121] and its

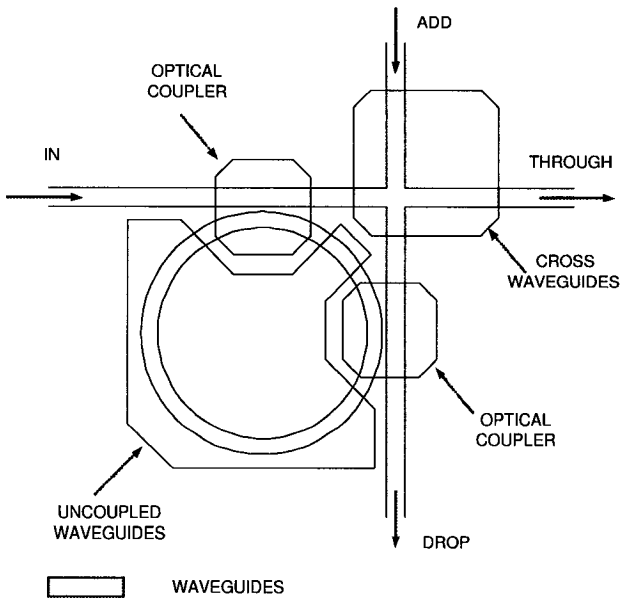

Figure 3.1: Decomposition of our Add-Drop Filter

matrix formalism [113]. The magnitude and phase transfer functions of our single-ring resonator based optical add-drop filter were obtained from its transfer and scattering transfer matrices. The transfer matrix representation defines the relation between the electromagnetic waves at the input ports and the waves at the exit ports, while the transfer scattering matrix representation represents the liner relation between the incident waves entering the filter and reflected waves exiting the filter.

In order to efficiently derive the transfer and scattering transfer matrices we decomposed our single ring resonator based add-drop filter into basic components such as optical couplers, uncoupled pair of waveguides, and pair of crossed waveguides. We modeled the basic components as appropriate types of generalized lumped-element 2×2 couplers introduced by Schwelb [115].

3.1.1 Model Decomposition and Representation

By looking carefully at our ring resonator based add-drop filter, depicted in Figure 3.1, we can identify its basic components. The filter is composed of two optical couplers, two uncoupled pair of dielectric waveguides, and a pair of crossed dielectric waveguides.

In the Figure 3.2 we illustrate the schematic representation of optical couplers, un-

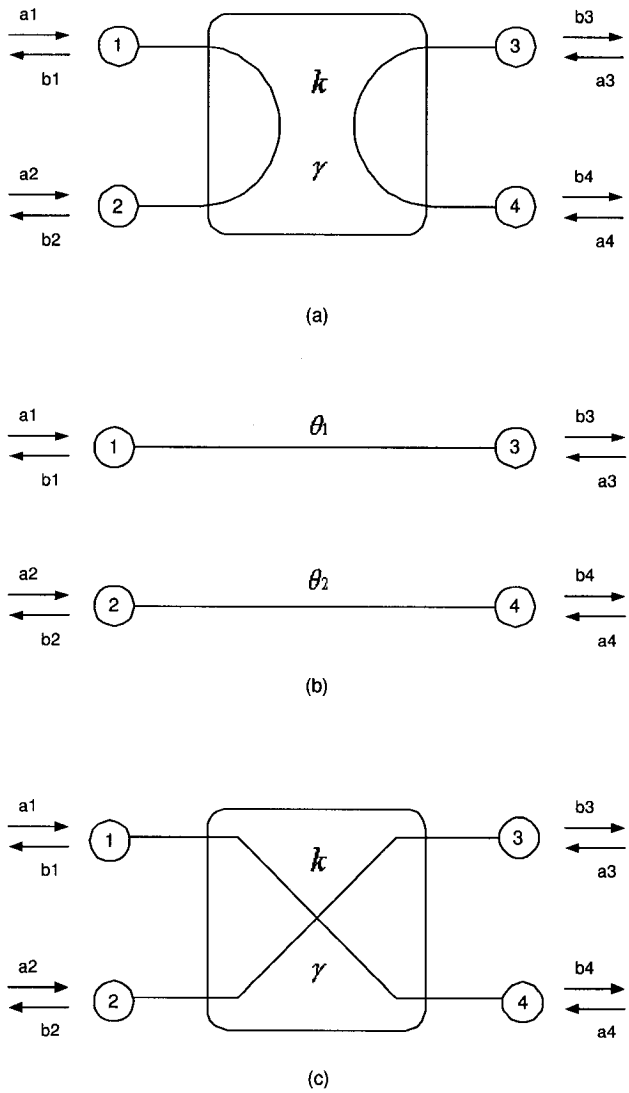

Figure 3.2: Single ring-resonator-based optical filter: (a) equivalent representation of an optical coupler, (b) equivalent representation of a resonator ring, (c) equivalent representation of a pair of crossed waveguides

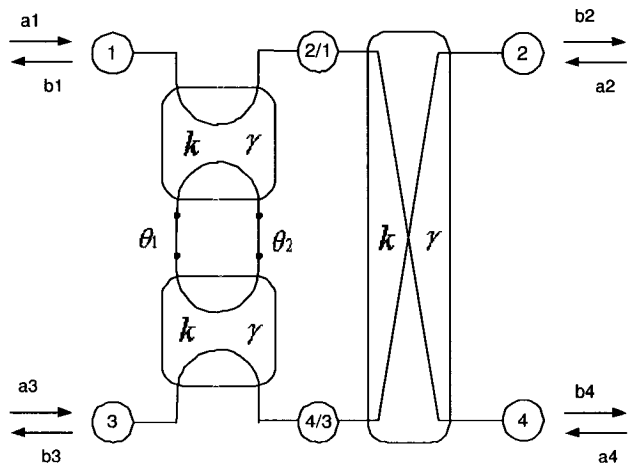

Figure 3.3: Equivalent Lattice Network of our Add-Drop Filter

coupled pair of transmission lines, and crossed waveguides, where a_i is the incident wave at port i, b_i is the reflected wave at port i, θ_i is the phase delay of the electromagnetic wave traveling through the transmission line i, k is power coupling coefficient, and γ is the scattering loss coefficient in the optical coupler.

The equivalent lattice network of our add-drop filter, depicted in Figure 3.3, is comprised of schematic representations of its basic components cascaded in series and parallel. To conveniently derive the transfer matrices of our add-drop filter we split the obtained equivalent lattice network in two parts the add-drop filter without crossed waveguides and the crossed waveguides.

3.1.2 Mode Number and Ring Radius

According to Suzuki et. al. [128], the mode number m_{ring} of a ring-resonator-based optical filter is

$$m_{ring} = \frac{L_{eff}}{\lambda_0} \tag{3.1}$$

and the effective length L_{eff} of the resonator ring is

$$L_{eff} = \frac{c}{FSR_{Hz}} \tag{3.2}$$

where λ_0 is the central wavelength of the filter, c is the speed of light in vacuum, and FSR_{Hz} is the free spectral range of the filter.

By substituting L_{eff} into Equation (3.1) we obtain a more convenient equation for the mode number m_{ring} of a ring-resonator-based optical filter

$$m_{ring} = \frac{c}{\lambda_0 \cdot FSR_{Hz}} \tag{3.3}$$

.

By the same account, the effective length L_{eff} of the resonator ring is

$$L_{eff} = L \cdot n_e \tag{3.4}$$

and

$$L_{eff} = \lambda_0 \cdot m_{ring} \tag{3.5}$$

where L is the physical length of the resonator ring, n_e is the refractive index of the optical material, λ_0 is the central wavelength of the filter, and m_{ring} is the mode number of the ring.

The ring radius r of the resonator ring is simply

$$r = \frac{L}{2\pi} \tag{3.6}$$

and by substituting L from Equation (3.4) and L_{eff} from Equation (3.5), into Equation (3.6) we obtain a more convenient equation of the radius r of the resonator ring

$$r = \frac{L_{eff}}{2\pi \cdot n_e} = \frac{\lambda_0 \cdot m_{ring}}{2\pi \cdot n_e} \tag{3.7}$$

.

3.1.3 The Transfer Matrices

The transfer matrix of the optical coupler $A_{coupler}$ is

$$A_{coupler} = \frac{j}{\sqrt{k}} \begin{pmatrix} 0 & \sqrt{1-k} & -\frac{1}{a} & 0 \\ -\sqrt{1-k} & 0 & 0 & a \\ -\frac{1}{a} & 0 & 0 & \sqrt{1-k} \\ 0 & a & -\sqrt{1-k} & 0 \end{pmatrix} \tag{3.8}$$

as shown by Schwelb [115], where

- k is the power coupling coefficient,
- γ is the loss coefficient in the optical coupler,
- a is the field magnitude loss, and is defined as the loss of magnitude of the electromagnetic field traveling through the optical coupler, $a = \sqrt{1-\gamma}$.

Likewise the transfer matrix of the uncoupled pair of waveguides A_{lines} is

$$A_{lines} = \begin{pmatrix} e^{j\theta_1} & 0 & 0 & 0 \\ 0 & e^{-j\theta_1} & 0 & 0 \\ 0 & 0 & e^{j\theta_2} & 0 \\ 0 & 0 & 0 & e^{-j\theta_2} \end{pmatrix} \tag{3.9}$$

where, $j = \sqrt{-1}$ and θ_i is the phase delay of the electromagnetic field traveling through the transmission line i, or the half round trip phase delay of the resonator ring, and can be expressed as it follows

$$\theta_i = (\beta_i - j\alpha_i)\pi r n_e \tag{3.10}$$

where β_i is the propagation coefficient of the transmission line, α_i is the loss coefficient of the transmission line, r is the radius of the resonator ring, and n_e is the refractive index of the resonator ring.

Since we take into account the small optical power exchange between the two waveguides, we shall model the pair of crossed waveguides as a type-2 generalized lumped-element 2×2 coupler with small coupling and coupler loss coefficients. Therefore, its transfer matrix A_{XW} is

$$A_{XW} = \begin{pmatrix} \frac{j\sqrt{k}}{a} & 0 & -\frac{\sqrt{1-k}}{a} & 0 \\ 0 & ja\sqrt{k} & 0 & a\sqrt{1-k} \\ -\frac{\sqrt{1-k}}{a} & 0 & \frac{j\sqrt{k}}{a} & 0 \\ 0 & a\sqrt{1-k} & 0 & ja\sqrt{k} \end{pmatrix} \tag{3.11}$$

where a, j, and k have the same significance as described earlier in this section.

According to the classical theory of cascaded transmission networks [137], the transfer matrix of our add-drop filter without crossed waveguides can be determined from the transfer matrix of its constituent components as follows

$$A_{ADF} = A_{coupler} \times A_{lines} \times A_{coupler} \tag{3.12}$$

and by substituting Equations (3.8), (3.9), and (3.11) into Equation (3.12) we obtain the transfer matrix of the add-drop filter without the crossed waveguides A_{ADF}.

Once A_{ADF} is obtained, the relation between the electromagnetic waves at the input ports and the waves at the exit ports of our add-drop filter without crossed waveguides can be expressed as follows

$$\begin{bmatrix} a_1 \\ b_1 \\ a_2 \\ b_2 \end{bmatrix} = A_{ADF} \begin{bmatrix} b_3 \\ a_3 \\ b_4 \\ a_4 \end{bmatrix} \tag{3.13}$$

where a_i and b_i, $i = 1, 2, 3, 4$, are the incident electromagnetic waves a_i and the reflected electromagnetic waves b_i at port i.

Likewise, given the transfer matrix A_{XW}, the relation between the electromagnetic waves at the input ports and the waves at the exit ports for the pair of crossed waveguides

is

$$\begin{bmatrix} a_1 \\ b_1 \\ a_2 \\ b_2 \end{bmatrix} = A_{XW} \begin{bmatrix} b_3 \\ a_3 \\ b_4 \\ a_4 \end{bmatrix} \tag{3.14}$$

By algebraically manipulating Equation (3.13) and Equation (3.14) such that

$$\begin{bmatrix} a_1 \\ b_1 \\ a_3 \\ b_3 \end{bmatrix} = A^{\diamond}_{ADF} \begin{bmatrix} b_2 \\ a_2 \\ b_4 \\ a_4 \end{bmatrix} \tag{3.15}$$

and

$$\begin{bmatrix} a_1 \\ b_1 \\ a_3 \\ b_3 \end{bmatrix} = A^{\diamond}_{XW} \begin{bmatrix} b_2 \\ a_2 \\ b_4 \\ a_4 \end{bmatrix} \tag{3.16}$$

we obtain the transformed transfer functions for the add-drop filter without crossed waveguides $A^{\diamond}_{ADF}$ and the transformed transfer matrix for the crossed waveguides $A^{\diamond}_{XW}$, respectively. The transformation is necessary due to the fact that the input signals are entering the constituent transmission networks through ports 1 and 3 and exit through ports 2 and 4 as opposed to entering through ports 1 and 2 and exiting through ports 3 and 4, as considered by Schwelb [115]. Therefore, according to the classical theory of cascaded transmission networks, the transfer matrix of the equivalent lattice network for our add-drop filter in Figure 3.3 is

$$A_{ADFX} = A^{\diamond}_{XW} \times A^{\diamond}_{ADF} \tag{3.17}$$

and by substituting the two results results into Equation (3.17) we obtain the transfer

matrix for our single-ring tuneable add-drop filter with crossed waveguides, A_{ADFX}.

Now we can express the relation between the electromagnetic waves at the input ports and the waves at the exit ports of our equivalent lattice network

$$\begin{bmatrix} a_1 \\ b_1 \\ a_2 \\ b_2 \end{bmatrix} = A_{ADFX} \begin{bmatrix} b_3 \\ a_3 \\ b_4 \\ a_4 \end{bmatrix} \tag{3.18}$$

along with the liner relation between the incident waves entering our equivalent lattice network and the waves reflected through the ports of our equivalent lattice network

$$\begin{bmatrix} b_1 \\ b_2 \\ b_3 \\ b_4 \end{bmatrix} = S_{ADFX} \begin{bmatrix} a_1 \\ a_2 \\ a_3 \\ a_4 \end{bmatrix} \tag{3.19}$$

where a_i and b_i, $i = 1, 2, 3, 4$, are respectively the incident and the reflected electromagnetic waves at port i.

Comparing Equation (3.19) with (3.18) one can see that the transfer scattering matrix S_{ADFX} is directly related to the transfer matrix A_{ADFX}. The transfer scattering matrix can be readily derived as outlined in [115].

$$S_{ADFX} = \begin{pmatrix} T_c T_A^{-1} & T_D - T_c T_A^{-1} T_B \\ T_C^{-1} & -T_D^{-1} T_A \end{pmatrix} \tag{3.20}$$

where T_A, T_B, T_C and T_D are 2×2 submatrices of T such that

$$T = \begin{pmatrix} T_A & T_B \\ T_C & T_D \end{pmatrix} = \Pi_{23} A_{ADFX} \Pi_{23} \tag{3.21}$$

and

$$\Pi_{23} = \begin{pmatrix} 1 & 0 & 0 & 0 \\ 0 & 0 & 1 & 0 \\ 0 & 1 & 0 & 0 \\ 0 & 0 & 0 & 1 \end{pmatrix} \tag{3.22}$$

We have therefore derived the transfer matrix A_{ADFX} and the transfer scattering matrix S_{ADFX} of our single-ring resonator based add-drop filter.

3.1.4 The Magnitude Response

The magnitude response between port i and port j of a linear system is the ratio between the magnitude I_j of the signal emerging from port j and the magnitude I_i of the signal entering the system through port i, $I_{ij} = I_j/I_i$.

To determine the magnitude transfer function between port 1 and ports $1, 2, 3, 4$ we excite the equivalent lattice network through port 1 with a unity incident wave. This is done by setting the incident waves $a_1 = 1$, $a_2 = 0$, $a_3 = 0$, $a_4 = 0$. The relation between the electromagnetic waves at the input ports and the waves at the exit ports of the equivalent lattice network becomes

$$\begin{bmatrix} 1 \\ b_1 \\ 0 \\ b_2 \end{bmatrix} = A_{ADFX} \begin{bmatrix} b_3 \\ 0 \\ b_4 \\ 0 \end{bmatrix} \tag{3.23}$$

and through algebraic manipulations of Equation (3.23) we obtain the system of linear equations (3.24)

$$\begin{bmatrix} 1 \\ 0 \\ 0 \\ 0 \end{bmatrix} = \begin{pmatrix} 0 & 0 & A_{ADFX}(1,1) & A_{ADFX}(1,3) \\ -1 & 0 & A_{ADFX}(2,1) & A_{ADFX}(2,3) \\ 0 & 0 & A_{ADFX}(3,1) & A_{ADFX}(3,3) \\ 0 & -1 & A_{ADFX}(4,1) & A_{ADFX}(4,3) \end{pmatrix} \begin{bmatrix} b_1 \\ b_2 \\ b_3 \\ b_4 \end{bmatrix} \tag{3.24}$$

where $A_{ADFX}(i,j)$ are elements (i,j) of matrix A_{ADFX}.

By solving the system of linear equations for b_j, $j = 1, 2, 3, 4$ we determine the magnitude of the reflected waves b_j of our equivalent lattice network.

The magnitude transfer function $I_{1j}(\lambda)$ between port $i = 1$ and port $j = 1, 2, 3, 4$ is

$$I_{1j}(\lambda) = \left|\frac{b_j}{a_1}\right|^2 \quad (\forall)j \in \{1, 2, 3, 4\}. \tag{3.25}$$

where λ is the wavelength of the optical signal.

Using a similar approach, we can derive the magnitude transfer functions between any input port i and output ports $j = 1, 2, 3, 4$ by exciting the equivalent lattice matrix through port i with a signal of unity intensity, i.e.

$$I_{ij}(\lambda) = \left|\frac{b_j}{a_i}\right|^2 \quad (\forall)j \in \{1, 2, 3, 4\} \tag{3.26}$$

3.1.5 The Phase Response

The phase response between port i and port j of a linear system is the difference between the phase Φ_j of the signal emerging from port j and the phase Φ_i of the signal entering the system through port i, $\Phi_{ij} = \Phi_j - \Phi_I$.

To determine the phase transfer function between port 1 and ports $1, 2, 3, 4$ we excite the equivalent lattice network through port 1 with a unity incident wave. This is done by setting the incident waves $a_1 = 1$, $a_2 = 0$, $a_3 = 0$, $a_4 = 0$. Then we compute the transfer scattering matrix as outlined in Section 3.1.3.

The phase transfer function $\Phi_{1j}(\lambda)$ between port $i = 1$ and port $j = 1, 2, 3, 4$ is

$$\Phi_{1j(\lambda)} = Im\{S_{ADFX}(i, j)\} \quad (\forall)i, j \in \{1, 2, 3, 4\}. \tag{3.27}$$

.

Using a similar approach, we can derive the phase transfer functions between any input port i and output ports $j = 1, 2, 3, 4$ by exciting the equivalent lattice matrix through port i with a signal of unity intensity

$$\Phi_{ij}(\lambda) = Im\{S_{ADFX}(i, j)\} \quad (\forall)i, j \in \{1, 2, 3, 4\}. \tag{3.28}$$

3.1.6 The Dynamic Range

At t_0, the central frequency λ_0 of the filter in Figure 3.1 is given by

$$\lambda_0 = \frac{2\pi r\ n_e}{m_{ring}} \tag{3.29}$$

.

By inspection, we see that there are three parameters influencing the central wavelength of the filter: the radius of the ring r; the refractive index of the ring waveguide n_e; and the mode number of the ring m_{ring}. Since the mode number is a fixed parameter of the filter, there are only two parameters we can vary in our attempt to tune the central frequency of the filter. The two parameters are the radius of the ring and the refractive index of the resonator ring waveguide.

Let r_t be the ring radius at temperature t, k_t the thermal expansion coefficient of the material, r_{t0} the ring radius at temperature t_0, and Δt the difference of temperature t-t_0, it follows that

$$r_t = r_{t_0}(1 + k_t \Delta t) \tag{3.30}$$

.

Likewise, let dn/dt be the thermo-optic coefficient of the material, $n_{e|t}$ the refractive index of the material at temperature t, and $n_{e|t_0}$ the refractive index of the material at temperature t_0, then

$$n_{e|t} = n_{e|t_0} + \frac{dn_e}{dt}\Delta t \tag{3.31}$$

.

By substituting Equation (3.30) and Equation (3.31) into Equation (3.29) for t_1 we obtain λ_1

$$\lambda_1 = \frac{2\pi}{m_{ring}} r_{t0}(1 + k_t \Delta t)(n_{e|t0} + \frac{dn_e}{dt}\Delta t) \tag{3.32}$$

assuming the whole length of the ring being heated with $\Delta t\ ^oK$, between t_0 and t_1.

It follows that the dynamic range of the filter is

$$\Delta\lambda_0 = \mid \lambda_0 - \lambda_1 \mid = \frac{2\pi r_0 \Delta t}{m_{ring}}(k_t + \frac{dn_e}{dt} + k_t \frac{dn_e}{dt}\Delta t) \tag{3.33}$$

where λ_0 is the central wavelength of the filter at t_0 and λ_1 the central wavelength of the filter at t_1.

3.2 Filter Design Procedure

Using the assumptions of Section 2.6 and the mathematical model discussed earlier, we can formulate the following design procedure:

(1) select the initial design parameters of the prototype filter in accordance to the target architecture of our tuneable OADM presented in Section 2.2
(2) determine the mode number and the radius of the resonator ring using Equation (3.3) and Equation (3.7), respectively
(3) determine the operating temperatures of the tuneable filter using Equation (3.33)
(4) determine the magnitude and phase transfer functions of the filter using the mathematical model presented in Section 3.1.4 and Section 3.1.5
(5) determine the performance characteristics of the filter from its transfer functions as per definitions presented in Section 2.5
(6) repeat the above to fine tune the design

The mathematical model of the tuneable add-drop filter has been coded in Matlab for further use in the design and analysis of our tuneable add-drop filters. Additional Matlab code has been developed to compute the performance parameters of the add-drop filter from its magnitude and phase transfer functions, as defined in Section 2.5.

3.3 Prototype Filter Design

(1) Initial Design Parameters

For the design of our tuneable add-drop filter prototype we shall select an ideal coupler loss coefficient $a = 1$ and an arbitrary coupling coefficient $k = 0.07$.

In accordance to the architecture of the tuneable OADM presented in Section 2.2, the initial design parameters for our tuneable add-drop filter prototype are channel spacing $C_s = 0.8nm$, number of channels per group of channels $N_{cg} = 4$, number of group of channels $N_g = 8$, total number of channels $N_c = 32$. Likewise, in order to accommodate four channels and account for the *all-through* position, we selected the free spectral range of the tuneable add-drop filter $FSR_{Hz} = 700GHz$.

Since the material considered for the design is hybrimer, as per assumption (1) in Section 2.6, the thermo-optical coefficient is $-2.0 \times 10^{-4}\ K^{-1}$, the thermal expansion coefficient is $10^{-6}\ K^{-1}$ and the refractive index at room temperature ($24.6°C$) is 1.47875.

For reader's convenience, a summary of the initial set of design parameters is presented as follows

Table 3.1: The initial design parameters of the tuneable add-drop filter prototype.

Parameter	Value	Units	Description
k	0.07		coupling coefficient
a	1		coupler loss coefficient
λ_0	1533.57	nm	central wavelength
$\Delta\lambda_0$	4	nm	dynamic range
n_e	1.47875		refractive index at $24.6°C$
dn/dt	-2×10^{-4}	K^{-1}	thermo-optic coefficient
k_t	10^{-6}	K^{-1}	thermal expansion coefficient
C_s	0.8	nm	channel spacing
FSR_{Hz}	700	GHz	free spectral range

(2) The Mode Number and The Ring Radius

By substituting the central wavelength λ_0 and the free spectral range FSR_{Hz} into Equation (3.3) we obtained the mode number of the resonator ring, $m_{ring} = 272.66$. Since the mode number must be an integer we truncated the value to $m_{ring} = 272$.

Next, by substituting m_{ring} into Equation (3.7) we obtained the ring radius of our filter prototype $r = 44.895\mu m$.

(3) The Operating Temperatures

We obtained the temperature difference $\Delta t = 7.71^oC$ for moving the central wavelength of the prototype filter by $\Delta\lambda_0 = 0.8nm$ from Equation (3.33) under the assumption[1] that only half of the resonator-ring is heated.

The computed operating temperatures of our tuneable add-drop filter prototype are presented as follows

Table 3.2: The operating temperatures of the tuneable add-drop filter prototype.

Channel	Wavelength $[nm]$	Temperature $[^oC]$
1	1529.57	63.17
2	1530.37	55.45
3	1531.17	47.74
4	1531.97	40.02
all-through	1533.57	24.6

(4) The Magnitude and Phase Transfer Functions

We determined the *add*, *drop*, and *through* magnitude and phase transfer functions of our tuneable add-drop filter prototype. The results are presented in the following three pages in Figures 3.4, 3.6, 3.8, and 3.9, respectively.

The *add* and *drop* magnitude transfer functions are almost identical, as one can see in Figure 3.4. The difference between the two transfer functions are marginal, e.g. at the resonant peak the difference is under $0.2dB$ as one can see in Figure 3.5. Although the *add* and *drop* phase transfer functions are no identical as one can see in Figure 3.6, their influence on performance, namely the group-velocity delay (τ), is almost identical as one can see in Figure 3.7. It is therefore reasonable to use the *drop* transfer functions

[1]The reason for making this assumption has been explained at point (7) in Section 2.6.

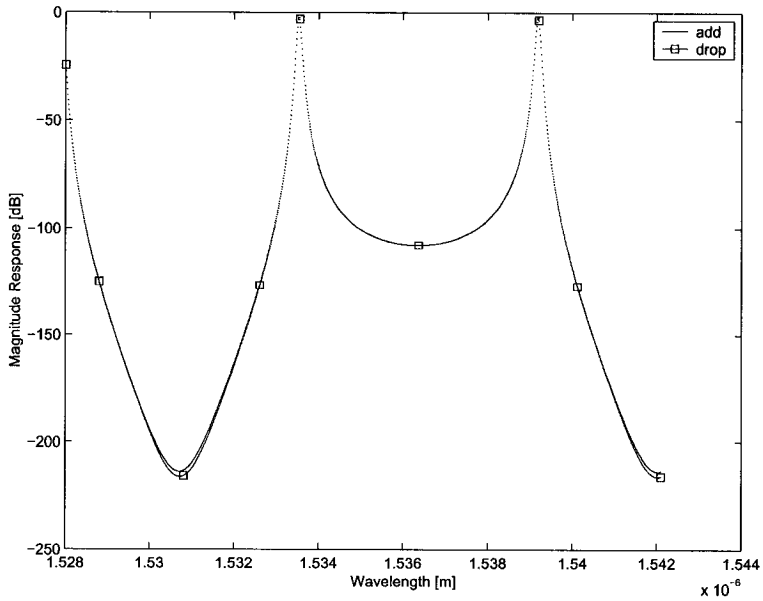

Figure 3.4: The *add* and *drop* magnitude response of our tuneable add-drop filter prototype.

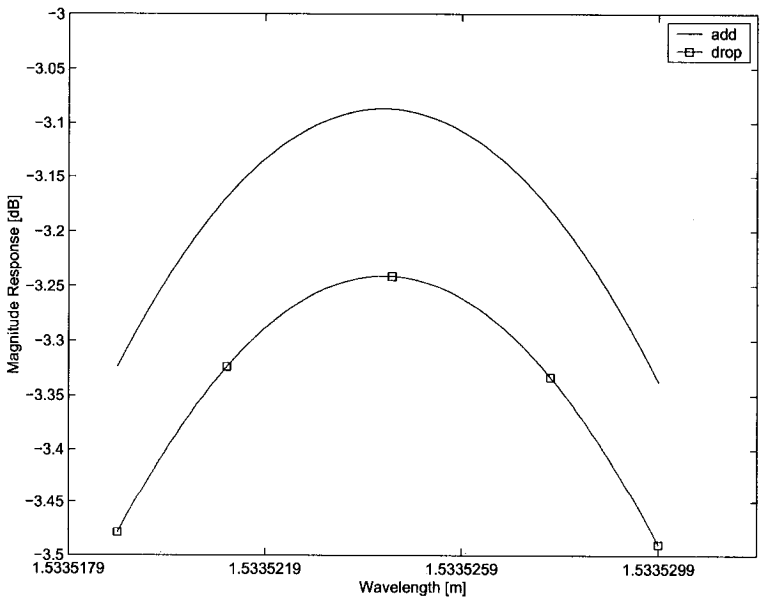

Figure 3.5: The *add* and *drop* magnitude response of our tuneable add-drop filter prototype, close up.

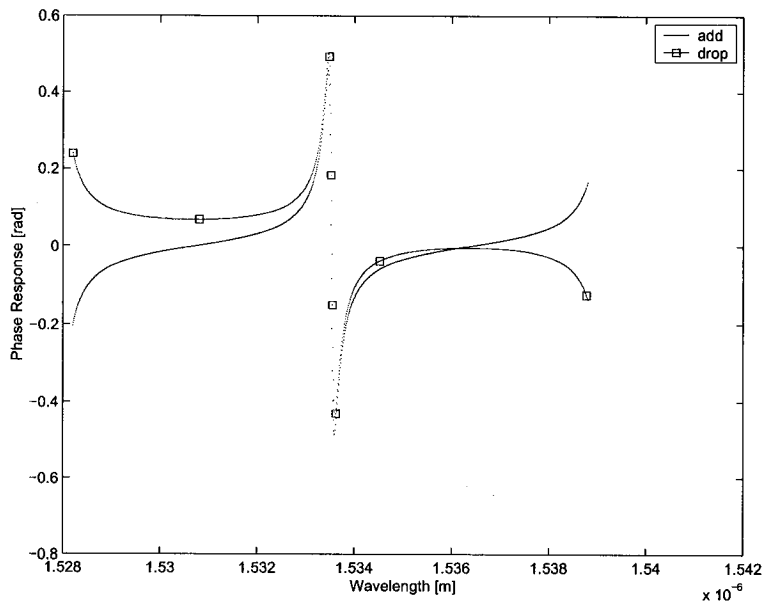

Figure 3.6: The *add* and *drop* phase response of our prototype filter

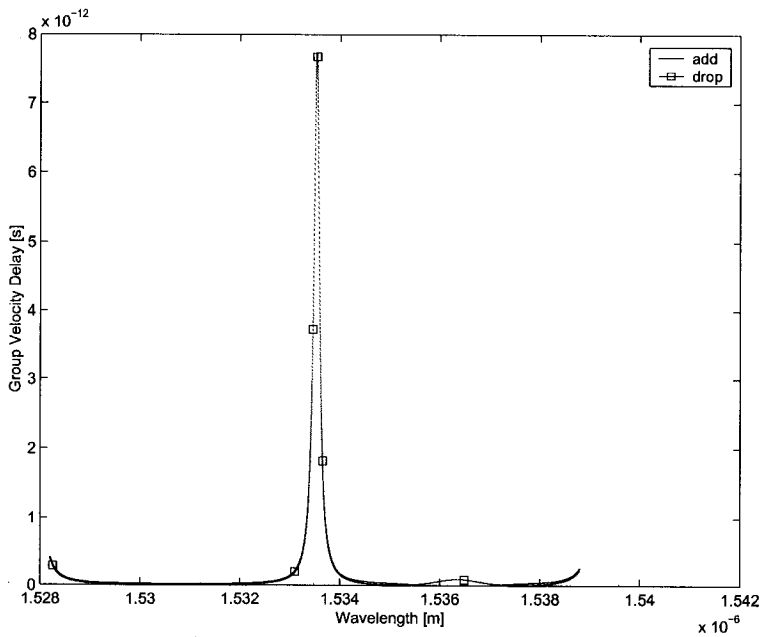

Figure 3.7: The *add* and *drop* differential group delay for our tuneable add-drop filter prototype.

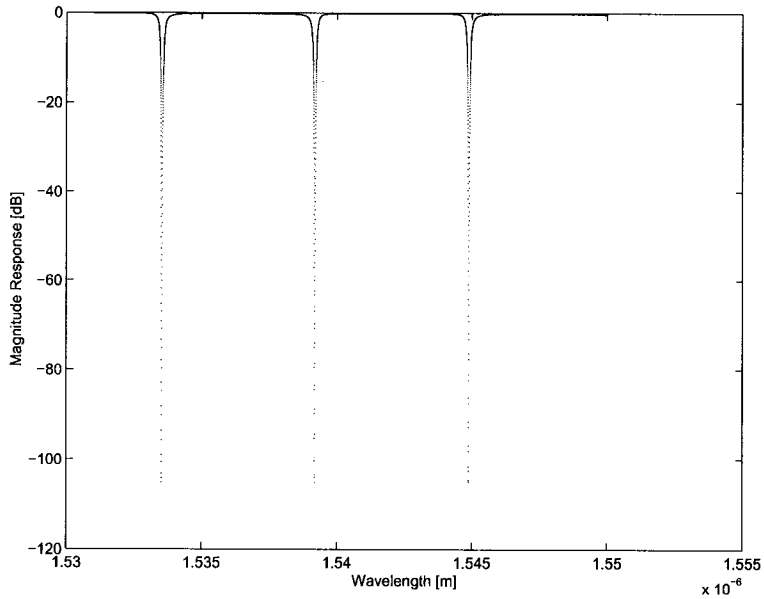

Figure 3.8: The *through* magnitude response of the tuneable add-drop filter prototype.

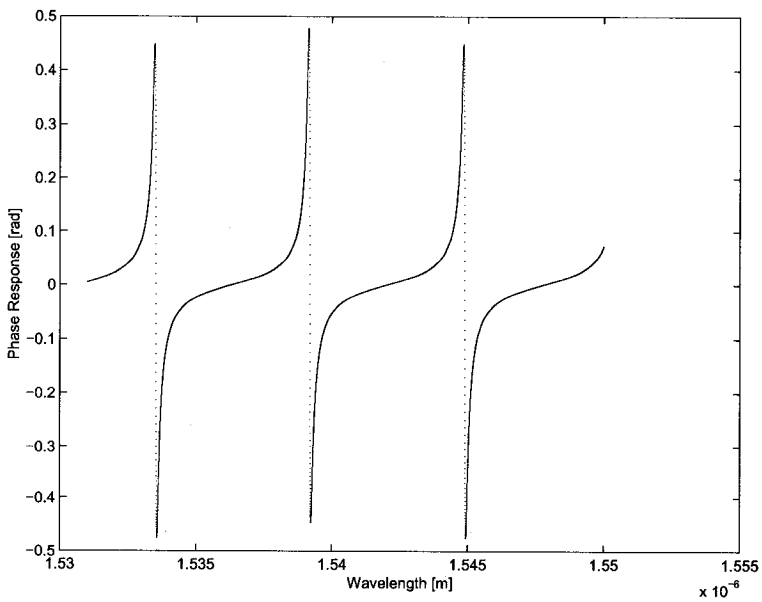

Figure 3.9: The *through* phase response of the tuneable add-drop filter prototype.

to determine both performance characteristics, called *add/drop* characteristics in the reminder of this work.

Our prototype filter exhibits a periodic *add/drop* and *through* magnitude and phase transfer functions. For example, equally spaced transmission peaks and maxima/minima of the phase values can be seen in Figure 3.4 and Figure 3.6, respectively. The shape of the magnitude transfer function within the free spectral range[2], indicates that the periodicity of our add-drop filter is twice its free spectral range. This features is inherent to our design due to the intersection between its *in-out* and *add-drop* waveguides. The intersection leads to a small exchange of optical power between the two waveguides and therefore introduces feedback path into the design. As a result, the transfer functions are asymmetrical in respect to the resonant peaks and the values of the adjacent and the non-adjacent cross talk are better on one side of the filter.

(5) The Performance Measures of the Prototype Filter

Using the additionally developed Matlab code, we computed the performance parameters of our prototype filter from its *add/drop* and *through* transfer functions determined at step (4).

The resulted performance measures are listed as follows

Table 3.3: The performance measures of the tuneable add-drop filter prototype.

Parameter	Value	Units	Description
$IL_{add/drop}$	0.16	dB	*add/drop* insertion loss
$IL_{throughadj}$	0.25	dB	*through* insertion loss for adjacent channel
$IL_{throughnon-adj}$	0.2	dB	*through* insertion loss for non-adjacent channel
$Xtalk_{adj}$	-132.89	dB	worst adjacent crosstalk
$Xtalk_{non-adj}$	-146.25	dB	worst non-adjacent crosstalk
BW_{FWHM}	0.037	nm	pass bandwidth at -3dB

[2]A definition of the free spectral range is provided in Section 2.5.

The obtained performance parameters indicate that the tuneable add-drop filter is feasible and may perform reasonably well in WDM transmission systems. However, as one can see in Table 3.3 the filter prototype exhibits a narrow pass bandwidth and a non-zero phase variation. The narrow pass bandwidth may prevent the optical signal to pass in the presence of laser chirp and/or central frequency variations, while the phase variation translates into group-velocity delays of the optical signal leading to signal dispersion in time and consequently to inter-symbol interference and high bit error rates [138]. It is therefore desirable to optimize the two transfer characteristics of our tuneable add-drop filter, namely its magnitude and phase transfer functions, if possible.

Chapter 4

Tuneable Add-Drop Filter Optimization

In this chapter, we shall optimize the design of our tuneable add-drop filter in an attempt to improve its performance, namely to minimize its insertion loss, decrease its adjacent cross talk, increase its *add/drop* pass bandwidth, and minimize its phase distortion. We shall identify the factors influencing the performance of our tuneable add-drop filter, analyse their influence, and determine their optimum values. Next, we shall design our optimized tuneable add-drop filter.

4.1 Influence of Filter Parameters on Performance

By inspecting the mathematical model of our tuneable add-drop filter, presented in Section 3.1, we can see from Equations (3.8) and (3.9) that the parameters influencing its performance are the loss coefficient of the waveguide (γ), the coupling coefficient (k), the coupler loss coefficient (a), and the effective length of the ring (L_{eff}). Since the effective length of the ring is directly influenced by the operating temperature, as detailed in Section 3.1.6, and the loss coefficient in waveguides does not have a significant influence on the performance, as established by Schwelb [115], we will focus our analysis on the variation of the operating temperature, the coupling coefficient, and the coupler loss coefficient.

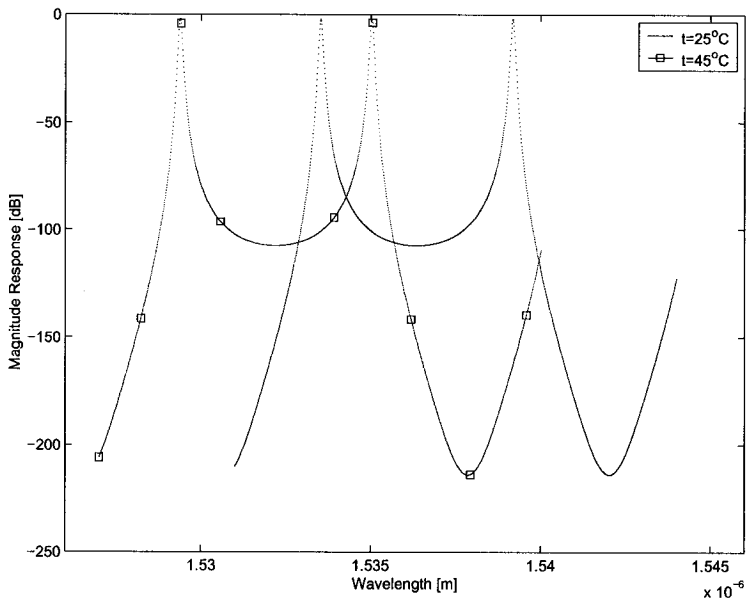

Figure 4.1: The influence of the temperature on the *add/drop* magnitude response.

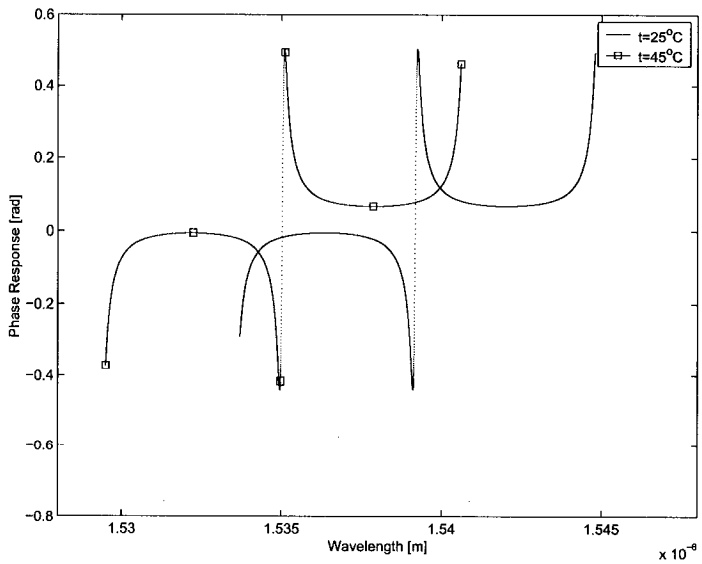

Figure 4.2: The influence of the temperature on the *add/drop* phase response.

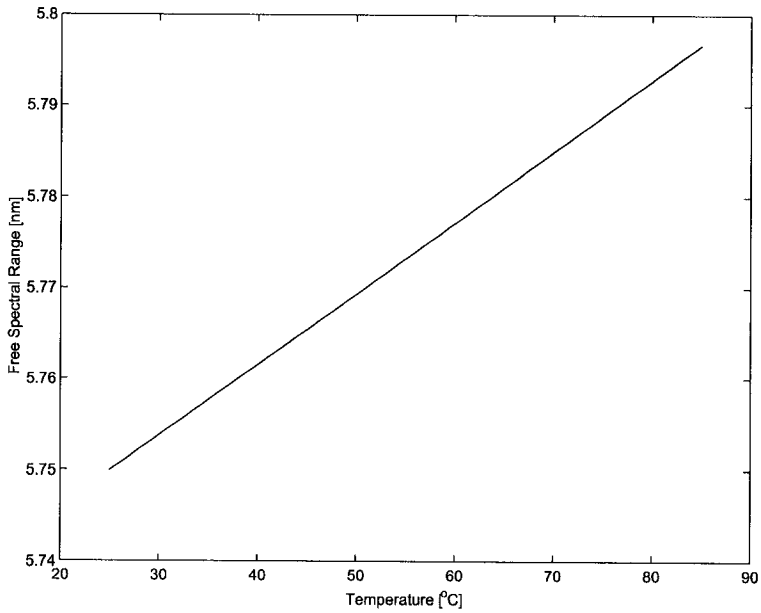

Figure 4.3: The influence of the temperature on the Free Spectral Range.

4.1.1 The Influence of Temperature

The effect of increasing the temperature of the resonator ring is a move of the central wavelength of the our add-drop filter towards shorter wavelengths, while a decrease does the opposite, as illustrated in Figure 4.1.

Along with the move of the central wavelength one can notice an increase of the free spectral range, as illustrated in Figure 4.3. Assuming the filter is designed for a free spectral range at least equal to the desired pass bandwidth at room temperature, it follows that an increase in temperature will further increase the free spectral range. Therefore, the free spectral range will be always larger or at least equal to the required pass bandwidth at any given operating temperature and the add-drop filter will operate properly.

However, in the case of building the add-drop filter from optical materials with positive thermo-optical coefficients the free spectral rage can become smaller than the required pass bandwidth of a channel, leading to more than one resonance peaks in the pass bandwidth, and disrupting the intended way of the filter operation.

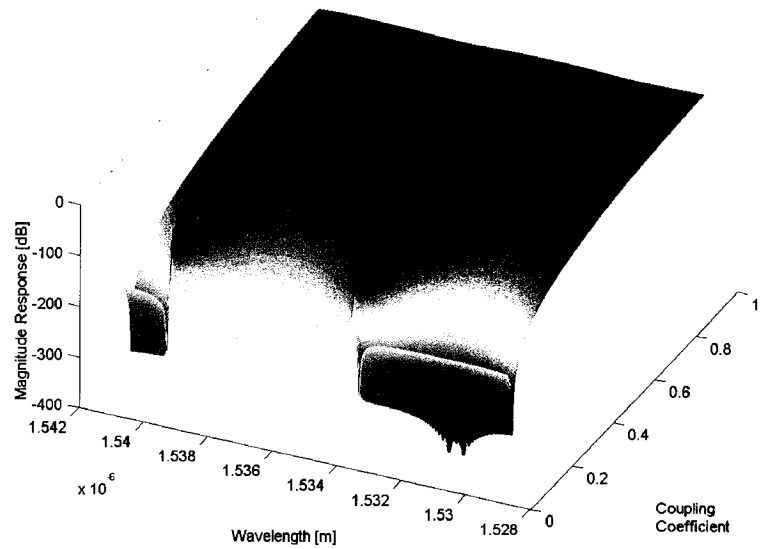

Figure 4.4: The influence of the Coupling Coefficient on the *add/drop* magnitude response.

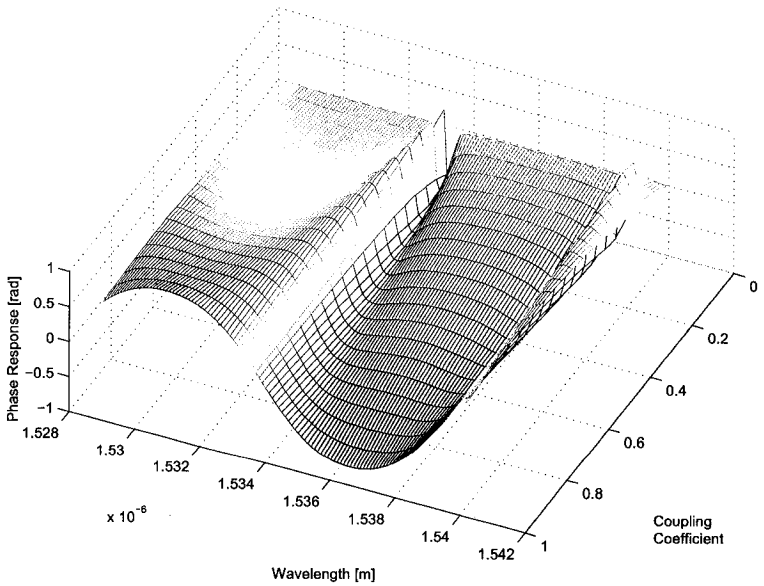

Figure 4.5: The influence of the Coupling Coefficient on the *add/drop* phase response.

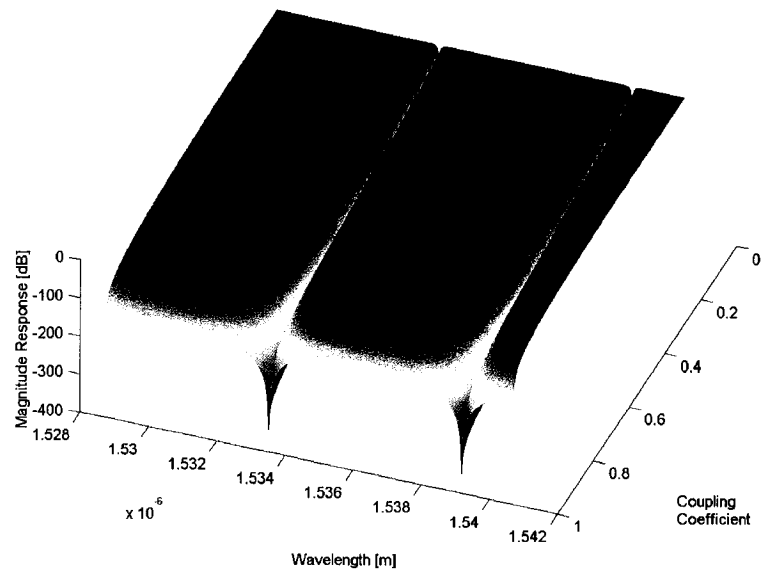

Figure 4.6: The influence of the Coupling Coefficient on the *through* magnitude response.

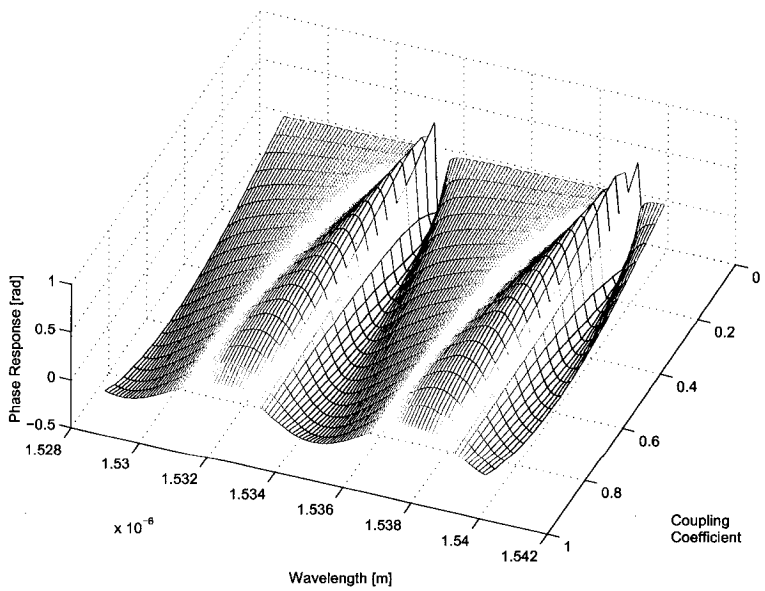

Figure 4.7: The influence of the Coupling Coefficient on the *through* phase response.

As one can see in Figure 4.2, an increase in the operating temperature of the resonator ring will sharply increase the phase distortion of the signal at the central wavelength of the filter. Further increases in temperature will sharply decrease the phase distortion followed by relative constant values and a sharp increase again. Decreasing the operating temperature of the resonator ring will have the opposite effect.

4.1.2 The Influence of the Coupling Coefficient

The influence of the coupling coefficient on the *add/drop* magnitude transfer function is illustrated in Figure 4.4[1], while its influence on the *through* magnitude is illustrated in Figure 4.6.

The *add/drop* magnitude transfer function at low coupling coefficient (e.g. 0.05) exhibits pass bandwidths of a few tenths of a nm (from 1533.51 nm to 1533.53 nm) and attenuations down to $-150dB$ at longer wavelengths (around 1536 nm) or down to $-300dB$ at shorter wavelengths (around 1532 nm). As the coupling coefficients increase towards unity the pass bandwidth of the filter increases towards infinity while the attenuation decreases towards $0dB$.

The *through* magnitude transfer function at large coupling coefficients (e.g 0.9) exhibits a pass bandwidth of a few nm (from 1533 nm to 1539 nm) with attenuation level around $20dB$ and a stop bandwidths around of a few tenths of nm (from 1533.5 nm to 1533.6 nm) with attenuation levels down to $-300dB$. As the coupling coefficients decrease towards zero the stop bandwidth decreases until eventually vanishes, the pass bandwidth increases towards infinity, and the attenuation levels approach $0dB$.

The influence of the coupling coefficient is presented in Figure 4.5 for the *add/drop* phase response and in Figure 4.7 for the *through* phase response.

For the *add/drop* phase response, it can be seen that the phase variation in respect to the wavelength is large in the pass bandwidth of the filter and almost inexistent elsewhere. As the coupling coefficients increase towards unity the phase variation decreases in the pass bandwidth and increases elsewhere.

For the *through* phase response, one can see that for small coupling coefficients the phase variation is large in the pass bandwidth of the filter and almost inexistent

[1]for better representation of features, the axis of coupling coefficient in Figure 4.4 are opposite to the axis of the subsequent figures

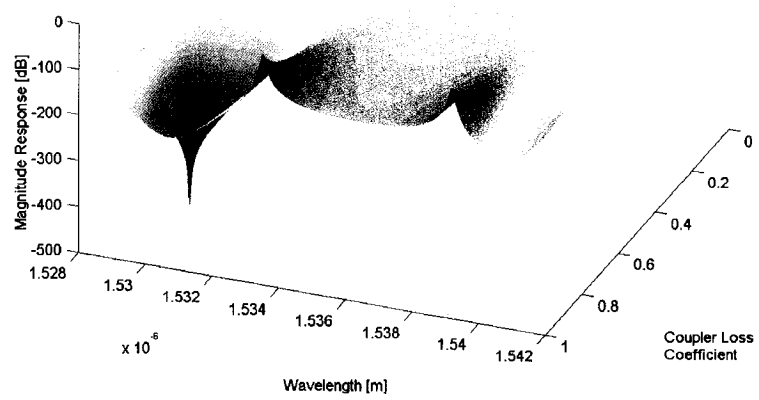

Figure 4.8: The influence of the Coupler Loss Coefficient on the *add/drop* magnitude response.

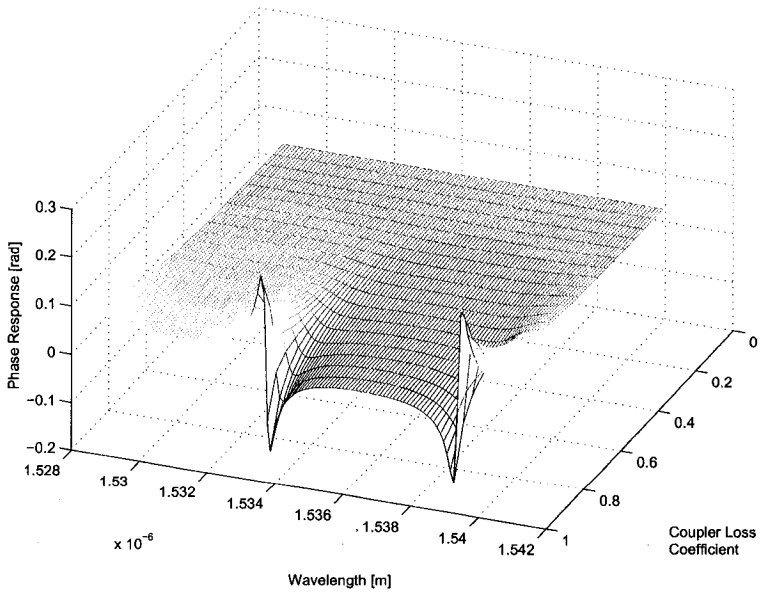

Figure 4.9: The influence of the Coupler Loss Coefficient on the *add/drop* phase response.

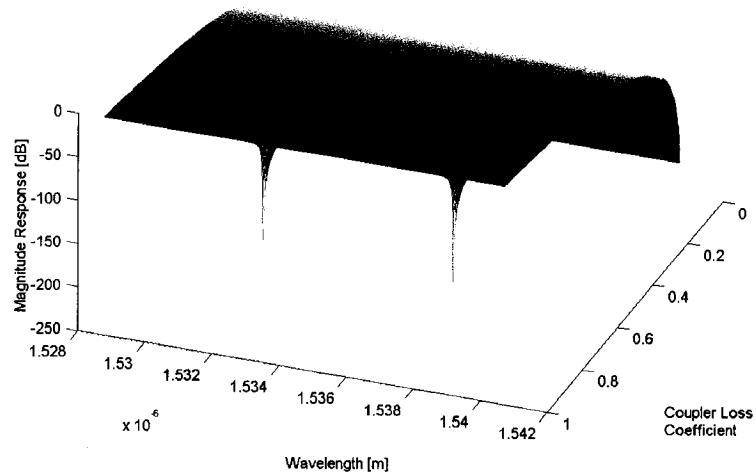

Figure 4.10: The influence of the Coupler Loss Coefficient on the *through* magnitude response.

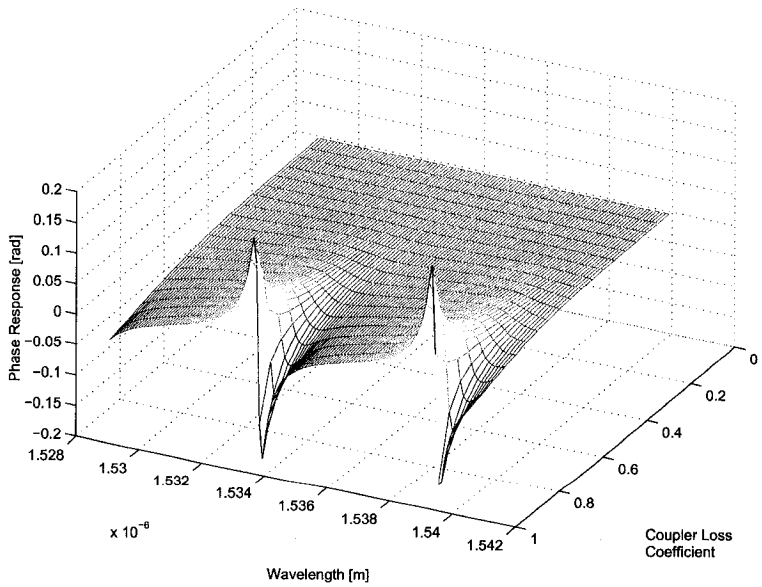

Figure 4.11: The influence of the Coupler Loss Coefficient on the *through* phase response.

elsewhere. As the coupling coefficients increase the phase variation decreases in the pass bandwidth and becomes present at all wavelengths.

4.1.3 The Influence of the Coupler Loss Coefficient

The influence of the coupler loss coefficient on the *add/drop* magnitude transfer function is illustrated in Figure 4.8, while its influence on the *through* magnitude transfer function is illustrated in Figure 4.10.

The *add/drop* magnitude transfer function exhibits at small coupler loss coefficients (e.g. 0.3) an infinite stop bandwidth with signal attenuations around $-150dB$ and no pass bandwidth. As the coupler loss coefficients increase towards unity, the attenuation levels approach $0dB$ (around 1533 nm and 1537 nm), remains $-150dB$ at longer wavelengths (around 1536 nm), and decreases to $-300dB$ at shorter wavelengths (around 1530 nm and 1532 nm). Likewise, the pass bandwidth is a few tenths of nm (from 1533.4 nm to 1533.6 nm) with attenuation levels of few dB.

The *through* magnitude transfer function exhibits at small coupler loss coefficients (e.g. 0.01) an infinite stop bandwidth with signal attenuations around $-250dB$. As the coupler loss coefficients increase towards unity, signal attenuations decrease down to $-250dB$ (around 1533 nm and 1539 nm) while the attenuation levels approach $0dB$ elsewhere. Likewise, the pass bandwidth is around a few tenths of nm (from 1533.5 nm to 1533.6 nm) with attenuation levels of few dB.

The influence of the coupler loss coefficient is presented in Figure 4.9 and Figure 4.11 for the *add/drop* and *through* phase transfer functions, respectively.

For both *add/drop* and *through* phase transfer functions one can see that there is no phase variation in respect to the wavelength at small coupler loss coefficients (e.g. 0.1). As the coupler loss coefficients increase towards unity the phase varies between 0.3 and -0.2 rad around the resonance wavelengths (approx. 1533 nm and 1539 nm) and marginally elsewhere.

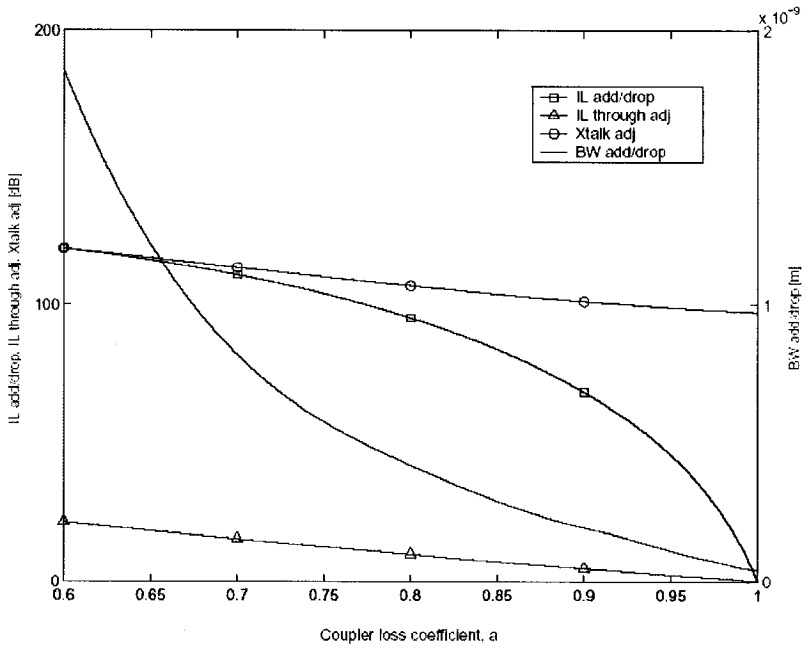

Figure 4.12: The influence of Coupler Loss Coefficient on the bandwidth, the adjacent crosstalk, and the *through* and *add/drop* insertion loss of the filter.

4.2 Coupler Loss Coefficient Optimization

The goal is to determine the value of the coupler loss coefficient that will minimize the *add/drop* insertion loss ($IL_{add/drop}$), the *through* adjacent insertion loss ($IL_{through-adj}$), and the adjacent cross talk ($Xtalk_{adj}$), while maximizing the *add/drop* pass bandwidth ($BW_{add/drop}$) at the same time.

Figure 4.12 illustrates the influence of the coupler loss coefficient on the *add/drop* insertion loss, the *through* insertion loss, the adjacent crosstalk, and the pass bandwidth of our filter. The presented parameters have been computed from the magnitude and phase transfer functions of add-drop filters with different coupler loss coefficients using the additional Matlab code developed in accordance with the definitions presented in Section 2.5, while the transfer functions have been computed using our Matlab implementation of the mathematical model presented in Section 3.1.

As one can see in Figure 4.12, the minima of the *add/drop* insertion loss ($IL_{add/drop}$), the *through* adjacent insertion loss ($IL_{through-adj}$), and the adjacent cross talk ($Xtalk_{adj}$) are exhibited at $a = 1$, while the maximum the *add/drop* pass bandwidth is exhibited

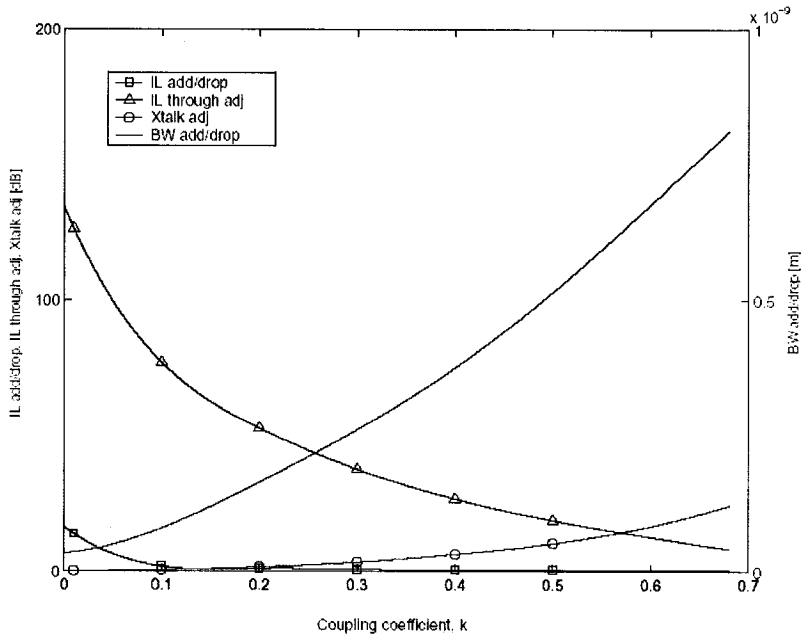

Figure 4.13: The influence of Coupling Coefficient on the bandwidth, the adjacent crosstalk, and the *through* and *add/drop* insertion loss of the filter.

at $a = 0$.

Since it is obvious that no possible values of the coupler loss coefficient will fully optimize our design, as per our optimization goal, it is reasonable to use for our filter design and its performance analysis a high achievable value $a = 0.998$ of the coupler loss coefficient. Similar values have been used by other people, e.g. Schwelb [115].

4.3 Coupling Coefficient Optimization

The goal is to determine the value of the coupling coefficient that will minimize the *add/drop* insertion loss ($IL_{add/drop}$), the *through* adjacent insertion loss ($IL_{through-adj}$), and the adjacent cross talk ($Xtalk_{adj}$), while maximizing the *add/drop* pass bandwidth ($BW_{add/drop}$) at the same time.

Figure 4.13 illustrates the influence of the coupler loss coefficient on the *add/drop* insertion loss, the *through* insertion loss, the adjacent crosstalk, and the pass bandwidth of our filter. The presented parameters have been computed form the magnitude and phase transfer functions of add-drop filters with different coupler loss coefficients using

the additional Matlab code developed in accordance with the definitions presented in Section 2.5, while the transfer functions have been computed using our Matlab implementation of the mathematical model presented in Section 3.1.

As one can see in Figure 4.13, the minimum *add/drop* insertion loss ($IL_{add/drop}$) is achieved at $k = 0$, while the minimum of the *through* adjacent insertion loss ($IL_{through-adj}$) and the minimum of the adjacent cross talk ($Xtalk_{adj}$) are exhibited at $k = 1$. Likewise, the maximum of the *add/drop* pass bandwidth is exhibited at $k = 0$. It is obvious that no possible values of the coupler loss coefficient will fully optimize our design. However, the optimum coupling coefficient for obtaining the minima for the *add/drop* and the *through* insertion loss is $k = 0.15$, while the optimum value of the coupling coefficient k that will maximize the *add/drop* pass bandwidth and minimize the adjacent cross talk is $k = 0.26$.

In general, larger *add/drop* pass bandwidths and smaller adjacent cross talk values are more desirable than smaller *add/drop* and *through* insertion losses. It is therefore reasonable to use for our filter design, $k = 0.26$, a coupler coefficient value which minimizes the $Xtalk_{adj}$ and the pass bandwidth $BW_{add/drop}$, while keeps the *add/drop* ($IL_{add/drop}$) and the *through* adjacent insertion loss ($IL_{through-adj}$) not far from their minima.

4.4 The Parameters of the Add-Drop Filter

Using the Matlab implementation of the mathematical model presented in Section 3.1, we computed the magnitude and transfer functions for all our tuneable add-drop filters with central wavelengths as presented in Section 2.4. Subsequently, we computed their performance parameters from its magnitude and phase transfer functions as defined in Section 2.5, using the additionally developed Matlab code.

In our computations, we used the coupling coefficient $k = 0.26$, the coupler loss coefficient $a = 0.998$, and all the design parameters presented in Table 3.1 with the exception of the coupling coefficient k and the coupler loss coefficient a. Since design parameters for the eight tuneable add-drop filters and their performance parameters are similar, we shall only present the parameters for filter ADF1.

Table 4.1: The initial set of design parameters for the tuneable add-drop filter ADF1.

Parameter	Value	Units	Description
k	0.26		coupling coefficient
a	0.998		coupler loss coefficient
λ_0	1533.57	nm	central wavelength
$\Delta\lambda_0$	4	nm	dynamic range
n_e	1.47875		refractive index at 24.6^oC
dn/dt	-2×10^{-4}	K^{-1}	thermo-optic coefficient
k_t	10^{-6}	K^{-1}	thermal expansion coefficient
C_s	0.8	nm	channel spacing
FSR_{Hz}	700	GHz	free spectral range
λ_{ch1}	1529.57	nm	central frequency of channel 1
λ_{ch2}	1530.37	nm	central frequency of channel 2
λ_{ch3}	1531.17	nm	central frequency of channel 3
λ_{ch4}	1531.97	nm	central frequency of channel 4
$\lambda_{all-through}$	1533.57	nm	central frequency in all-through position

Table 4.2: The computed performance measures of the tuneable add-drop filter ADF1.

Parameter	Value	Units	Description
BW_{FWHM}	0.221	nm	*add/drop* pass bandwidth
$IL_{add/drop}$	0.77	dB	*add/drop* insertion loss
$IL_{throughadj}$	2.7	dB	*through* adjacent insertion loss
$IL_{throughnon-adj}$	1.15	dB	*through* non-adjacent insertion loss
$Xtalk_{adj}$	-43	dB	worst adjacent crosstalk
$Xtalk_{non-adj}$	-62.2	dB	worst non-adjacent crosstalk
t_{ch1}	63.15	^oC	temperature for channel 1 add/drop
t_{ch2}	55.44	^oC	temperature for channel 2 add/drop
t_{ch3}	47.73	^oC	temperature for channel 3 add/drop
t_{ch4}	40.02	^oC	temperature for channel 4 add/drop
$t_{all-through}$	24.6	^oC	temperature for all channels through

Chapter 5

Performance Characteristics of the Tuneable OADM

In this chapter, we shall analyse the performance of our sparse tuneable OADM by determining its performance parameters such as insertion loss, channel pass bandwidth, adjacent cross talk, non-adjacent cross talk, and group delay. We shall present the mathematical model developed to determine the magnitude and phase transfer functions of our tuneable OADM from the transfer functions of its constituent components. Next, we shall determine its magnitude and phase transfer functions and present its performance parameters.

The mathematical model shall reflect the fact that our sparse tuneable OADM is comprised of two eight-channel phased-array planar devices interconnected through eight tuneable ring resonator-based filters in a so-called transmission lattice, as illustrated in Figure 2.2, and described in Sections 2.2 and 2.3.

5.1 Mathematical Model

The phase array devices, namely the optical multiplexer and optical demultiplexer, are time-invariant systems that behave linearly with respect to their input and have all their parameters stationary in time. Likewise, our sparse tuneable OADM is a time invariant system as per considerations in Section 2.6.

The classical theory of spectral analysis of signals [137, 139] has demonstrated that the response of linear time-invariant systems can be expressed in Z-domain as the equivalent transfer function obtained through multiplication of the transfer functions of its constituent components, while the equivalent phase shift is the sum of the phase shifts

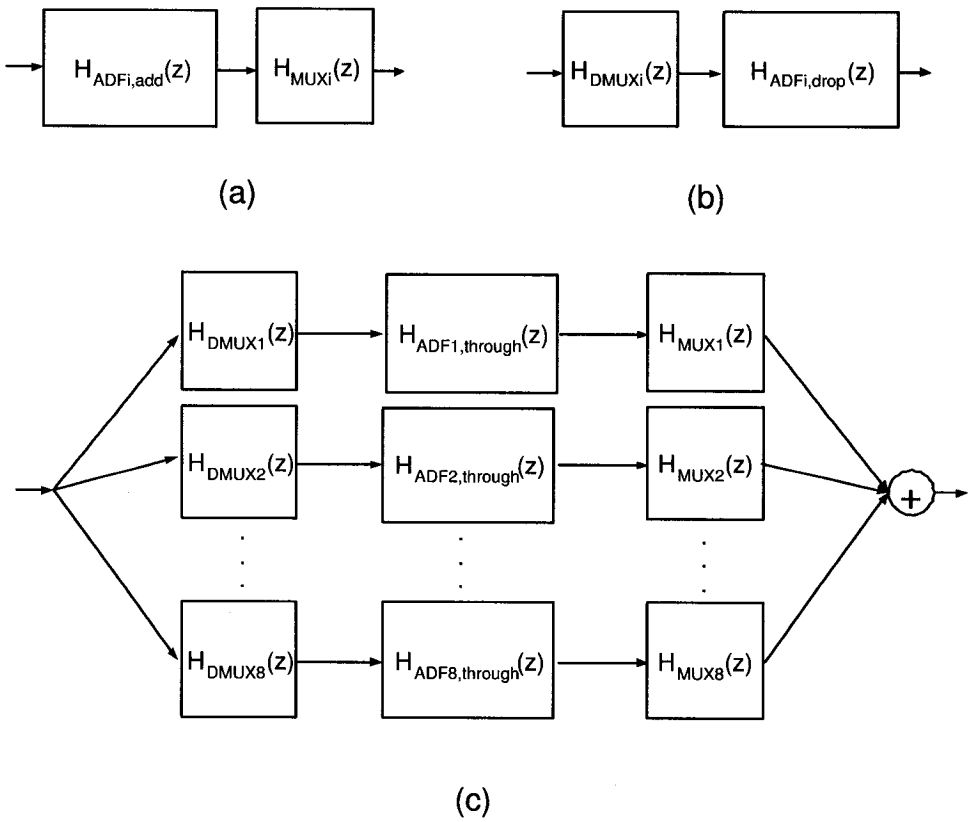

Figure 5.1: The equivalent representation of our tuneable OADM for the *add* (a), the *drop* (b) , and the *through* (c).

of its constituent components.

In accordance with its architecture, we can therefore represent our sparse tuneable OADM as a transmission lattice, illustrated in Figure 5.1 (a), (b), and (c) for *add*, *drop* and *through*, respectively.

The *add* and *drop* equivalent transmission lattice are equivalent, since the *add* and *drop* transfer functions are identical, as determined at point (4) in Section 3.3, and both addition and multiplication are commutative. It is therefore reasonable to use the equivalent representation in Figure 5.1 (a) to determine the transfer functions for both *add* and *drop* equivalent network lattices. For *through* we shall use the equivalent representation from Figure 5.1 (c).

The *add/drop* magnitude response $I_{i,add/drop}(\lambda)$ for channel i of our tuneable OADM

is

$$I_{i,add/drop}(\lambda) = I_{DMUXi}(\lambda) \cdot I_{ADFi,add/drop}(\lambda) \tag{5.1}$$

while its *through* magnitude response $I_{through}(\lambda)$ is

$$I_{through}(\lambda) = \sum_{i=1}^{8}(I_{DMUXi}(\lambda) \cdot I_{ADFi,through}(\lambda) \cdot I_{MUXi}(\lambda)) \tag{5.2}$$

where $I_{DMUXi}(\lambda)$ is the magnitude response of the i^{th} channel of the phase-array demultiplexer, $I_{ADFi,through}(\lambda)$ is the magnitude response of the i^{th} tuneable add-drop filters, and $I_{MUXi}(\lambda)$ is the magnitude response of the i^{th} channel of the phase-array multiplexer.

Likewise, the *add/drop* phase response $\Phi_{i,add/drop}(\lambda)$ of channel i of our tuneable OADM is

$$\Phi_{i,add/drop}(\lambda) = \Phi_{DMUXi}(\lambda) + \Phi_{ADFi,add/drop}(\lambda) \tag{5.3}$$

while its *through* phase response $\Phi_{through}(\lambda)$ is

$$\Phi_{through}(\lambda) = \sum_{i=1}^{8}(\Phi_{DMUXi}(\lambda) + \Phi_{ADFi,through}(\lambda) + \Phi_{MUXi}(\lambda)) \tag{5.4}$$

where $\Phi_{DMUXi}(\lambda)$ is phase response of channel i of the phase-array demultiplexer, $\Phi_{ADFi,through}(\lambda)$ is the *through* phase response of the i^{th} tuneable add-drop filters, and $\Phi_{MUXi}(\lambda)$ is the phase response of the i^{th} channel of the phase-array multiplexer.

5.2 Performance Characteristics of the Constituent Components

The magnitude transfer functions of the phased-array demultiplexer $I_{DMUXi}(\lambda)$ and phase-array multiplexer $I_{MUXi}(\lambda)$, $i = 1, .., 8$, are considered quasi-rectangular as per

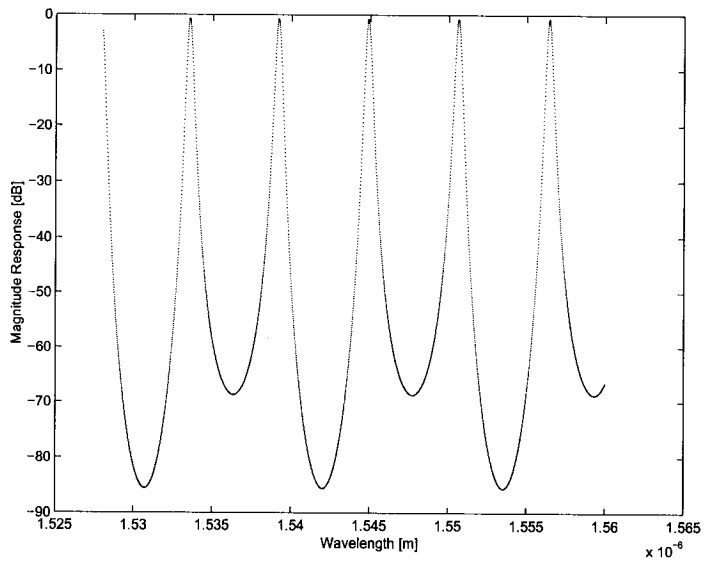

Figure 5.2: The *add/drop* magnitude response of ADF1 in all-through position.

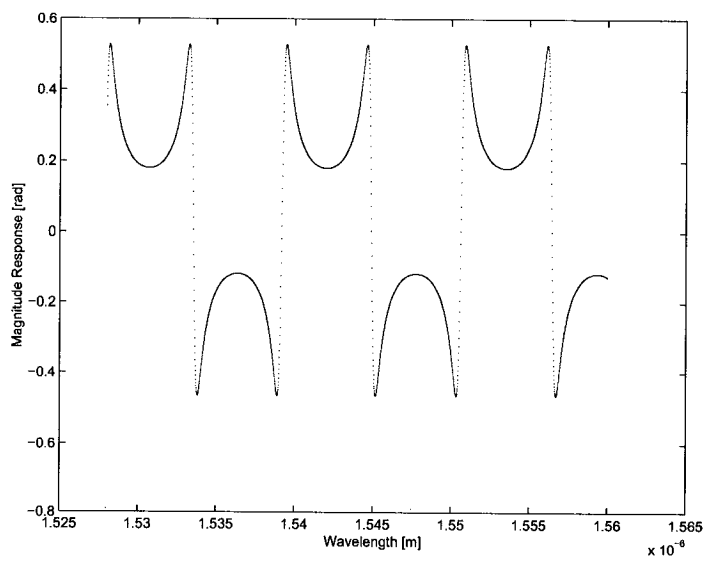

Figure 5.3: The *add/drop* phase response of ADF1 in all-through position.

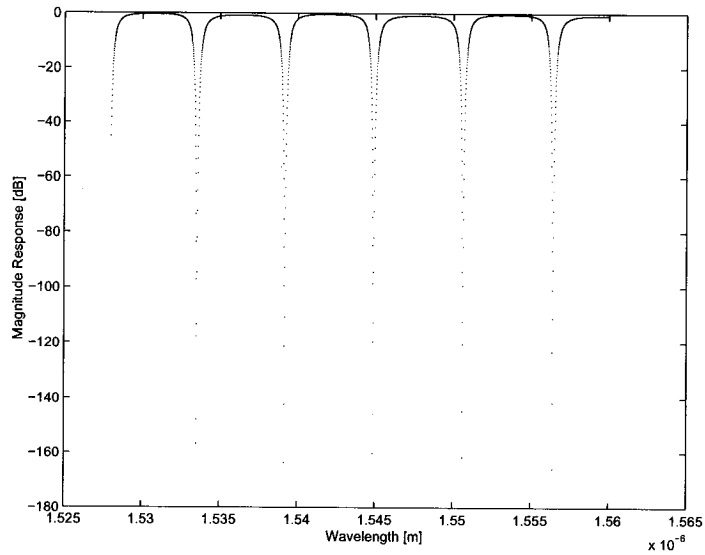

Figure 5.4: The *through* magnitude response of ADF1 in all-through position.

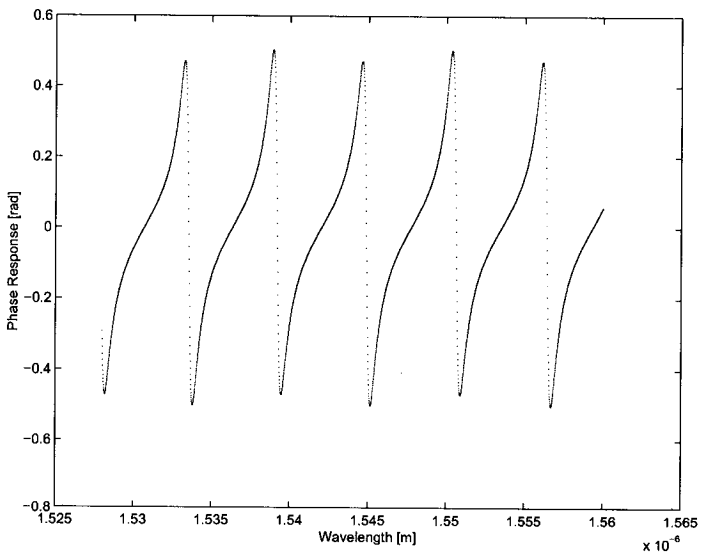

Figure 5.5: The *through* phase response of ADF1 in all-through position.

design proposed by Dragone [136], while the phase transfer functions $\Phi_{DMUXi}(\lambda)$ and $\Phi_{MUXi}(\lambda)$, $i = 1, .., 8$, are ideal as per assumption (5) in Section 2.6.

The magnitude $I_{ADFi}(\lambda)$ and the phase $\Phi_{ADFi}(\lambda)$ transfer functions have been computed for all eight add-drop filter using the optimum filter design parameters determined and presented in Section 4.4. Since all the add-drop filters exhibit similar transfer characteristics, we shall only present here the transfer functions for tuneable add-drop filter $ADF1$. Its *add/drop* and *through* magnitude and phase transfer functions are presented in Figure 5.2, 5.3, 5.4, and 5.5, respectively.

One can see in Figure 5.2 and 5.4 that the magnitude transfer functions exhibit periodic variation with the wavelength. The *add/drop* magnitude transfer function exhibits magnitude peaks around the central wavelengths and magnitude valleys elsewhere, while the *through* magnitude transfer function exhibits magnitude valleys around the central wavelengths and magnitude peaks elsewhere. In both cases, the magnitude peaks favour the transmission of optical signals with wavelengths in that region while the magnitude valleys block their transmission.

The phase transfer functions also exhibit a periodic variation with the wavelength for the *add/drop* and *through* signals, as one can see in Figure 5.3 and 5.5. This kind of phase variation is detrimental to the performance of the add-drop filter in transmission systems, since phase variations within optical signals lead to group delay variations, bit pulse dispersion, inter-symbol interference, and therefore increased bit error rates.

All the other tuneable add-drop filters exhibit similar characteristics with the only difference that their central wavelengths, in the *all-through* position, are 1541.57, 1545.57, 1549.57, 1553.57, 1557.57, and 1561.57 *nm*, respectively.

5.3 The Performance Characteristics

The magnitude and phase transfer functions of our sparse tuneable OADM can now be obtained by substituting the transfer functions of its constituent components into Equations (5.1), (5.2), (5.3) and (5.4). Subsequently its performance parameters can be determined and its performance evaluated.

The magnitude transfer functions for the *add/drop* and *through* are presented in Figure 5.6 and 5.8, respectively. One can see that the tuneable OADM properly adds,

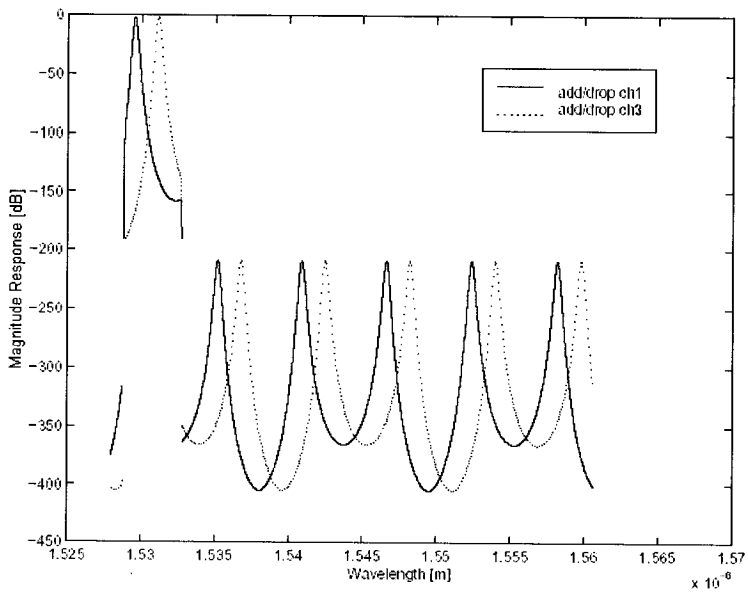

Figure 5.6: The *add/drop* magnitude response of our tuneable OADM with ADF1 tuned to channel 1 and 3, respectively; all other add-drop filters in all-through position.

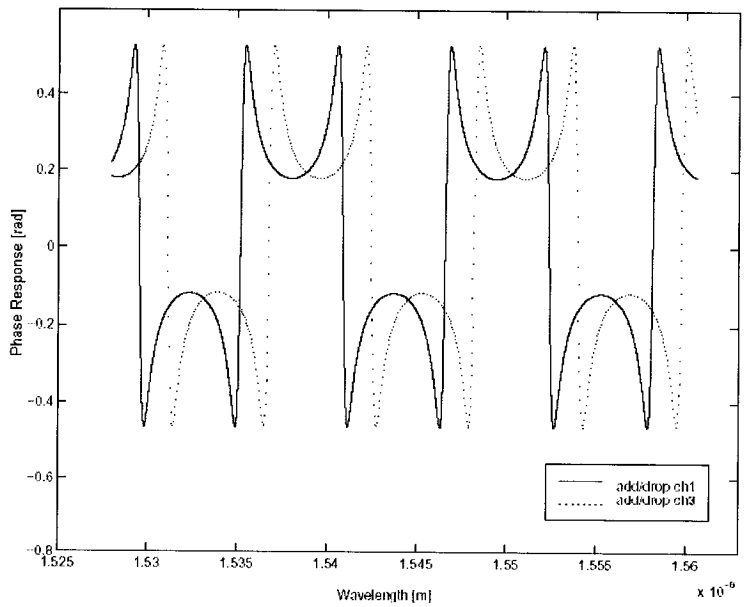

Figure 5.7: The *add/drop* phase response of our tuneable OADM with ADF1 tuned to channel 1 an 3, respectively; all other add-drop filters in all-through position.

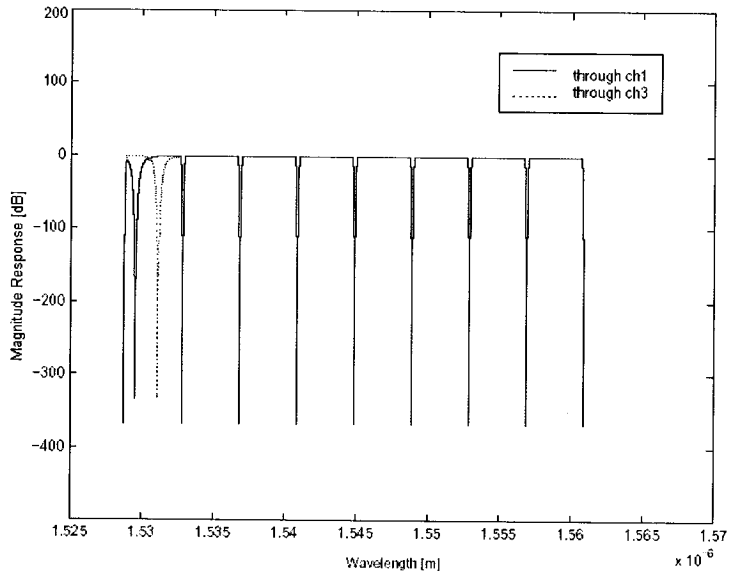

Figure 5.8: The *through* magnitude response of our tuneable OADM with ADF1 tuned to channel 1 an 3, respectively; all other add-drop filters in all-through position.

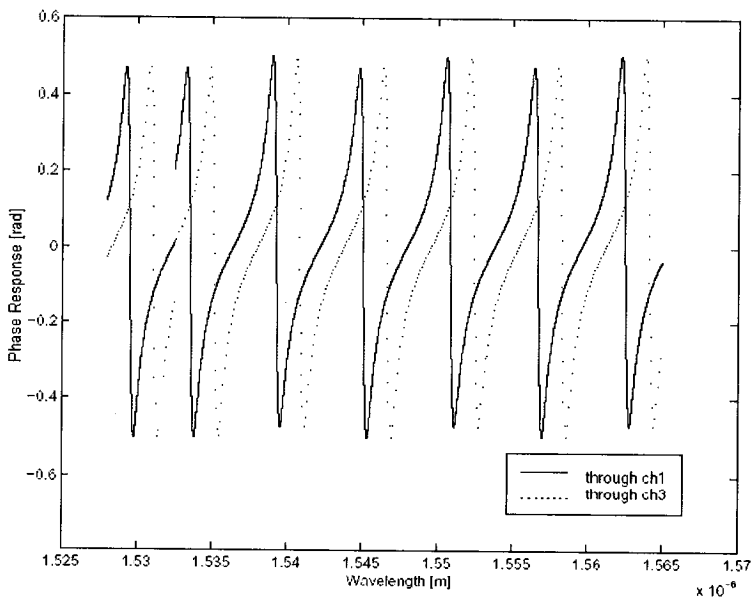

Figure 5.9: The *through* phase response of our tuneable OADM with ADF1 tuned to channel 1 an 3, respectively; all other add-drop filters in all-through position.

drops, and/or passes through the selected channel without affecting the other channels.

The phase transfer functions for the *add/drop* and *through* presented in Figure 5.7 and 5.9 show that the tuneable OADM exhibits certain phase distortions in the pass bandwidth of the selected *add/drop* and outside of the stop bandwidth in the *through* channels.

Subsequently, we computed the performance parameters such as insertion loss, channel pass bandwidth, adjacent cross talk, non-adjacent cross talk, and group delay from the magnitude and phase transfer functions presented in Figure 5.6, 5.8, 5.7 and 5.9. All the performance parameters have be computed according to their definitions presented in Section 2.5.

A summary of the design parameters of the tuneable OADM is listed bellow

Table 5.1: The design parameters for the sparse tuneable OADM.

Parameter	Value	Units	Description
B	*C-band*		transmission band
N_c	32		number of channels
N_g	8		number of group of channels
N_{cg}	4		number of channel per group
AD_{factor}	0.25		add-drop factor
C_s	0.8	nm	channel spacing in nm

The performance parameters of the tuneable OADM are presented as follows

Table 5.2: The performance parameters for the sparse tuneable OADM.

Parameter	Value	Units	Description
BW_{FWHM}	0.221	nm	*add/drop* pass bandwidth
$IL_{add/drop}$	0.77	dB	*add/drop* insertion loss

$IL_{throughadj}$	2.7	dB	*through* adjacent insertion loss
$IL_{throughnon-adj}$	1.15	dB	*through* non-adjacent insertion loss
$Xtalk_{adj}$	-43	dB	worst adjacent crosstalk
$Xtalk_{non-adj}$	-62.2	dB	worst non-adjacent crosstalk
$\tau_{add/drop}$	less than 2	ps	*add/drop* group delay
$\tau_{through}$	less than 1.8	ps	*through* group delay

The operating temperatures of the filter $ADF1$ are listed bellow

Table 5.3: The operating temperatures for the tuneable add-drop filter $ADF1$.

Parameter	Value	Units	Description
λ_{ch1}	1529.57	nm	central frequency at 63.15^oC
λ_{ch2}	1530.37	nm	central frequency at 55.44^oC
λ_{ch3}	1531.17	nm	central frequency at 47.73^oC
λ_{ch4}	1531.97	nm	central frequency at 40.02^oC
$\lambda_{all-through}$	1533.57	nm	central frequency at 24.6^oC

All the obtained values for the performance parameters such as insertion loss, channel pass bandwidth, adjacent cross talk, non-adjacent cross talk, and group delay strongly indicate the our tuneable OADM can be employed in WDM optical networks/transmission systems.

The operating temperatures are bounded between 24.6^oC and 63.15^oC, as one can see in Table 5.3, and are strictly characteristic to the add-drop filter $ADF1$. The operating temperatures for all the other add-drop filters $ADF2$, $ADF3$, .., $ADF8$ can be the same, given that the tuneable add-drop filters are designed accordingly, or slightly different but within similar bounds.

Chapter 6

Performance Evaluation in All-Optical Networks

In this chapter, we shall evaluate the performance of our tuneable OADM in linear, ring, and mesh all-optical networks/transmission systems using Optsim, an optical transmission systems simulator. We shall devise and present the component models, the network models, and the simulation scenarios that shall be used to evaluate the performance in terms of optical power spectra, bit error rates, optical signal to noise ratios, eye diagrams, and maximum number of cascadable sparse tuneable OADM.

6.1 Simulation Approach

Our performance evaluation employs an optical transmission system simulator, called Optsim [129]. We shall use it to devise and develop component models, simulation scenarios, and network models. The simulation model of the tuneable OADM shall reflect its architecture presented in Section 2.2 and performance characteristics determined in Section 5.3, while the network models shall reflect the devised simulation scenarios. Additional component models shall be developed for other required network components such as optical transmitters and optical receivers. All additional component models shall reflect the behaviour of realistic devices.

Our simulation approach shall comprise two steps:

- A general frequency-domain simulation of the entire network to identify the most affected channel and the worst-case simulation scenario
- A frequency/time-domain simulation of the most affected channel in the worst-case scenario

The first step represents a preliminary understanding of the performance. The simulation employs a so-called spectral simulation technique where optical signals are propagated as power spectra and each component is characterized by its magnitude transfer functions. Spectral simulation technique is a simplified technique that does not consider phase distortion and fiber non-linearities (e.g. Raman effect). Average signal powers, optical spectra, and optical signal to noise ratio shall be estimated at every point in the network/transmission system and the worst-case path shall be identified.

The second step, a frequency/time-domain simulation [129], shall be performed to determine the performance of the most affected channel in the worst-case scenario. The simulation shall consider the phase distortion in various components and the linear and non-linear effects in the transmission media. A preliminary spectral propagation technique simulation shall be run to initialize the component requiring the value of the input average power in order to be properly modeled (e.g. optical amplifiers). Next, a frequency/time-domain variable bandwidth simulation technique shall be employed to estimate average signal powers, optical spectra, optical signal to noise ratios, and bit error rates at desired points in the network/transmission system.

All the electromagnetic fields are assumed to have arbitrary modulations, frequencies, phases, and polarizations and shall be simulated as stochastic processes using a Monte-Carlo approach. The simulations shall take into account all the linear and non-linear effects in the fiber, along with additional transmission impairments such as insertion loss, cross talk, polarization-dependant loss, polarization mode dispersion, chromatic dispersion, transmitter chirp, and both magnitude and phase distortion due to filtering. The noise shall be propagated at the same time with the signals, and all signals shall be represented by sets of samples in time and frequency domain as described in [131].

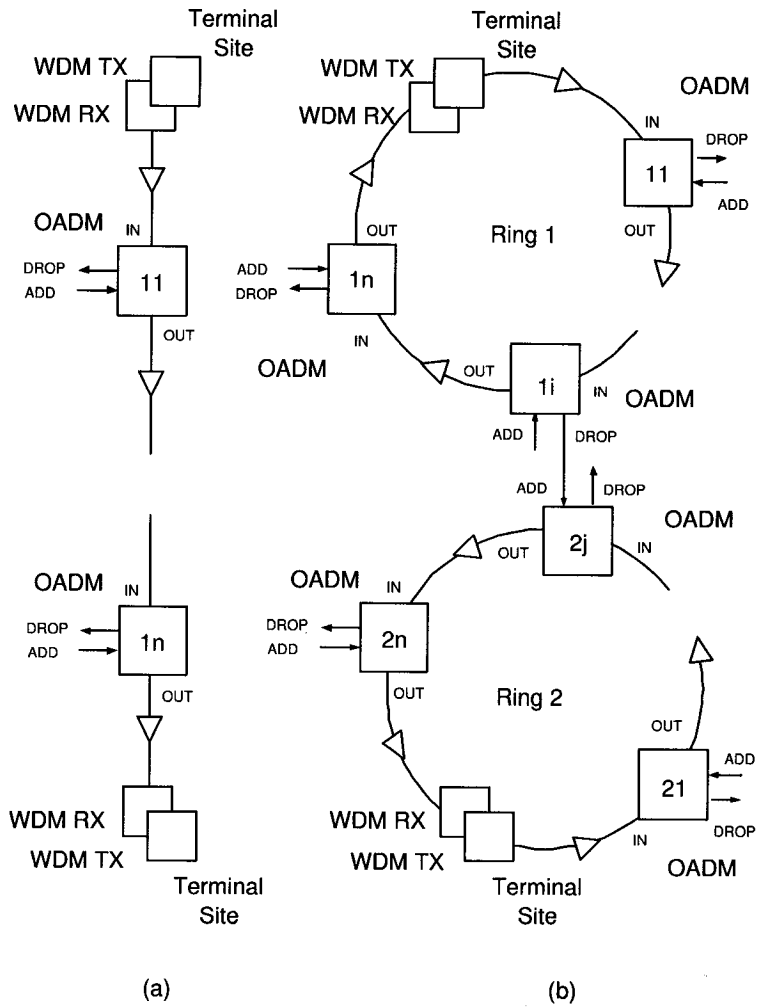

Figure 6.1: The linear/mesh/single-ring (a) and double-ring (b) scenario.

During the second simulation step, we shall evaluate the performance of our tuneable OADM in terms of optical signal to noise ratio, bit error rate, eye diagrams, and maximum number of cascadable OADM in linear, single-ring, double-ring, and mesh all-optical networks/transmission systems.

6.2 Simulation Scenarios

Since at the transmission level all-optical mesh networks/transmission systems with ideal optical cross-connects[1] and single-ring all-optical networks/transmission systems are

[1]All the optical cross connects are ideal as per assumption (8) in Section 2.6.

fundamentally linear, we devised two simulation scenarios for our performance analysis: a linear/mesh/single-ring and a double-ring scenario. All-optical networks/transmission systems with more than two rings are supersets of the double-ring scenario featuring additional *drop-add* connections and will not be considered because we do not think their analysis will provide additional information and insight.

The Linear/Mesh/Single-Ring

In the linear/mesh/single-ring simulation scenario a tuneable OADM is connected to an upstream OADM in a *out-in* manner, as illustrated in Figure 6.1 (a), and any channel can be added and/or dropped at any add-drop node while the other channels pass untouched towards their destination. The maximum number of channels that can be added and/or dropped at any add-drop node is eight.

The Double-Ring

In the double-ring simulation scenario a tuneable OADM is connected to the upstream OADM in a *out-in* manner with the exception of the two OADMs connecting the two adjacent rings which are also connected in a *drop-add* manner as illustrated in Figure 6.1 (b). Any channel can be added and/or dropped at any add-drop node while the other channels pass unaffected towards their destination. The maximum number of channels that can be added and/or dropped at any add-drop node is eight.

6.3 Simulation Models

We developed a system model of our sparse tuneable OADM that reflects its functionality and performance characteristics. In addition, we developed system models of the optical receivers, the optical transmitters, and both linear/mesh/single-ring and double-ring scenarios used in our simulations.

6.3.1 The Component Models

The Tuneable OADM Model

The tuneable OADM component model illustrated in Figure 6.2 is comprised of one demultiplexer model (DMUX), eight add-drop filter models (ADFi, $I = 1, 2, .., 8$), and one

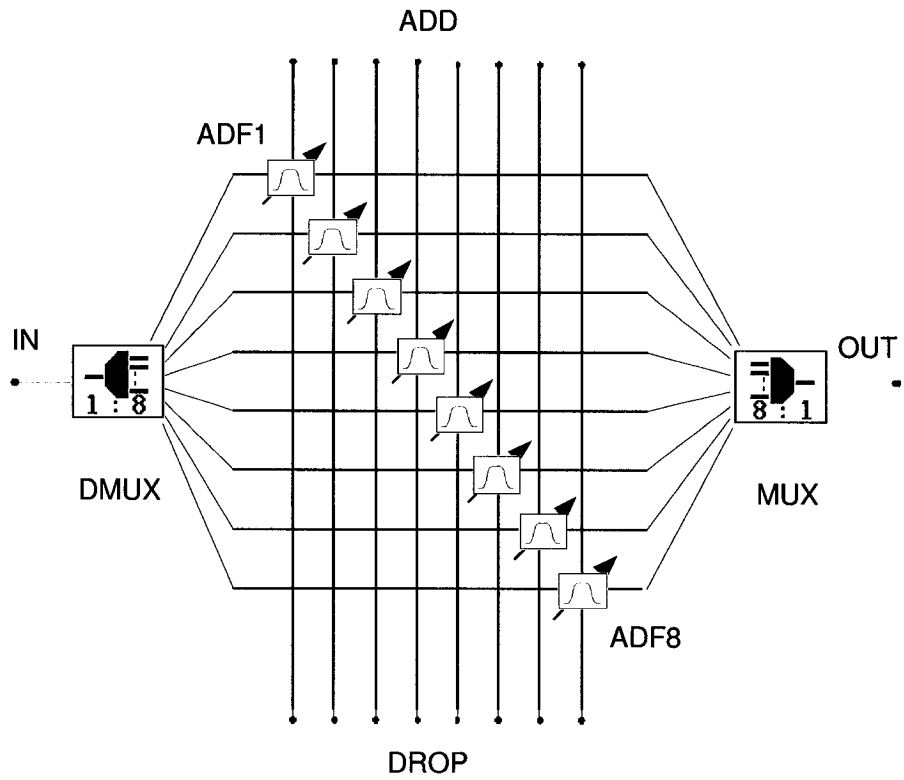

Figure 6.2: The tuneable OADM model.

multiplexer (MUX) model. The transfer characteristic of the multiplexer and demultiplexer models reflects the magnitude and phase transfer functions as per assumptions outlined in Section 2.6, while the tuneable add-drop filter models reflect the magnitude and phase transfer functions of the respective filter computed in Section 4.4.

The position of the central wavelength of the add-drop filter can be selected such that it can simulate all the optical channel passing through, add-drop filter in *all-through* position, or add/drop any of the optical channels covered by the tuneable add-drop filter.

The WDM Transmitter Model

The WDM transmitter model, illustrated in Figure 6.3, represents a generic single channel transmitter equipped with a pseudo-random-bit-sequence data source (Datasource), a non-return to zero (NRZ) data encoder, a Lorenzian continuous wave laser (CW Lorenzian), and an external Mach-Zehnder modulator (sin^2MZ).

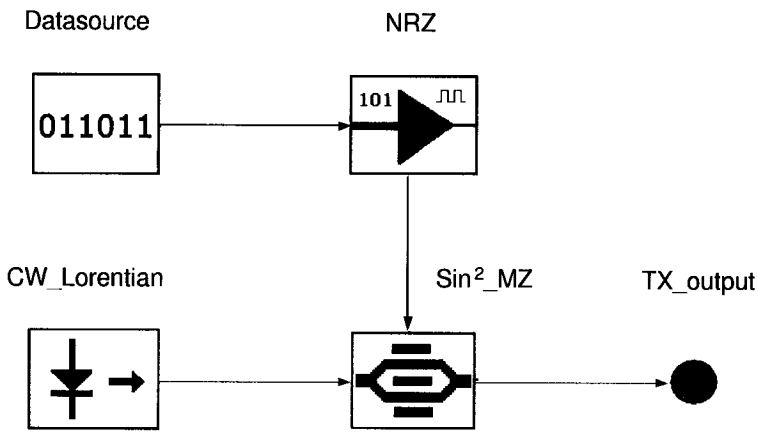

Figure 6.3: The single channel WDM transmitter model.

The simulation parameters of the optical transmitter as presented as follows

Table 6.1: The simulation parameters of the optical transmitter model

Characteristic	Default Value	Units
PRBS sequence degree	7	
laser central wavelength	1529.57	nm
laser power	0	dBm
laser linewidth	0.1	nm
bit rate	1	Gbit/s
modulator extinction ratio	30	dB
modulator chirp factor	0	
modulator excess loss	3	

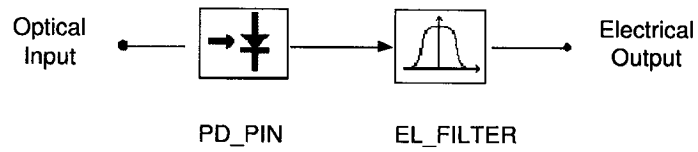

Figure 6.4: The optical receiver model.

The Optical Receiver Model

The optical receiver model, depicted in Figure 6.4, has been developed as a modified version of a asynchronous ASK single-channel optical receiver present in the Optsim library. The model consists of an ideal PIN photodiode (PD_PIN), and a 5th order lowpass Bessel filter (EL_FILTER) with selectable 3 dB bandwidth.

The parameters of the optical receiver model are presented as follows

Table 6.2: The simulation parameters of the optical receiver model

Characteristic	Default Value	Units
Type	PIN Photodiode	
Quantum Efficiency	0.798	
Responsivity	1	A/W
Quantum noise	Off	
Dark Current	0	nA
Single-Pole Electrical Filtering	Off	
-3dB Bandwidth	0.1	GHz

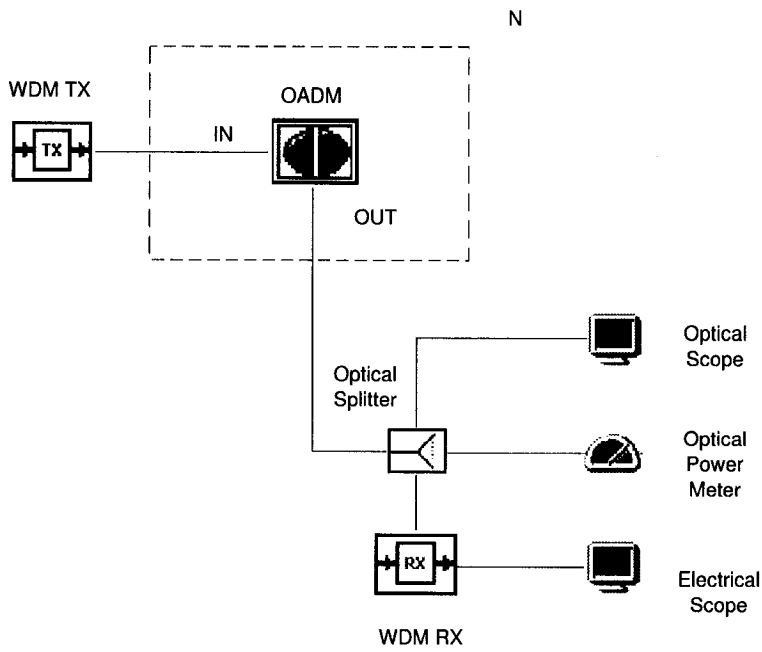

Figure 6.5: The liner/mesh/single-ring network model.

6.3.2 The Simulation Scenario Models

The Liner/Mesh/Single-Ring Model

In the liner/mesh/single-ring scenario model, all N tuneable OADM models are *out-in* connected in a single chain as illustrated in Figure 6.5. The multichannel transmitter model from the terminal site is connected to the *in* port of the first tuneable OADM model, the *out* port of the i^{th} tuneable OADM model is connected to the *in* port of the $(i+1)^{st}$ tuneable OADM model, and the multichannel receiver model is connected to the *out* of the last tuneable OADM model. Additional traffic can be added through the *add* port of any tuneable OADM, while traffic can be dropped through any *drop* port of any tuneable OADM model. Terminal sites do not contain any tuneable OADMs but allow adding and/or dropping of all the channels at the same time. Virtual optical instruments such as optical scopes, optical power meters, and electrical scopes are readily available in the Optsim library and can be freely employed to evaluate the performance of any optical channel.

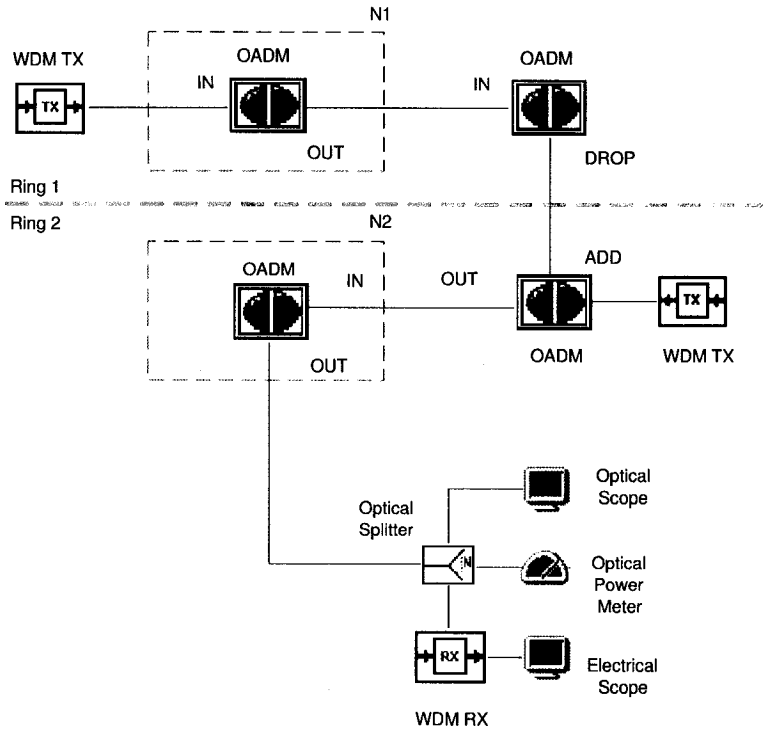

Figure 6.6: The double-ring network model.

The Double-Ring Model

The double-ring scenario model illustrated in Figure 6.6 is comprised of two rings of N1 and N2 tuneable OADM models, respectively. The multichannel transmitter model at the terminal site is connected to the *in* port of the first tuneable OADM model, the *out* port of the i^{th} tuneable OADM model is connected to the *in* port of the $(i+1)^{st}$ tuneable OADM model in Ring 1, and the multichannel receiver model is connected to the *out* of the last tuneable OADM model in the Ring 2. The two rings are arbitrarily connected through the *drop* port of any of the tuneable OADM model from the first ring and the *add* port of any tuneable OADM model form the second ring. Additional traffic can be added through the *add* port of any tuneable OADM. Terminal sites do not contain any tuneable OADMs and allow adding and/or dropping of all the channels at the same time. Optical instruments such as optical scopes, optical power meters, and electrical scopes can be freely employed to evaluate the performance of any optical channel.

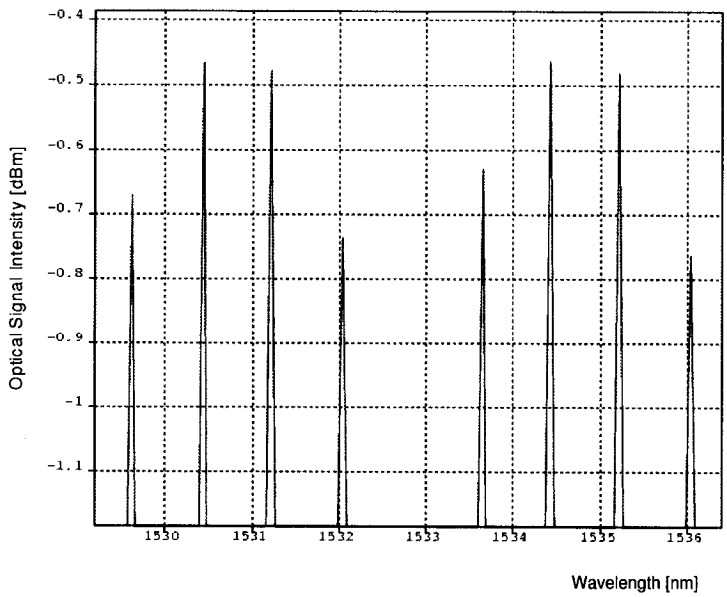

(a)

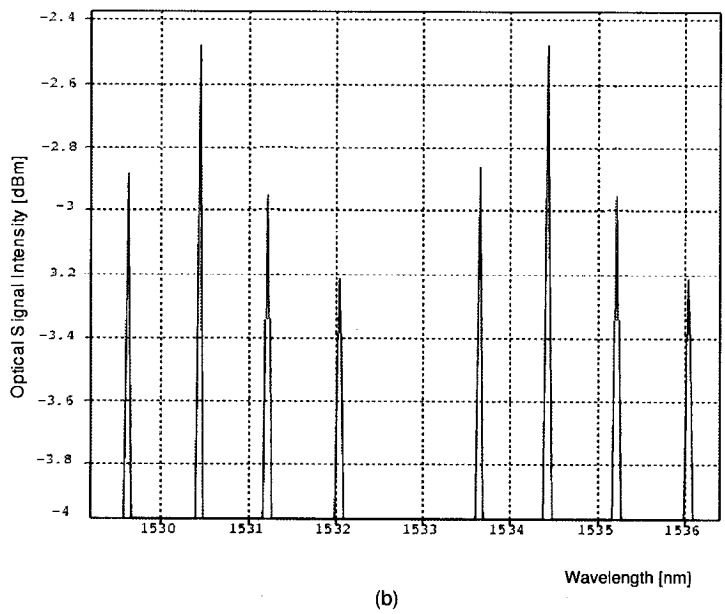

(b)

Figure 6.7: The most affected channel for the linear/mesh/single-ring (a) and the double-ring (b) scenario.

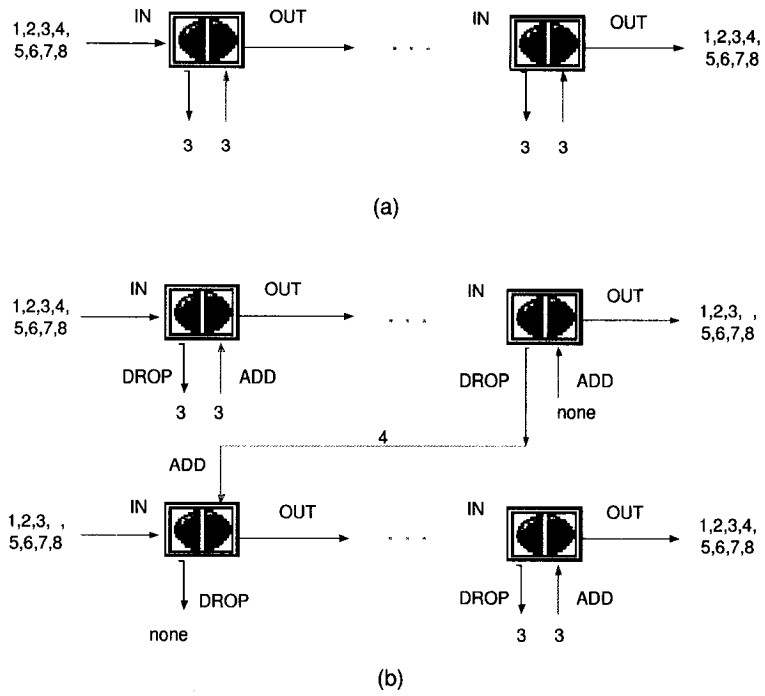

Figure 6.8: The simulated worst-case for the linear/mesh/single-ring (a) and the double-ring (b) scenario.

6.4 Performance Evaluation

As outlined in the beginning of the chapter, at first we shall identify the most affected channel and next we shall evaluate the performance of the most affected channel in the two simulation scenarios described in Section 6.2. In the latter step, we shall evaluate the cross talk, the optical signal to noise, the eye diagrams, and the ratio the bit error rate for a variable number of cascaded OADMs. The cross talk and the optical signal to noise ratio shall be estimated using optical scopes, while the eye diagrams and the bit error rate shall be obtained using electrical scopes, both virtual instruments of the transmission system simulator. The number of simulated bits shall be 512, the bit rate $10Gbit/s$, the total simulated time $51.2ns$, the number of samples per bit is 568, the overall amplitude error $0.01dB$, the overall group delay error 0.04, and the confidence interval is 95% of the times. The simulated optical fiber spans shall have lengths of 0 km (back-to-back scenario) and lengths of 10 km. The back-to-back scenario shall be used as a performance baseline.

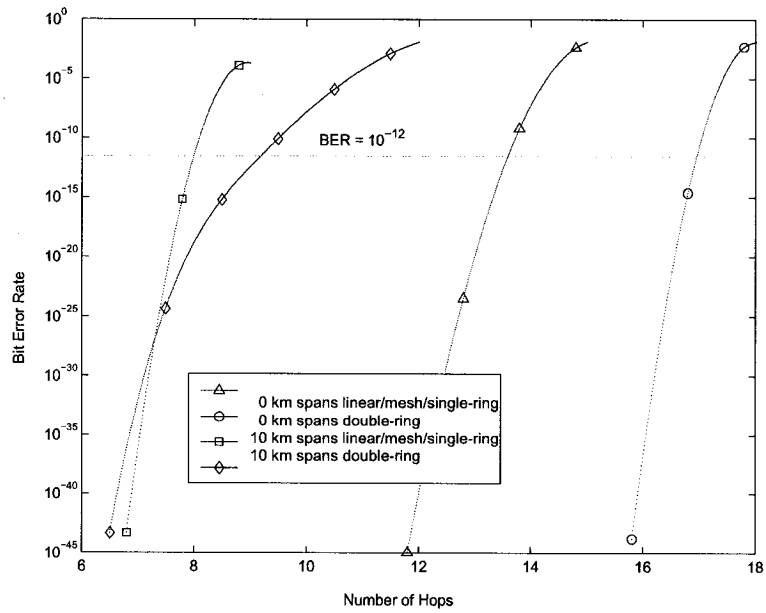

Figure 6.9: The variation of the BER with the number of cascaded tuneable OADMs.

6.4.1 The Most Affected Channel and the Worst-Case Scenario

We shall identify the most affected channel by running frequency-domain, spectral propagation technique simulations in the linear/mesh/single-ring and the double-ring simulation scenarios. Next, we shall analyse additional factors that further impact the most affected channel and identify the worst-case simulation scenario for each case.

We launched 32 optical channels, $i = 1, 2, .., 32$ as per channel allocation plan in Section 2.4, through both the linear/mesh/single-ring and the double-ring scenario models. In the linear/mesh/single-ring case the number of tuneable OADMs was $N = 1$, while in the double-ring case the number of tuneable OADMs were $N_1 = 1$ and $N_2 = 2$ in the first ring and in the second ring, respectively.

All the launched signals had initially the same optical power, 0 dBm or 1 mW, but experienced different levels of attenuation after passing through the two transmission systems. In both cases, the most affected channel was the fourth channel of each group of channels, as one can see in Figure 6.7(a) and (b) where two adjacent groups of 4channels are shown. The attenuation of its optical power was approximately 0.25 dB larger than the one experience by the second channel of each group, which is the least affected

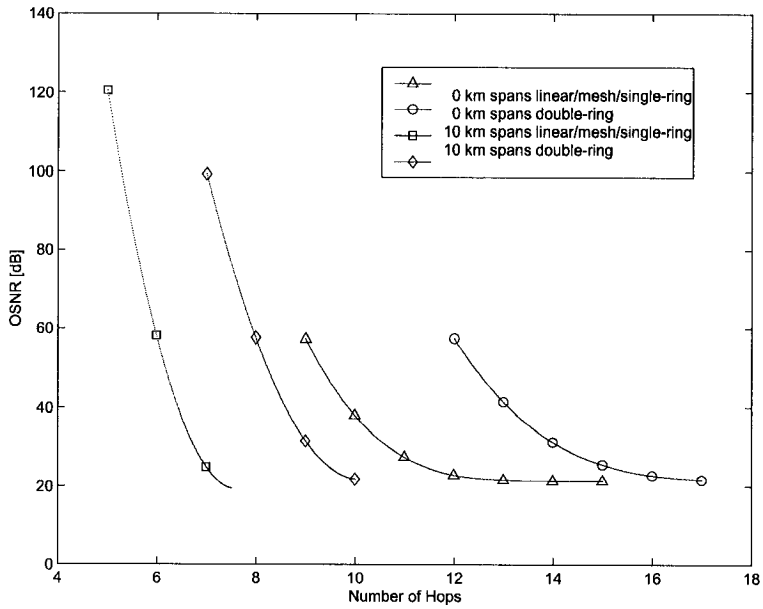

Figure 6.10: The variation of the OSNR with the number of cascaded tuneable OADMs.

channel. Since the most affected channels are 4, 8, 12, 16, 20, 24, 28, and 32 and the channels are equally affected, it is reasonable to focus our further performance analysis only on channel 4.

Optical signals transmitted through an optical channel experience a number of adverse effects such as transmitter chirp, linear and non-linear effects in transmission media, phase and magnitude distortions incurred in the add-drop nodes, and receiver noise. Our simulations take into account all those adverse effects in the component models: transmitter chirp in the transmitter model, liner and non-linear effects in the fiber in the fiber model, phase and magnitude distortion in OADM nodes in the OADM model, and receiver noise in the receiver model.

The influence of the tuneable add-drop filters is dependent on their overall configuration and tuning position. We shall therefore analyse the performance of channel 4 while adding and dropping channel 3 at each OADM site, as illustrated in Figure 6.8. It is reasonable to assert that this is the worst-case for the two simulation scenarios, since by systematically adding and dropping channel 3 we shall maximize the influence of the insertion loss and cross talk on channel 4, already the most affected optical channel.

The total number of simulated channels is eight because of limited simulation capa-

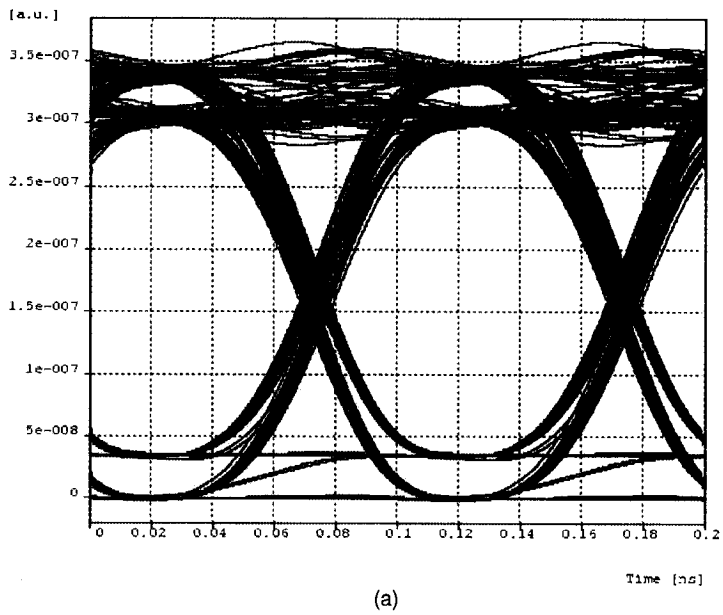

(a)

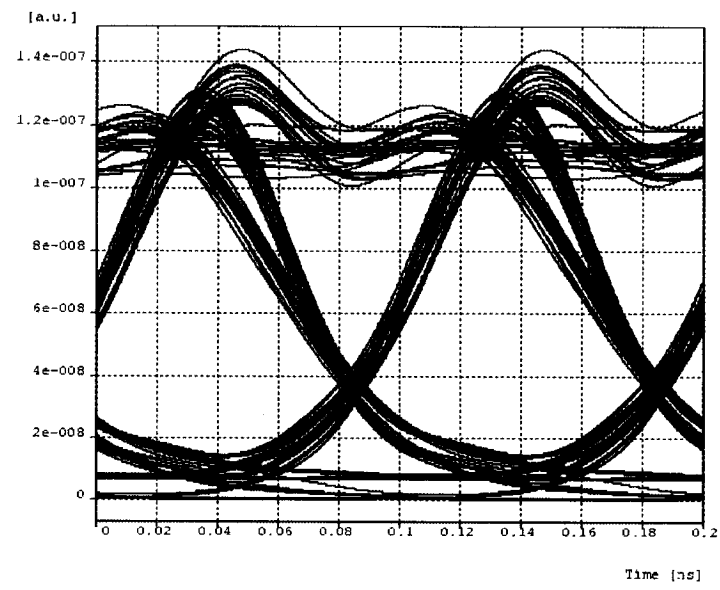

(b)

Figure 6.11: The eye diagrams for channel 4 after 7 hops (a) and 8 hops (b) in a back-to-back linear/mesh/single-ring scenario.

bilities featured by Optsim. However, since the influence of the channels not accounted for in our simulation is marginal, we do not foresee any loss in the quality of our results.

6.4.2 The Bit Error Rate

The simulated results of the bit error rate for linear/mesh/single-ring and double-ring all-optical transmission networks are presented in Figure 6.9. The tuneable OADM were cascaded back-to-back as illustrated in Figure 6.5 and Figure 6.6, respectively. Subsequently the tuneable OADM were connected by 10km fiber spans of single mode fiber. The optical channels were launched in accordance to the worst-case simulation scenarios, illustrated in Figure 6.8.

One can se that the bit error rate increases with the number of cascaded tuneable OADM as well as with the length of the fiber spans between the tuneable OADMs until eventually becomes unity. According to the ITU recommendations [134], bit error rates exceeding 10^{-9} for optical transmission systems with single channels, or 10^{-12} for multiple channel (WDM) optical transmission systems are not acceptable.

6.4.3 The Optical Signal to Noise Ratio

The results for the optical signal to noise ratio (OSNR) are presented in Figure 6.10 for linear/mesh/single-ring and double-ring all-optical transmission networks. The tuneable OADM were cascaded back-to-back and subsequently connected by 10km fiber spans of single mode fiber as illustrated in Figure 6.5 and Figure 6.6, respectively. The optical channels were launched in accordance to the worst-case simulation scenarios, illustrated in Figure 6.8.

One can see that the optical signal to noise ratio decreases with the number of cascaded tuneable OADM as well as with the length of the fiber spans between the tuneable OADMs until eventually becomes zero. Since optical signal to noise ratio is directly connected with the bit error rate [138]

$$BER = \frac{1}{2} exp(-\frac{OSNR}{8}) \tag{6.1}$$

the results are in good agreement with the bit error rate results.

6.4.4 The Eye Diagrams

The tuneable OADM were cascaded back-to-back and subsequently through 10km fiber spans of single mode fiber, as illustrated in Figure 6.5 and Figure 6.6, respectively. The optical channels were launched in accordance to the worst-case simulation scenarios, illustrated in Figure 6.8.

Since the eye diagrams represent qualitative information only that shall not be further used in our analysis we shall only present the eye diagrams for the linear/mesh/single-ring case with $N = 7$ and $N = 8$ cascaded tuneable OADMs connected through 10km of standard single mode fiber, illustrated in Figure 6.11 (a) and (b), respectively.

Our simulation results clearly indicated a degradation of the received signal for transmission systems with longer transmission links and more cascaded OADMs. The results were in agreement with the bit error rate and optical signal to noise ratios results presented earlier in this section. Low bit error rates and high optical signal to noise ratios corresponded to a open eye diagrams, while high bit error rates and low optical signal to noise ratios corresponded to closed eye diagrams.

6.4.5 The Maximum Number of Cascadeable Tuneable OADMs

We can determine the maximum number of cascaded tuneable OADMs from Figure 6.9 by considering 10^{-12} the maximum acceptable BER, as recommended by the International Telecommunication Union, Study Group 15 [134].

The maximum number of cascadeable tuneable OADMs for linear/mesh/single-ring and double-ring all-optical networks/transmission systems are presented as follows

Table 6.3: The maximum number of cascadeable tuneable OADMs

Network Type	Maximum Cascades	Span Length
linear/mesh/single-ring	13	0 km
double-ring	16	0 km
linear/mesh/single-ring	7	10 km
double-ring	9	10 km

Chapter 7

Design Guidelines

Based on our design experience, we believe that one can design sparse tuneable OADMs with a smaller or larger number of channels, group of channels, and/or channel spacing. Similarly, different channel allocation plans, new or different optical materials, and transmission bands can be employed. However, a lager number of channels means either phase array devices with a larger number of channels of add-drop tuneable filters with larger free spectral ranges. Phase array devices with a larger number of channels may prove more difficult to manufacture while add-drop filters with larger free spectral ranges will clearly feature worse performance characteristics in terms of insertion loss due to the increased scattering loss in the dielectric walls of the resonator rings. Moreover, achieving larger dynamic ranges the filters requires larger operating temperature, which will eventually lead to degradation of the stability and the reliability of the hybrimer used in our design.

Smaller channel spacing means that the cross talk values must be improved to maintain the same level of performance at the transmission system level. Improved cross talk levels translates into narrower pass bandwiths, which may render the add-drop filter and therefore the sparse tuneable OADM unusable.

Larger groups of channels require add-drop filters with larger free spectral ranges which have drawbacks in terms of performance characteristics and feasibility, as outlined above in this section. Smaller groups of channels will not bring any benefits to the performance of the tuneable OADM and/or the transmission system, in fact will render unavailable more of the transmission bandwidth of the optical fiber, as more skipped channels will be required.

Changing the channel allocation plan is required if any of the above number of channels, size of the group of channels, or channel spacing has been changed. Since the channel allocation plan is directly connected to the number of channels, size of the group of channels, and the channel spacing any change in the performance of the tuneable OADM will be occur as a result of changing these parameters, as described above in this section.

Since the proposed architecture is technology independent, designing and manufacturing sparse tuneable OADMs using other add/drop filter technologies is conceivable. Employing new or existing optical materials with better performance in terms of stability, thermal expansion coefficient, refractive index, thermo-optical coefficient will beneficially influence the performance characteristics of the sparse tuneable OADM, while designs supporting different transmission bands such as L and S band can be manufactured with minimal changes in the provided design of the tuneable add-drop filters.

Since in practice the radiation/bending loss may be larger than assumed in our design, one can get lower performance characteristics in manufactured tuneable OADMs based on our design.

Chapter 8

Conclusions

We have designed in this research a tuneable OADM optical subsystem consisting of eight tuneable ring resonator-based optical filters and two eight-channel phase arrays devices in a planar arrangement. The design takes advantage of the main limitation of single ring resonator-based optical filters, namely the rather limited free spectral range and in effect the limited number of communication channels that can be processed. The tuneable filters provide add and drop functions of selected sparse channels whereas the phase arrays devices provide demultiplexing and multiplexing functions for the inbound, respectively the outbound channels.

The coupled mode theory, its transfer matrix formalism, and the theory of spectral analysis of signals had been used to carry out the design and the performance analysis of our tuneable add-drop filters, the main components of our tuneable optical add-drop multiplexer. It had been determined that a hybrimer ring resonator with 44.895 μm radius, 0.26 coupling coefficient, and 0.998 coupler loss coefficients has a free spectral range of 718.7 GHz, an add/drop insertion loss of 0.77 dB, and a full width half maximum bandwidth of 0.221 nm, making this add-drop filter attractive for wavelength division multiplexing applications.

A wavelength-domain step coupled with a time/frequency-domain step, has been used to analyse the performance of the tuneable OADM in linear, single-ring, double-ring, and mesh all-optical wavelength-division multiplexing networks/transmission systems. It was demonstrated that the tuneable OADM could be successfully employed in un-amplified linear, single-ring, double-ring, and mesh all-optical wavelength-division multiplexing networks/transmission systems with bit rates up to 10 Gbit/s.

The maximum number of cascaded sparse tuneable OADMs in our design is 13 for back-to-back linear/mesh/single-ring, 7 for linear/mesh/single-ring with 10 km spans of standard single mode fiber, 16 for back-to-back double-ring, and 9 for double-ring architectures with 10 km spans of standard single mode fiber.

Further Work

Simulating the performance of our tuneable OADM using alternate methods (e.g finite difference time-domain) shall further validate our mathematical models, while comparing the performance of our design with the performance of similar designs based on alternate technologies such as fiber/planar Bragg gratings, Mach-Zehnder interferometers, and micro electro-mechanical systems, acousto-optic filters, or semiconductor optical amplifiers shall place our work in a broader context.

Evaluating the performance of our tuneable OADM in all-optical networks/transmission systems with more than two non-amplified rings or systems with amplified architectures would be of practical interest. Other types of optical fiber, with different transmission characteristics such as polarization mode dispersion, polarization dependent loss and optical power loss, or other types of optical transmitters or receivers can also be considered to gain more insight.

Manufacturing the proposed design shall ultimately prove the feasibility of the device, field trials shall demonstrate its applicability in all-optical networks/transmission systems, while novel optical materials, manufacturing processes, and control circuitry shall improve our design. Detailed heat analysis of the proposed design shall prove mandatory in order to identify methods of preventing the heat from spreading throughout the entire optical chip.

Appendix A

The Wavelength Allocation Plan

Table A.1 and Table A.2 present the central wavelengths associated with the optical channels and the *all-through* position of our tuneable add-drop filters, respectively.

Table A.1: The central wavelengths of the optical channels

Number	Central Wavelength	Units	Group Number
1	1529.57	*nm*	1
2	1530.37	*nm*	1
3	1531.17	*nm*	1
4	1531.97	*nm*	1
skipped	1532.77	*nm*	
5	1533.57	*nm*	2
6	1534.37	*nm*	2
7	1535.17	*nm*	2
8	1535.97	*nm*	2
skipped	1536.77	*nm*	
9	1537.57	*nm*	3
10	1538.37	*nm*	3
11	1539.17	*nm*	3
12	1539.97	*nm*	3
skipped	1540.77	*nm*	

13	1541.57	nm	4
14	1542.37	nm	4
15	1543.17	nm	4
16	1543.97	nm	4
skipped	1544.77	nm	
17	1545.57	nm	5
18	1546.37	nm	5
19	1547.17	nm	5
20	1547.97	nm	5
skipped	1548.77	nm	
21	1549.57	nm	6
22	1550.37	nm	6
23	1551.17	nm	6
24	1551.97	nm	6
skipped	1552.77	nm	
25	1553.57	nm	7
26	1554.37	nm	7
27	1555.17	nm	7
28	1555.97	nm	7
skipped	1556.77	nm	
29	1557.57	nm	8
30	1558.37	nm	8
31	1559.17	nm	8
32	1559.97	nm	8

Table A.2: The central wavelengths for the *all- through* position

Add-Drop Filter	All-Through Central Wavelength	Units Units	Covered Group of Channels
ADF1	1533.57	*nm*	1
ADF2	1537.57	*nm*	2
ADF3	1541.57	*nm*	3
ADF4	1545.57	*nm*	4
ADF5	1549.57	*nm*	5
ADF6	1553.57	*nm*	6
ADF7	1557.57	*nm*	7
ADF8	1561.57	*nm*	8

Appendix B

The Simulation Parameters

Since most of the simulation parameters are identical, we shall represent only one set, the simulation parameters used in the 10 km linear/mesh/single-ring simulation scenario. The parameters are organized in sections and each section contains the simulation parameters used in a specific component model (e.g. optical transmitter). The simulation parameters are parameters used in every each section and establish the simulation bandwidth, total simulation time, allowable errors, simulation bit rate, and simulation accuracy, among others.

General Parameters

Simulation center frequency in Time Domain [THz]: 194.39627815
Simulation center wavelength in Time Domain [nm]: 1542.38183156
Simulation bandwidth in Time Domain [THz]: 4.544
Simulation bandwidth in Time Domain [nm]: 36.0530873966
Reference bit rate [Gbit/s]: 10
Total simulated time span [ns]: 51.2
Total simulated time span in number of bits: 512
Optical field representation: Single polarization
Random parameters seed: 1
Simulation Accuracy Defaults: Tight
Enforcement: Strict
Overall Amplitude Error [dB]: 0.01
Overall Group Delay Error [ps]: 0.04
Peak Power Detection Averaging [ps]: 0.176056338028

resulting in averaging over simulation time-samples: 2

Maximum non-linear phase shift over a spatial step [degrees]: 0.25

Level of suppression of FWM Artifacts [dB]: 25

Samples per bit: 568

Corresponding Simulated Bit-Rate [Gbit/s]: 10

Time Domain Frequency Lower Limit [THz]: 192.124278151

Time Domain Wavelength Lower Limit [nm]: 1524.35593996

Time Domain Frequency Upper Limit [THz]: 196.66827815

Time Domain Wavelength Upper Limit [nm]: 1560.40902735

Frequency Lower Limit [THz]: 191.556278151

Wavelength Lower Limit [nm]: 1519.96610771

Frequency Upper Limit [THz]: 197.23627815

Wavelength Upper Limit [nm]: 1565.0359304

Simulation center frequency [THz]: 194.39627815

Simulation center wavelength [nm]: 1542.50101906

Simulation bandwidth [THz]: 5.68

Simulation bandwidth [nm]: 45.0698226921

Raman Amplifier simulation accuracy: 1e-06

Optical Transmitter

PRBS_sequence_degree: 7

bit_rate: 10

laser_linewidth: 0.1

laser_power_dBm: p

laser_wavelength: 1531.17

modulator_chirp_factor: 0

modulator_excess_loss: 3

modulator_extincion_ratio: 30

Demultiplexer

Filter Data Filename: DMUX.DAT

File Format: Wavelength/Frequency: Wavelength

File Format: Description options: Amplitude Only

File Format: Absolute/Relative frequency: Absolute

File Format: Linear/dB: dB

Smoothing: No

Smoothing factor: Undefined

Offset [THz]: 0

Offset [nm]: 0

Filter scaling: 1

Actual Filter Amplitude and Group Delay Plot: Yes

Reference Frequency [THz]: Undefined

Reference Wavelength [nm]: Undefined

Optical Filter ADF1

Notch Filter: Bandpass

Filter Data Filename: ADF_drop_026.DAT

File Format: Wavelength/Frequency: Wavelength

File Format: Description options: Phase

File Format: Absolute/Relative frequency: Absolute

File Format: Linear/dB: dB

Smoothing: No

Smoothing factor: Undefined

Offset [THz]: 0.504214324949

Offset [nm]: -4.00000000001

Filter scaling: 1

Actual Filter Amplitude and Group Delay Plot: Yes

Reference Frequency [THz]: Undefined

Reference Wavelength [nm]: Undefined

Multiplexer

Notch Filter: Bandpass

Filter Data Filename: MUX.DAT

File Format: Wavelength/Frequency: Wavelength

File Format: Description options: Amplitude Only

File Format: Absolute/Relative frequency: Absolute

File Format: Linear/dB: dB

Smoothing: No

Smoothing factor: Undefined

Offset [THz]: 0

Offset [nm]: 0

Filter scaling: 1

Actual Filter Amplitude and Group Delay Plot: Yes

Reference Frequency [THz]: Undefined

Reference Wavelength [nm]: Undefined

Optical Fiber

Type: Fiber

Name: Standard_SM

Location: Current model

Loss [dB/Km]: 0.2

Dispersion at the reference frequency [ps/nm/km]: 16

Dispersion at the reference frequency $[ps^2/km]$: -20.4071711919

Dispersion derivative at the reference frequency $[ps/nm^2/km]$: 0.07

Dispersion derivative at the reference frequency $[ps^3/km]$: 0.147458657676

Zero-Dispersion Frequency [THz]: 215.440338317

Zero-Dispersion Wavelength [nm]: 1391.53354633

Dispersion Statistical Distribution: Uniform

Dispersion standard deviation [ps/nm/km]: 0

β_2 standard deviation $[ps^2/km]$: 0

Zero-Dispersion Frequency Standard Deviation [THz]: 0

Zero-Dispersion Wavelength Standard Deviation [nm]: 0

Dispersion Correlation Length [Km]: 20

Fiber Non-Linearity Coefficient [1/W/km]: 1.26677123128

Fiber Average Beat Length [m]: 5

Birefringence Correlation Length [km]: 0.2

Beat Length Standard Deviation [m]: 0.5

Fiber PMD $[ps/km^0.5]$: 0.1

Reference Frequency for Dispersion [THz]: 193.414489032

Reference Wavelength for Dispersion [nm]: 1550

Loss From File: No

Loss FileName: Undefined

Loss File Format: Frequency

Reference Frequency for Loss [THz]: 193.414489032

Reference Wavelength for Loss [nm]: 1550

Loss derivative at the reference frequency [dB/Km/THz]: 0

Loss second derivative at the reference frequency $[dB/Km/THz^2]$: 0

Dispersion From File: No

Dispersion FileName: Undefined

Dispersion File Format: β_2 vs. Frequency

Dispersion second derivative at the reference frequency $[ps^4/km]$: 0

Dispersion third derivative at the reference frequency $[ps^5/km]$: 0

Non Linear Refractive Index: 2.5e-20

Core Effective Area $[10^{-12}m^2]$: 80.0000000004

Raman Constant: 0.18

First Raman Time Constant [fs]: 12.2

Second Raman Time Constant [fs]: 32

Reference Frequency for Non Linearity [THz]: 193.414489032

Reference Wavelength for Non Linearity [nm]: 1550

Reference Frequency for Raman Profile [THz]: 299.792458

Reference Wavelength for Raman Profile [nm]: 1000

Raman Profile Type: Lorentzian

Raman Profile Filename: Undefined

Raman File Format Type: Frequency

Rayleigh Scattering Type: Ideal

Rayleigh Capture Factor [dB]: Undefined

Reflectivity Type: Ideal

Input Reflectivity [dB]: Undefined

Output Reflectivity [dB]: Undefined

Custom Scaling of Raman Profile: No

Custom Scaling Filename: Undefined

Custom Raman Profile Type: gr

Used Loss Profile: File derived coefficients

Optical Amplifier

Block Type: Optical Amplifier Fixed Gain

Force time domain gain computation: No

Gain Shape: Flat

Gain [dB]: 25

Gain Shape from file: Undefined

Noise: Yes

Noise Figure: Flat

F [dB]: 4.5

F [lin]: 2.81838293126

Noise from file: Undefined

Optical Receiver

Type: PIN Photodiode

Quantum Efficiency: 0.798190356045

Responsivity (at reference frequency) [A/W] : 1

Quantum noise: Off

Dark Current [nA]: 0

Single-Pole Electrical Filtering: Off

-3dB Bandwidth [GHz]: Undefined

Optical Scope

Block Type: Optical Probe

Start Time [ns]: Undefined

End Time [ns]: Undefined

Sampling Factor: 1

Measure time-span: Whole

Electrical Scope

Block Type: Electrical Scope

Nominal Bit Rate [Gbit/s]: 10

Time Resolution: Automatic

Number of visualized points per bit: Undefined

Start Time [ns]: Undefined

End Time [ns]: Undefined

Samples per bit: 568

Corresponding Simulated Bit-Rate [Gbit/s]: 10

Measure time-span: Whole

Bibliography

[1] T.E. Stern and K. Bala. *Multiwavelength Optical Networks: A Layered Approach.* A-W CSE Professional, 1999.

[2] E. Karasan and E. Ayanoglu. Performance of WDM transport networks. *IEEE Selected Areas in Communications*, 16:1081–1096, 1998.

[3] S. Kawanishi, H. Takara, K. Uchiyama, I. Shake, O. Kamatani, and H. Takahashi. 1.4 Tbit/s (200 Gbit/s × 7 ch) 50 km optical transmission experiment. *IEEE Electronics Letters*, 33:1716–1717, 1997.

[4] J. Inoue, H. Sotobayashi, W. Chujo, and H. Kawaguchi. 80-Gbit/s OTDM signal transmission over 208-km standard fiber using midspan optical phase conjugation. *IEEE Electronics Letters*, 38:819–821, 2002.

[5] H. Sotobayashi. OCDM techniques for improved spectral efficiency. *CLEO Lasers and Electro-Optics*, 2:853–854, 2002.

[6] K. Fukuchi, T. Kasamatsu, M. Morie, R. Ohhira, T. Ito, K. Sekiya, D. Ogasahara, and T. Ono. 10.92-Tb/s (273×40-gb/s) triple-band/ultra-dense WDM optical-repeatered transmission experiment. *Optical Fiber Communications Conference*, 4:PD24–P1–3, 2001.

[7] S. Bigo, Y. Frignac, G. Charlet, W. Idler, S. Borne, H. Gross, R. Dischler, W. Poehlmann, P. Tran, , and C. Simonneau. 10.2 Tbit/s (256×42.7 Gbit/s PDM/WDM) transmission over 100 km TeraLight fiber with 1.28 bit/s/Hz spectral efficiency. *Optical Fiber Communications Conference*, 4:PD25–P1–3, 2001.

[8] R. Olshansky, V. Lanzisera, and P. Hill. Design and performance of wideband subcarrier multiplexed lightwave systems. *ECOC Optical Communications*, pages 143–146, 1988.

[9] R. Olshansky, V. Lanzisera, and P. Hill. Subcarrier multiplexed lightwave networks for broadband distribution. *ICC 89 and BOSTONICC/89*, pages 982–986, 1989.

[10] R. Hui, B. Zhu, R. Huang, C.T. Allen, K.R. Demarest, and D. Richards. Subcarrier

multiplexing for high-speed optical transmission. *IEEE Lightwave Technology*, 20:417–427, 2002.

[11] M.A. Al-Mumin and G. Li. WDM/SCM optical fiber backbone for 60 Ghz wireless systems. *Microwave Photonics*, pages 61–64, 2001.

[12] H. Sotobayashi, W. Chujo, and K. Kitayama. 1.52 Tbit/s OCDM/WDM (4 OCDM×19 WDM×20 Gbit/s) transmission experiment. *IEEE Electronics Letters*, 37:700–701, 2001.

[13] H. Sotobayashi, W. Chujo, and K. Kitayama. 1.6-b/s/Hz 6.4-Tb/s QPSK-OCDM/WDM (4 OCDM × 40 WDM × 40 Gb/s) transmission experiment using optical hard thresholding. *IEEE Photonics Technology Letters*, 14:555–557, 2002.

[14] H. Sotobayashi, W. Chujo, and T.Ozeki. Hierarchical hybrid OTDM/WDM network. *IEEE Laser and Electro-Optics Society*, pages 47–48, 2002.

[15] T. Pfeiffer, J. Kissing, J.-P. Elbers, B. Deppisch, M. Witte, H. Schmuck, and E.Voges. Coarse WDM/CDM/TDM concept for optical packet transmission in metropolitan and access networks supporting 400 channels at 2.5 Gb/s peak rate. *IEEE Lightwave Technology*, 18:1928–1938, 2000.

[16] G.C. Wilson, J.-M. Delavaux, A. Srivastava, C. Hullin, C. McIntosh, C.G. Bethea, and C. Wolf. Long-haul DWDM/SCM transmission of 64- and 256-QAM using electroabsorption modulated laser transmitters. *IEEE Photonics Technology Letters*, 14:1184–1186, 2002.

[17] J.-M. Delavaux, G.C. Wilson, C. Hullin, B. Neyret, and C. Bethea. QAM-PON and super PON for access distribution networks. *Optical Fiber Communications Conference*, 3:WN2 –1–3, 2001.

[18] R. Olshansky. Subcarrier multiplexed lightwave networks for broadband distribution. *Broadband Analog Optoelectronics: Devices and Systems*, pages 9–10, 1990.

[19] J.-P. Hamaide, A. Bertaina, S. Bigo, and Y. Frignac. High-throughput WDM transmission. *IEEE Lasers and Electro-Optics Society*, 2:476–477, 2000.

[20] A. Birman. Computing approximate blocking probabilities for a class of all-optical networks. *Selected Areas in Communications*, 14:852–857, 1996.

[21] A. Sridharan and K.N. Sivarajan. Blocking in all-optical networks. *INFOCOM Computer Communications*, 2:990–999, 2000.

[22] Y. Zhu and G.N. Rouskas. A path decomposition approach for computing blocking probabilities in wavelength-routing networks. *IEEE/ACM Transactions on*

Networking, 8:747–762, 2000.

[23] B. Ramamurthy and B. Mukherjee. Wavelength conversion in WDM networking. *Selected Areas in Communications*, 16:1061–1073, 1998.

[24] S. Subramaniam and M. Azizoglu. All-optical networks with sparse wavelength conversion. *IEEE/ACM Transactions on Networking*, 4:544–557, 1996.

[25] B. Schein and E. Modiano. Quantifying the benefit of configurability in circuit-switched WDM ring networks with limited ports per node. *IEEE Lightwave Technology*, 19:821–829, 2001.

[26] M. Kovaceviv and A.S. Acampora. Benefits of wavelenght translation in all-optical clear-channel networks. *IEEE Selected Areas in Communications*, 14:886–880, 1996.

[27] K.C. Lee and V.O.K. Li. A wavelength convertible network. *IEEE Lightwave Technology*, pages 962–970, 1993.

[28] J. Yates, J. Lacey, D. Everitt, and M. Summerfield. Limited-range wavelength translation in all-optical networks. *INFOCOM Computer Communications*, 3:954–961, 1996.

[29] P. Tang and O. Eknoyan. Rapidly tunable polarisation independent optical add drop multiplexer. *IEEE Electronics Letters*, 38:242–244, 2002.

[30] K. Eda, H. Asakura, M. Iida, and K. Hagiwara. Novel high performance wavelength selective devices for densly spaced WDM HD-CATV systems. *ECOC Optical Communications*, pages WeC8–2, 1991.

[31] M.S. Wu, G.S. Li, W. Yuen, and C.J. Chang-Hasnain. Widely tunable 1.5 μm micromechanical optical filter using AlOx/AlGaAs DBR. *IEEE Electronics Letters*, 33:1702–1703, 1997.

[32] K.W. Cheung, M.M. Choy, and H. Kobrinski. Electronic wavelength tuning using acousto-optic tunable filter with broad continuous tuning range and narrow channel spacing. *IEEE Photonic Technology Letters*, 1:38–40, 1989.

[33] T.E. Dimmick, D.A. Satorius, and G.L. Burdge. All-fiber acousto-optic tunable bandpass filter. *Optical Fiber Communications Conference*, pages WJ3–1, 2000.

[34] H. Toba, K. Oda, K. Nakanishi, N.Shibata, K. Nosu, N. Takato, and M. Fukuda. 100-channel optical FDM transmission/distribution at 622 Mb/s over 50 km. *Optical Fiber Communications Conference*, page PD1, 1990.

[35] C. Kostrzewa, R. Moosburger, G. Fishchbeck, B. Schuppert, and K. Petermann.

Tunable polymer optical add/drop filter for multiwavelength networks. *IEEE Photonics Technology Letters*, 11:1487–1489, 1997.

[36] F. Genereux, G. Baldenberger, C. Pare, P.Y. Cortes, J. Lauzon, and S. LaRochelle. Narrowband add/drop filter optically tunable over the C-band. *CLEO Lasers and Electro-Optics*, page CMI5, 2002.

[37] J. Peerlings, A. Dehe, A. Vogt, M. Tilsch, C. Hebeler, F. Langenhan, P. Meissner, and H.L. Hartnagel. Long resonator micromachined tunable GaAs-AlAs Fabry-Perot filter. *IEEE Photonic Technology Letters*, 9:1235–1237, 1997.

[38] H.K. Tsang, M.W.K. Mak, L.Y. Chan, J.B.D. Soole, C. Youstsey, and I. Adesida. Etched cavity InGaAsP/InP waveguide Fabry-Perot tunable by current injection. *IEEE Lightwave Technology*, 17:1890–1895, 1999.

[39] K. Hirabayashi, H. Tsuda, and T. Kurokawa. Tuneable liquid-crystal Fabry-Perot interferometer filter for WDM communication systems. *IEEE Lightwave Technology*, 11:2033–2043, 1993.

[40] S. Matsumoto, K. Hirabayashi, S. Sakata, and T. Hayashi. Tunable wavelength filter using nano-sized dropets of liquid crystal. *IEEE Photonic Technology Letters*, 11:442–444, 1999.

[41] D. Sadot and E. Boimovich. Tunable optical filters for dense WDM networks. *IEEE Communications Magazine*, 36:50–55, 1998.

[42] C.G.H. Roeloffzen, F. Horst, B.J. Offrein, R. Germann, G.L. Bona, H.W.M. Salemink, and R.M. de Ridder. Tunable passband flattened 1-from-16 binary tree structured add-after-drop multiplexer using SiON waveguide technology. *IEEE Photonics Technology Letters*, 12:1201–1203, 2000.

[43] T. Augustsson. Proposal of a phase shifted bragg grating assisted MZI for add-drop multiplexing. *Optoelectronics*, 56:205–208, 2001.

[44] M. Horita, Y. Matsushima, and S. Tanaka. Wavelength tunable optical add and drop multiplexer utilising coupled semiconductor waveguides. *Optical Communication*, 1:115–116, 1998.

[45] L.D. Garrett, A.H. Gnauck, L.H. Spiekman, and J.M. Wiesenfeld. Dynamic add/drop of 8-of-16 10 Gb/s channels in 440 km semiconductor-optical-amplifier-based WDM system. *Optical Fiber Communications Conference*, 4:284–286, 2000.

[46] J.K. Rhee, F. Garcia, A. Ellis, ' Hallock B, T. Kennedy, T. Lackey, R.G. Lindquist, J.P. Kondis, B.A. Scott, J.M.Harris, D. Wolf, and M. Dugan. Variable passband

optical add/drop multiplexer using wavelength selective switch. *Optical Communication*, pages 550–551, 2001.

[47] C.H. Yoon, H. Kim, and J.D. Shin. A tunable optical add-drop multiplexer using a fiber-optic tappered delay-line transversal filter. *CLEO Lasers and Electro-Optics*, pages 785–786, 1999.

[48] J.E. Ford, V.A.Aksyuk, D.J. Bishop, and J.A. Walker. Wavelength add-drop switching using tilting micromirrors. *IEEE Lightwave Technology*, 17:904–911, 1999.

[49] C.Pu, L.Y. Lin, E.L. Goldstein, and R.W. Tkach. Client-configurable eight-channel optical add/drop multiplexer using micromachining technology. *IEEE Photonics Technology Letters*, 12:1665–1667, 2000.

[50] H. Miyata, Y. Kaito, Y. Kai, H. Onaka, T. Nakazawa, M. Doi, M. Seino, T. Chikama, Y. Kotaki, K. Wakao, M. Komiyama, T. Kunikane, H. Yonetani, and Y. Sakai. Fully dynamic and reconfigurable optical add/drop multiplexer on 0.8 nm channel spacing using AOTF and 32-wave tunable LD module. *Optical Fiber Communications Conference*, 4:287–289, 2000.

[51] H. Okayama, Y. Ozeki, and T. Kunii. Dynamic wavelength selective add/drop node comprising tunable gratings. *IEEE Electronics Letters*, 33:881–882, 1997.

[52] P. Leisching, H. Bock, A. Richter, D. Stoll, and G. Fischer. Optical add/drop multiplexer for dynamic channel routing. *IEEE Electronics Letters*, 35:591–592, 1999.

[53] L. Eladada, D. Pant R. Blomquist M. Maxfield, G. Boudoughian, C. Poga, and R.A. Norrwood. Thermo-optic planar polymer Bragg grating OADM with broad tuning range. *IEEE Photonics Technology Letters*, 11:448–450, 1999.

[54] G. Barozzi, M.A. Davis, W.A. Helm, M. Lo Papa, F. Meli, and M.A. Putnam. Configurable OADM based on novel tunable Bragg grating. *CLEO Lasers and Electro-Optics*, 2:549–550, 2000.

[55] J. Kim and B. Lee. Bidirectional wavelength add-drop multiplexer using multiport optical circulators and fiber Bragg gratings. *IEEE Photonics Technology Letters*, 12:561–563, 2000.

[56] A.V. Tran, W.D. Zhong, R.S. Tucker, and K. Song. Reconfigurable multichannel OADM incorporating eight-port optical circulator and fiber Bragg gratings. *IEEE*

Photonics Technology Letters, 13:1100–1102, 2001.

[57] T. Almeida, P.S. Andre, A.N. Pinto, J.L. Pinto, and M. Pousa. Tunable transparent and cost effective optical add-drop multiplexer based on fiber Bragg grating for DWDM networks. *Digest of the LEOS Summer Topical Meetings*, page 2, 2001.

[58] R. Blomquist, R. Eldada, L. Glass, C. Nonvood, R.A. Poga, and C. Shing Yin. Integrated multichannel OADMs using polymer Bragg grating MZIs. *IEEE Photonics Technology Letters*, 10:1416 –1418, 1998.

[59] A.Q. Liu and X.M. Zhang. A MEMS pitch-tunable grating add/drop multiplexers. *IEEE/LEOS International Conference on Optical MEMS*, pages 25–26, 2000.

[60] T. Augustsson. Proposal of a Bragg grating assisted MMIMI-coupler for tunable add-drop multiplexing. *IEEE Photonics Technology Letters*, 13:1011–1013, 2001.

[61] Y. Urino, N. Ofusa, T. Saito, T. Shimoda, and T. Hanada. Optical add-drop multiplexer with grating-loaded directional coupler. *CLEO Lasers and Electro-Optics*, pages 1141–1142, 1999.

[62] X.M. Zhang and A.Q. Liu. Thermally tunable polymer Bragg grating OADMs. page MB5, 2000.

[63] K. Saito, T. Sano, H. Suganuma, K. Takahashi, and M. Tamura. Reconfigurable optical add/drop multiplexer using passive temperature-compensated wavelength tunable fiber Bragg grating. *Optical Fiber Communications Conference*, 3:WDD93–WD1–3, 2001.

[64] Dominik G. Rabus. *Realization of Optical Filters using Ring Resonators with Integrated Semiconductor Optical Amplifiers in GaInAsP/InP.* PhD Thesis - Technical University of Berlin, 2002.

[65] L.R. Chen. Tunable phase-shifted long-period gratings by refractive index-shifting. *Electrical and Computer Engineering*, 1:453–457, 2001.

[66] P. Tayebati, P.D. Wang, D. Vakhshoori, and R.N. Sacks. Widely tunable Fabry-Perot filter using Ga(Al)As-AlOx deformable mirrors. *IEEE Photonic Technology Letters*, 10:394–396, 1998.

[67] J. Lamperski. Discretely tunable multi cavity FFP filter for standard WDM frequency grid. *Electronic Components and Technology*, pages 1572–1575, 2000.

[68] S.E Miller. Integrated optics: An introduction. *Bell Systems Technology*, 48:2059–2069, 1969.

[69] R. Marz. *Integrated Optics design and modeling systems.* Artech House Publishers,

1995.

[70] E.A.J. Marcatilli. Bends in optical dielectric waveguides. *Bell Systems Technology*, 48:2103–2132, 1969.

[71] N.Q. Ngo and L.N. Binh. Novel realization of monotonic Butterworth-type lowpass and highpass and and bandpass optical filters using phase-modulated fiber-optic interferometers and ring resonators. *IEEE Lightwave Technology*, 12:827–841, 1994.

[72] K. Oda, N. Takato, and H. Toba. A wide-FSR waveguide double-ring resonator for optical FDM transmission systems. *IEEE Lightwave Technology*, 9:728–736, 1991.

[73] J. Zhang and J.W.Y. Lit. All-fiber compound ring resonator with a ring filter. *IEEE Lightwave Technology*, 12:1256–1262, 1994.

[74] B.E. Little, J.S. Foresi, G. Steinmeyer, E.R. Thoen, S.T. Chu, H.A. Haus, E.P. Ippen, L.C. Kimerling, and W. Greene. Ultra-compact Si-SiO2 microring resonator optical channel dropping filters. *IEEE Photonics Technology Letters*, 10:549–551, 1998.

[75] B.E.Little, S.T. Chu, W. Pan, D. Ripin, T. Kaneko, Y. Kokubun, and E. Ippen. Vertically coupled glass microring resonator channel dropping filters. *IEEE Photonics Technology Letters*, 11:215–217, 1999.

[76] R. Grover, P.P. Absil, V. Van;, J.V. Hryniewicz, B.E. Little, O. King, F.G. Johnson, L.C. Calhoun, and P.T. Ho. Vertically coupled GaAs-AlGaAs and GaInAsP-InP microring resonators. *Optical Fiber Communications Conference*, 3:WK2–1–3, 2000.

[77] P.P. Absil, J.V. Hryniewicz, B.E. Little, F.G. Johnson, K.J. Ritter, and P.T. Ho. Vertically coupled GaAs-AlGaAs and GaInAsP-InP microring resonators. *IEEE Photonics Technology Letters*, 13:49–51, 2001.

[78] M.K. Chin, C. Youtsey, W. Zhao, T. Pierson, Z. Ren, S.L. Wu, L. Wang, Y.G. Zhao, and S.T. Ho. GaAs microcavity channel-dropping filter based on a race-track resonator. *IEEE Photonics Technology Letters*, 11:1620–1622, 1999.

[79] R. Grover, V. Van, T.A. Ibrahim, P.P. Absil, L.C. Calhoun, F.G. Johnson, J.V. Hryniewicz, and P.T. Ho. Parallel-cascaded semiconductor microring resonators for high-order and wide-FSR filters. *IEEE Lightwave Technology*, 20:900–905,

2002.

[80] S.T. Chu, B.E. Little, W. Pan, T. Kaneko, S. Sato, and Y. Kokubun. An eight-channel add-drop filter using vertically coupled microring resonators over a cross grid. *IEEE Photonics Technology Letters*, 11:691–693, 1999.

[81] B.E. Little, S.T. Chu, W. Pan, T. Kaneko, and Y. Kokubun. Microring resonator arrays for VLSI photonics. *IEEE Photonics Technology Letters*, 12:323–325, 2000.

[82] D.W. Wilmot. Macroscopic single-mode waveguide for the construction of optical components, 1964.

[83] E.A.J. Marcatilli. Dielectric rectangular waveguide and directional coupler for integrated optics. *Bell Systems Technology*, 48:2079–2102, 1969.

[84] R. Marz. *Integrated Optics design and modeling systems*, chapter Waveguide Theory, pages 39–85. Artech House Publishers, 1995.

[85] G. Fischbeck, R. Moosburger, M. Topper, and K. Petermann. Design concept for singlemode polymer waveguides. *IEEE Electronics Letters*, 32:212–213, 1996.

[86] G.N. de Brabander, J.T. Boyd, and H.E. Jackson. Single polarization optical waveguide on silicon. *Quantum Electronics*, 27:575–579, 1991.

[87] B. Jalali, P.D. Trinh, S. Yegnanarayanan, and F. Coppinger. Guided-wave optics in silicon-on-insulator technology, 1996.

[88] S. Tanahashi, K. Kaneko, , and M. Terasawa. Single-mode optical waveguide using siloxane polymer on Cu-polyimide substrate. *Electronic Components and Technology Conference*, pages 189–193, 1995.

[89] J.D. Bickford and G.R. Branner. Ultra-broadband high-directivity directional coupler design. *Microwave Symposium*, 2:595–598, 1988.

[90] R.J. Deri, N. Yasuoka, M. Makiuchi, A. Kuramata, O. Wada, and S. Yamakoshi. Low-loss optical directional coupler on InP. *Quantum Electronics*, 25:1355–1356, 1989.

[91] P.D. Trinh, S. Yegnanarayanan, and B. Jalali. Integrated optical directional couplers in silicon-on-insulator. *IEEE Electronics Letters*, 31:2097–2099, 1995.

[92] T.A Ramadan, R. Scarmozzino, and R.M. Osgood Jr. Adiabatic couplers: design rules and optimization. *IEEE Lightwave Technology*, 16:277–283, 1998.

[93] T. Saida, A. Himeno, M. Okuno, A. Sugita, and K. Okamoto. Silica-based 2×2 multimode interference coupler with arbitrary power splitting ratio. *IEEE Electronics Letters*, 35:2031–2033, 1999.

[94] A. Takagi, K. Jinguji, and M. Kawachi. Design and fabrication of broad-band silica-based optical waveguide couplers with asymmetric structure. *Quantum Electronics*, 28:848–855, 1992.

[95] R. Marz. *Integrated Optics design and modeling systems*, chapter Codirectional Coupling, pages 169–216. Artech House Publishers, 1995.

[96] O. Brynggahl. Image formation using self-imaging technique. *Optical Society of America*, 63:416–418, 1973.

[97] R.Ulrich and T. Kamiya. Self-imaging in homogeneous planar optical waveguides. *Applied Physics Letters*, 68:583–592, 1975.

[98] L.B. Soldano and E.C.M. Pennings. Optical multi-mode interference devices based on self-imaging: principles and applications. *IEEE Lightwave Technology*, 13:615–627, 1995.

[99] L.B. Soldano, F.B. Veerman, M.K. Smit, B.H. Verbeek, A.H. Dubost, and E.C.M. Pennings. Planar monomode optical couplers based on multimode interference effects. *IEEE Lightwave Technology*, 10:1848–1850, 1992.

[100] J.M. Heaton and R.M. Jenkins. General matrix theory of self-imaging in multimode interference (MMI) couplers. *IEEE Photonics Technology Letters*, 11:212–214, 1999.

[101] N.S. Lagali, M.R. Paiam, and R.I. MacDonald. Theory of variable-ratio power splitters using multimode interference couplers. *IEEE Photonics Technology Letters*, 11:665–667, 1999.

[102] E.C.M. Pennings, R. van Roijen, B.H. Verbeek, R.J. Deri, and L.B. Soldano. Ultracompact multimode interference waveguide devices. *CLEO Lasers and Electro-Optics*, pages 193–194, 1993.

[103] D.S. Levy, R. Scarmozzino, Y.M. Li, and R.M. Osgood Jr. A new design for ultracompact multimode interference-based 2×2 couplers. *IEEE Photonics Technology Letters*, 10:96–98, 1998.

[104] Y. Ma, S. Park, L. Wang, and S.T. Ho. Ultracompact multimode interference 3-db coupler with strong lateral confinement by deep dry etching. *IEEE Photonics Technology Letters*, 12:492–494, 2000.

[105] F.B. Veerman, P.J. Schalkwijk, E.C.M. Pennings, M.K. Smit, and B.H. Verbeek. An optical passive 3 dB TMI-coupler with reduced fabrication tolerance sensitivity. *IEEE Lightwave Technology*, 10:306–311, 1992.

[106] P.A. Besse, M. Bachmann, H. Melchior, L.B. Soldano, and M.K. Smit. Optical bandwidth and fabrication tolerances of multimode interference couplers. *IEEE Lightwave Technology*, 13:1004–1009, 1994.

[107] T. Kudou, K. Shimizu, K. Harada, , and T. Ozeki. Synthesis of grating lattice circuits. *IEEE Lightwave Technology*, 2:347, 1999.

[108] C.K. Madsen and J.H. Zhao. *Optical Filter Design and Analysis: A Signal Processing Approach.* Wiley, 1999.

[109] A. Melloni and M. Martinelli. Synthesis of direct-coupled-resonators bandpass filters for WDM systems. *IEEE Lightwave Technology*, 2:296–303, 2002.

[110] B. E. Little, S. T. Chu, H. A. Haus, J. Foresi, , and J.-P. Laine. Microring resonator channel dropping filters. *IEEE Lightwave Technology*, 15:998–1005, 1997.

[111] A. Yariv. Universal relations for coupling of optical power between microresonators and dielectric waveguides. *IEEE Electronics Letters*, 36:321–322, 2000.

[112] A. Yariv. Critical coupling and its control in optical waveguide-ring resonator systems. *Photonics Technology Letters*, 14:483–485, 2002.

[113] F. Sanchez. Matrix algebra for all-fiber optical resonators. *IEEE Lightwave Technology*, 9:838–844, 1991.

[114] J. Capmany and M.A. Muriel. A new transfer matrix formalism for the analysis of fiber ring resonators: compound coupled structures for FDMA demultiplexing. *IEEE Lightwave Technology*, 8:1904–1919, 1990.

[115] O. Schwelb. Generalized analysis for a class of linear interferometric networks. Part I. Analysis. *IEEE Transactions on Microwave Theory and Techniques*, 46:1399–1408, 1998.

[116] S. C. Hagness, D. Rafizadeh, S. T. Ho, and A. Taflove. FDTD microcavity simulations: design and experimental realization of waveguide-coupled single-mode ring and whispering-gallery-mode disk resonators. *IEEE Lightwave Technology*, 15:2154–2165, 1997.

[117] S. C. Hagness, D. Rafizadeh, S. T. Ho, , and A. Taflove. High-Q microcavity ring and disk resonators: FDTD analysis of resonance and coupling characteristics. *IEEE Transaction on Antennas and Propagation*, 2:1236 –1239, 1997.

[118] S.E. Miller. Coupled wave theory and waveguide applications. *Bell Systems Technology*, 33:853–871, 1954.

[119] S.A Schelkunoff. Conversion of Maxwell's equations into generalized telegraphist's

equations. *Bell Systems Technology*, 34:995–1043, 1955.

[120] A. Yariv. Coupled mode theory for guided-wave optics. *Quantum Electronics*, QE-9:919–933, 1973.

[121] H.A. Haus and W. Huang. Coupled-mode theory. *IEEE Proceedings*, 79:1505–1518, 1991.

[122] N.Q. Ngo and L.N. Binh. Novel realization of monotonic butterworth-type lowpass and highpass and and bandpass optical filters using phase-modulated fiber-optic interferometers and ring resonators. *IEEE Lightwave Technology*, 12:827–840, 1994.

[123] R. Orta, P. Savi, R. Tascone, , and D. Trinchero. Synthesis of multiplering-resonator filter for optical systems. *IEEE Photonics Letters*, 7:1447–1449, 1995.

[124] G.S. Pandian and F.E. Seraji. Optical pulse response of a fiber ring resonator. *IEEE Proceedings*, 138:235–239, 1991.

[125] R.M. de Ridder and R. Stoffer. Finite-difference time-domain modelling of photonic crystal structures. *IEE Colloquium - Transparent Optical Networks*, pages 22–25, 2001.

[126] T.T. Chi, R.J. Burkholder, and R. Lee. The application of FDTD in hybrid methods for cavity scattering analysis. *IEEE Transaction on Antennas and Propagation*, 43:1082–1090, 1995.

[127] K.S. Kunz and R.J. Luebbers. *The Finite Difference Time Domain Method for Electromagnetics.* CRC Press and Boca Raton, 1993.

[128] S. Suzuki, K. Oda, , and Y. Hibino. Integrated-optic douple ring resonators with a wide free spectral range of 100 GHz. *IEEE Lightwave Technology*, 13:1766–1771, 1995.

[129] A. Carena, V. Curri, R. Gaudino, P. Poggiolini, and S. Benedetto. A time-domain optical transmission system simulation package accounting for nonlinear and polarization-related effects in fiber. *IEEE Selected Areas in Communications*, 15:751–765, 1997.

[130] M.C. Jeruchim. *Simulation of Communication Systems: Modeling and Methodology and and Techniques.* Plenum Publishing Corporation, 2001.

[131] T.T. Chi, R.J. Burkholder, and R. Lee. The application of FDTD in hybrid methods for cavity scattering analysis. *IEEE Transaction on Antennas and Propagation*, 43:1082–1090, 1995.

[132] V. Craciun and O. W.W. Yang. Ring resonator-based sparse reconfigurable optical add-drop multiplexer. Part I: Filter analysis. *ITCOM - Active and Passive Optical Components for WDM Communications*, 2003 - to appear.

[133] V. Craciun and O. W. W. Yang. Ring resonator-based sparse reconfigurable optical add-drop multiplexer. Part II: Node level analysis. *ITCOM - Optical Transmission Systems and Equipment for WDM Networking*, 2003 - to apper.

[134] ITU-T Study Group 15. *Series G: ITU-T Recommandation G.692 - Characteristics of optical components and sub-systems.* International Communication Union, 1998.

[135] E.-S. Kang, J.Y. Bae, and B.-S. Bae. Measurement of thermo-optic coefficients in sol-gel hybrid glass films. *Sol-Gel Science and Technology*, 26:981–984, 2003.

[136] C. Dragone. Planar 1× N optical multiplexer with nearly ideal response. *IEEE Photonics Technology Letters*, 14:1545–1547, 2002.

[137] M. Javid and E. Brenner. *Analysis and transmission and and filtering of signals.* McGraw-Hill, 1963.

[138] G.P. Agrawal. *Fiber-Optic Communication Systems.* Wiley Series in Microwave and Optical Engineering, 1997.

[139] S.W. Smith. *The Scientist & Engineer's Guide to Digital Signal Processing.* California Technical Publishing, 1998.